Volume 39 No. 2 2009
ISSN 0146-6453
ISBN 978-0-7020-4186-0

ICRP

Annals of the ICRP

ICRP Publication 110

Adult Reference Computational Phantoms

ELSEVIER

Annals of the ICRP

ICRP PUBLICATION 110
(with accompanying ICRP CD 4)

Adult Reference Computational Phantoms

Joint ICRP/ICRU Report

Editor
C.H. CLEMENT

PUBLISHED FOR

The International Commission on Radiological Protection

and

The International Commission on Radiation Units and Measurements

by

ELSEVIER

Subscription Information

Publication information: *Annals of the ICRP* (ISSN 0146-6453). *Annals of the ICRP*, and the Publications series preceding it, have been published by Pergamon since 1958. In 1991, Pergamon became part of the Elsevier family of imprints. Elsevier carries forward the name and reputation of a publishing house dating from 1580. Elsevier is an integral partner with the scientific, technical and health communities, delivering superior information products and services that foster communication, build insights, and enable individual and collective advancement in scientific research and health care.
Subscription prices are available upon request from the Publisher or from the Elsevier Customer Service Department nearest you or from this journal's website (http://intl.elsevierhealth.com/journals/icrp). Further information is available on this journal and other Elsevier products through Elsevier's website (http://www.elsevier.com). Subscriptions are accepted on a prepaid basis only and are entered on a calendar year basis. Issues are sent by standard mail (surface within Europe, air delivery outside Europe). Priority rates are available upon request. Claims for missing issues should be made within six months of the date of dispatch.

Orders, claims, and journal enquiries: please contact the Elsevier Customer Service Department nearest you:

St. Louis: Elsevier Customer Service Department, 3251 Riverport Lane, Maryland Heights, MO 63043, USA; phone: (800) 6542452 [toll free within the USA]; (+1) (314) 4478871 [outside the USA]; fax: (+1) (314) 4478029; e-mail: JournalsCustomerService-usa@elsevier.com

Oxford: Elsevier Customer Service Department, The Boulevard, Langford Lane, Kidlington, Oxford OX5 1GB, UK; phone: (+44) (1865) 843434; fax: (+44) (1865) 843970; e-mail: JournalsCustomerService-EMEA@elsevier.com

Tokyo: Elsevier Customer Service Department, 4F Higashi-Azabu, 1-Chome Bldg, 1-9-15 Higashi-Azabu, Minato-ku, Tokyo 106-0044, Japan; phone: (+81) (3) 5561 5037; fax: (+81) (3) 5561 5047; e-mail: JournalsCustomerServiceJapan@elsevier.com

Singapore: Elsevier Customer Service Department, 3 Killiney Road, #08-01 Winsland House I, Singapore 239519; phone: (+65) 63490222; fax: (+65) 67331510; e-mail: JoumalsCustomerServiceAPAC@elsevier.com

Back Issues

This journal is indexed/abstracted in App. Health Phy. Abstr., Biosis Data., CBS and SSSA/CISA/ECA/ISMEC, and Scopus.

♾ The paper used in this publication meets the minimum requirements of ANSI/NISO Z39.48-1992 (Permanence of Paper).

USA mailing notice: *Annals of the ICRP* (ISSN 0146-6453) is published bi-monthly by Elsevier Ltd, The Boulevard, Langford Lane, Kidlington, Oxford OX5 1GB, UK. Periodical postage paid at Rahway NJ and additional mailing offices.

USA POSTMASTER: Send change of address to *Annals of the ICRP*, Elsevier Customer Service Department, 3251 Riverport Lane, Maryland Heights, MO 63043, USA.

AIRFREIGHT AND MAILING in USA by Mercury International Limited, 365 Blair Road, Avenel, NJ 07001.

ISBN 978-0-7020-4186-0
ISSN 0146-6453

Published bi-monthly.

Printed by Polestar Wheatons Ltd, Exeter, UK

Annals of the ICRP

Published on behalf of the International Commission on Radiological Protection

Aims and Scope

The International Commission on Radiological Protection (ICRP) is the primary body in protection against ionising radiation. ICRP is a registered charity and is thus an independent non-governmental organisation created by the 1928 International Congress of Radiology to advance for the public benefit the science of radiological protection. The ICRP provides recommendations and guidance on protection against the risks associated with ionising radiation, from artificial sources widely used in medicine, general industry and nuclear enterprises, and from naturally occurring sources. These reports and recommendations are published four times each year on behalf of the ICRP as the journal *Annals of the ICRP*. Each issue provides in-depth coverage of a specific subject area.

Subscribers to the journal receive each new report as soon as it appears so that they are kept up to date on the latest developments in this important field. While many subscribers prefer to acquire a complete set of ICRP reports and recommendations, single issues of the journal are also available separately for those individuals and organizations needing a single report covering their own field of interest. Please order through your bookseller, subscription agent, or direct from the publisher.

ICRP is composed of a Main Commission and five standing Committees on: radiation effects, doses from radiation exposure, protection in medicine, the application of ICRP recommendations, and protection of the environment, all served by a small Scientific Secretariat. The Main Commission consists of twelve members and a Chair. Committees typically comprise 15–20 members. Biologists and medical doctors dominate the current membership; physicists are also well represented.

ICRP uses Working Parties to develop ideas and Task Groups to prepare its reports. A Task Group is usually chaired by an ICRP Committee member and usually contains a majority of specialists from outside ICRP. Thus, ICRP is an independent international network of specialists in various fields of radiological protection. At any one time, about one hundred eminent scientists are actively involved in the work of ICRP. The Task Groups are assigned the responsibility for drafting documents on various subjects, which are reviewed and finally approved by the Main Commission. These documents are then published as the *Annals of the ICRP*.

This report was compiled by a Subgroup of the Task Group on Dose Calculations of ICRP Committee 2. The membership was as follows:

M. Zankl (Chairperson)
K.F. Eckerman
N. Petoussi-Henss
W.E. Bolch
H.G. Menzel

ELSEVIER

ICRP Publication 110

Annals of the ICRP

Adult Reference Computational Phantoms

ICRP PUBLICATION 110
Approved by ICRP in October 2007 and
adopted by ICRU in October 2008

Abstract–This report describes the development and intended use of the computational phantoms of the Reference Male and Reference Female. In its 2007 Recommendations, ICRP adopted these computational phantoms for forthcoming updates of organ dose coefficients for both internal and external radiation sources (ICRP, 2007). The phantoms are based on medical image data of real people, yet are consistent with the data given in *Publication 89* (ICRP, 2002) on the reference anatomical and physiological parameters for both male and female subjects. The reference phantoms are constructed after modifying the voxel models (Golem and Laura) of two individuals whose body height and mass resembled the reference data. The organ masses of both models were adjusted to the ICRP data on the adult Reference Male and Reference Female, without compromising their anatomic realism. This report describes the methods used for this process and the characteristics of the resulting computational phantoms.

Chapter 1 summarises the main reasons for constructing these phantoms – voxel phantoms being the state of the art, and the necessity for compliance with the anatomical characteristics of the Reference Male and Reference Female given in *Publication 89* (ICRP, 2002). Chapter 2 summarises the specifications of the computational phantoms with respect to external dimensions and the source and target regions that are required. Chapter 3 characterises the previously segmented voxel models (Golem and Laura) that are the origins of the reference phantoms. Chapter 4 sketches the modifications that had to be applied to these models to create voxel models of the Reference Male and Reference Female. Chapter 5 is a description of the resulting reference computational phantoms of the Reference Male and Reference Female. Finally, Chapter 6 indicates their applications and highlights their limitations.

The phantoms' technical descriptions are contained in Annexes A–H, which represent the larger part of this report. The numerical data representing the phantoms are contained on an electronic data storage medium (CD-ROM) that accompanies the printed publication. One of the aims of this report is to assist those who wish to implement the phantoms for their own calculations.

Furthermore, to illustrate the uses of these phantoms, graphical illustrations of conversion coefficients for some external and internal exposures are included in Annexes I–L.

A comprehensive set of recommended values will be published in separate reports. Finally, Annex M presents a description of the data files on the CD-ROM.

Keywords: Computational phantoms; Voxel models; Reference Male; Reference Female

References

ICRP, 2002. Basic anatomical and physiological data for use in radiological protection: reference values. ICRP Publication 89. Ann. ICRP 32(3–4).

ICRP, 2007. The 2007 Recommendations of the International Commission on Radiological Protection. ICRP Publication 103. Ann. ICRP 37(2–4).

ELSEVIER

ICRP Publication 110

Annals of the ICRP

Editorial

REALISTIC REFERENCE PHANTOMS: AN ICRP/ICRU JOINT EFFORT

In London in 1925, at the first International Congress of Radiology (ICR), the predecessor to the International Commission on Radiation Units and Measurements (ICRU) was created as the International X-ray Unit Committee. The International X-ray and Radium Protection Committee, predecessor to the International Commission on Radiological Protection (ICRP), was created in Stockholm in 1928 at the second ICR. Thus, ICRP and ICRU have a shared origin and many common interests.

Although both organisations function independently, until the 1970s they usually met at the time and place of the ICR. They shared (and still share) many interests and, at times, many members including Lauriston Taylor, a pioneer and giant in the field of radiological protection.

This publication represents a renewed collaboration between the two organisations, being the first in a series of planned joint efforts, with contributions from members of both ICRP and ICRU. In this case, ICRP has taken the lead, while ICRU will take the lead for some of the forthcoming publications.

In addition, this report is vital to the full implementation of the 2007 Recommendations of ICRP (ICRP, 2007). The Recommendations formally define 'reference phantoms' as 'voxel phantoms for the human body...'. The current report delivers the most important of these voxel phantoms: the adult male and adult female.

Practical radiological protection for workers and the general public uses dosimetric quantities which quantify the exposure to ionising radiation appropriately for the implementation of the fundamental principles of limitation and optimisation. Radiation protection regulations and guidelines for demonstration of compliance are formulated in terms of reference or standard individuals. ICRP and ICRU have established a system of protection and operational dosimetric quantities which are based on reference data, models, and phantoms, and which have been shown to provide a satisfactory conceptual and practicable procedure for risk management of the low dose exposures of concern in radiological protection.

It was recognised long before the introduction of the current system of protection and operational quantities that exposure assessment and monitoring of humans exposed to ionising radiation from external sources and from incorporated radionuclides requires the use of models and phantoms characterizing reference individuals. This led to the development of phantoms, i.e. physical models of the human body such as the 'Rando' phantom (Alderson et al., 1962), and computational anthropo-

morphic models such as the MIRD model (Fisher and Snyder, 1967) which mathematically described the geometries of the body and its organs.

This important facet of radiation dosimetry has also been an important part of the work by ICRP and ICRU.

ICRP first presented data on standard man in ICRP *Publication 2* Report of Committee II on Permissible Dose for Internal Radiation (ICRP, 1960) as it formulated the concept of permissible doses for workers from incorporated radionuclides. In 1975, ICRP *Publication 23* on Reference Man (ICRP, 1975) was published. It contained comprehensive information on anatomical, morphological, and physiological data, and provided a systematic and consistent set of reference data for reference individuals. The most recent publication on this subject, and replacing ICRP *Publication 23*, is ICRP *Publication 89* (ICRP, 2002), which provides reference values for both male and female subjects of six different ages from newborn to adult.

One of ICRU's objectives is to provide guidance on radiation measurements in all areas of application of ionising radiation. So-called standard phantoms for radiotherapy applications were introduced in ICRU Report 10d (ICRU, 1963) and ICRU Report 23 (ICRU, 1973). These phantoms have simple geometry, e.g. cubic water phantoms used to compare measurements under standard conditions of irradiation. For the definition of operational quantities, ICRU introduced a reference computational phantom, the ICRU sphere, 30-cm diameter, composed of ICRU tissue (ICRU, 1980). ICRU Report 48 (ICRU, 1992) was a review on phantoms and computational models in therapy, diagnosis, and protection.

In this joint ICRP/ICRU report, reference computational phantoms of the adult male and adult female are introduced. These phantoms will be for use by ICRP and ICRU to derive organ dose conversion coefficients for external and internal exposure, following the revisions introduced in ICRP *Publication 103* (ICRP, 2007).

These phantoms were also constructed to be consistent with the external dimensions and masses of organs and tissues in ICRP *Publication 89* and thus are complementary to that document. The reference phantoms are voxel based and have been derived from tomographic imaging data of a male and female patient. Thus, they reflect an anatomically realistic spatial distribution of organs and tissues with a high degree of consistency with the reference values in ICRP *Publication 89*. Furthermore, the technique applied in the construction of the phantoms from the medical imaging, as described in some detail in the report, also permitted the identification of all organs and tissues, including those explicitly noted in the definition of effective dose, thus enabling the full implementation of the recommendations in *Publication 103* with regard to the reference dose conversion coefficients. The treatment of the anatomical properties of the skeleton in these reference phantoms will allow detailed skeletal dosimetry to be performed and deserves special mention. Reference organ conversion coefficients for exposure to incorporated radionuclides will, of course, be evaluated using ICRP reference biokinetic and dosimetric models, including an update of the *Publication 66* (ICRP, 1994) Human Respiratory Tract Model, and the *Publication 100* (ICRP, 2006) Human Alimentary Tract Model.

All reference dosimetric data used for dosimetry, dose assessment, and monitoring in radiological protection for exposure of adults will, in the future, be based on

calculations and evaluations using these reference phantoms. Reference phantoms for persons of younger ages are in the process of being prepared using a similar approach; in particular, consistency with ICRP *Publication 89* will be assured.

In recent years, a number of computational phantoms have been published by various authors for a variety of purposes and applications based on tomographic imaging data of individuals. The principal purpose of the phantoms presented here is in the evaluation of reference dosimetric data by ICRP and ICRU, in particular reference organ dose conversion coefficients, thus enabling the determination of effective dose. In spite of this intended limited application, the report also contains a CD with the phantoms and guidance regarding how to use these phantoms in radiation transport calculations. Thus, the phantoms can also be used for other applications. However, any other application must respect the manner of construction of these particular phantoms and their relationship to the reference anatomical data of ICRP *Publication 89*. In particular, it must be remembered that the phantoms represent reference persons, and any potential application with regard to a particular individual can be associated with substantial uncertainties.

Hans-Georg Menzel (ICRP/ICRU)
Christopher Clement (ICRP)
Paul DeLuca (ICRU)

References

Alderson, S.W., Lanzl, L.H., Rollins, M., Spira, J., 1962. An instrumented phantom system for analog computation of treatment plans. Am. J. Roentgenol. 87, 185–195.

Fisher, H.L., Snyder, W.S., 1967. Distribution of Dose in the Body from a Source of Gamma Rays Distributed Uniformly in an Organ. ORNL-4168. Oak Ridge National Laboratory, Oak Ridge, TN.

ICRP, 1960. Report of Committee II on Permissible Dose for Internal Radiation. ICRP Publication 2. Pergamon Press, Oxford.

ICRP, 1975. Reference Man: Anatomical, Physiological and Metabolic Characteristics. ICRP Publication 23. Pergamon Press, Oxford.

ICRP, 1994. Human respiratory tract model for radiological protection. ICRP Publication 66. Ann. ICRP 24(1–3).

ICRP, 2002. Basic anatomical and physiological data for use in radiological protection: reference values. ICRP Publication 89. Ann. ICRP 32(3–4).

ICRP, 2006. Human alimentary tract model for radiological protection. ICRP Publication 100. Ann. ICRP 36(1–2).

ICRP, 2007. The 2007 Recommendations of the International Commission on Radiological Protection. ICRP Publication 103. Ann. ICRP 37(2–4).

ICRU, 1963. Clinical Dosimetry. ICRU Report 10d. International Commission on Radiation Units and Measurements, Bethesda, MD.

ICRU, 1973. Measurement of Absorbed Dose in a Phantom Irradiated by a Single Beam of X or Gamma Rays. ICRU Report 23. International Commission on Radiation Units and Measurements, Bethesda, MD.

ICRU, 1980. Radiation Quantities and Units. ICRU Report 33. International Commission on Radiation Units and Measurements, Bethesda, MD.

ICRU, 1992. Phantoms and Computational Models in Therapy, Diagnosis and Protection. ICRU Report 48. International Commission on Radiation Units and Measurements, Bethesda, MD.

CONTENTS

PREFACE

This report provides a summary of the methods and procedures used to create the computational phantoms corresponding to the adult Reference Male and Reference Female from individual-specific tomographic data. The methods and procedures used in this activity have been reported in numerous publications. These phantoms are designed specifically for calculation of the radiological protection quantities corresponding to the effective dose concept of the 2007 Recommendations of the Commission. The phantoms are presented to the radiation protection community in numerical format, with identification of source and target regions of the body in the CD inserted at the back cover of this publication. Due to the numerical nature of the phantoms and earlier publication of the characteristics of the adult Reference Male and Reference Female, this document was not provided for public consultation. The authors acknowledge the comments received from the ICRP Committees, the International Commission on Radiation Units and Measurements (ICRU), and selected expert reviewers.

Although being released as an ICRP publication, the present report is a joint publication of ICRP and ICRU.

This report was compiled by a Subgroup of the Task Group on Dose Calculations of ICRP Committee 2. The membership was as follows:

M. Zankl (Chairperson)	K.F. Eckerman	N. Petoussi-Henss
W.E. Bolch	H.G. Menzel	

The membership of the Task Group on Dose Calculations of ICRP Committee 2 during the preparation of this report was:

2001–2005 (full members)

K.F. Eckerman (Chairman)	W.E. Bolch	A. Phipps
H.G. Menzel (Vice-Chair, External Dosimetry)	N. Hertel	B.R.L. Siebert
D. Nosske (Vice-Chair, Internal Dosimetry)	N. Petoussi-Henss	M. Zankl
V. Berkovski		

2001–2005 (corresponding members)

L. Bertelli	G.M. Kendall	A.R. Reddy
A. Endo	R. Leggett	R. Richardson
T. Fell	I. Likhtarev	M.G. Stabin
J. Hunt	G. Miller	A. Ulanovsky
L. Johansson	M. Pelliccioni	X.G. Xu

2005–2009 (full members)

W.E. Bolch (Chairman, 2007–2009)	E. Blanchardon	M. Pelliccioni
K.F. Eckerman (Chairman, 2005–2007)	A. Endo	A. Phipps (2005–2007)

D. Nosske (Vice-Chair, Internal Dosimetry)	N. Hertel	M. Zankl
N. Petoussi-Henss (Vice-Chair, External Dosimetry)	J. Hunt	
V. Berkovski	H.G. Menzel (2005–2007)	

2005–2009 (corresponding members)

L. Bertelli	R. Richardson	A. Ulanovsky
T. Fell	M.G. Stabin	X.G. Xu

The membership of ICRP Committee 2 during the preparation of this report was:

2001–2005

C. Streffer (Chairman)	F.A. Fry	H.G. Paretzke
M. Balonov	J. Inaba	A.S. Pradhan
B.B. Boecker	I.A. Likhtarev	J.W. Stather (Vice-Chairman)
A. Bouville	J.L. Lipsztein	D. Taylor (Secretary)
G. Dietze	H.G. Menzel	Y.Z. Zhou
K.F. Eckerman	H. Métivier	

2005–2009

H.G. Menzel (Chairman, 2007–2009)	G. Dietze	H.G. Paretzke
C. Streffer (Chairman, 2005–2007)	K.F. Eckerman	F. Paquet
M. Balonov	J.D. Harrison (Secretary)	A.S. Pradhan
V. Berkovski	N. Ishigure	J.W. Stather
W.E. Bolch	P. Jacob (2007–2009)	(2005–2007)
A. Bouville	J.L. Lipsztein	Y.Z. Zhou

The ICRU sponsors of the report were:

H.G. Menzel H.G. Paretzke

Members of ICRU during the preparation of this report were:

P.M. DeLuca (Chairman)	D.T.L. Jones	H. Tatsuzaki
P. Dawson	H.G. Menzel	A. Wambersie
K. Doi	B.D. Michael	G.F. Whitmore
R.A. Gahbauer	H.G. Paretzke	
M. Inokuti	S.M. Seltzer	

MAIN POINTS

- **The phantoms presented in this document are the official computational models representing the Reference Male and Reference Female (ICRP, 2002,2007). These reference computational models are based on computed tomographic data of real people and, hence, are digital three-dimensional representations of human anatomy.**

- **For the construction of the reference computational models, tomographic data sets were selected of individuals with external dimensions close to the reference data. From these data, voxel phantoms were segmented and then adjusted to the reference values given in *Publication 89* (ICRP, 2002).**

- **Most relevant source and target regions are adjusted to their reference mass values with high precision. Exceptions and limitations are discussed.**

- **The phantoms' technical descriptions are contained in a series of annexes that form the larger part of this report.**

- **The numerical data representing the phantoms are contained on an electronic data storage medium (CD-ROM) that accompanies the printed document. One of the aims of this report is to assist those who wish to implement the phantoms for their own calculations.**

References

ICRP, 2002. Basic anatomical and physiological data for use in radiological protection: reference values. ICRP Publication 89. Ann. ICRP 32(3–4).

ICRP, 2007. The 2007 Recommendations of the International Commission on Radiological Protection. ICRP Publication 103. Ann. ICRP 37(2–4).

EXECUTIVE SUMMARY

(a) This report describes the development and intended use of the computational phantoms of the Reference Male and Reference Female. In its 2007 Recommendations, ICRP adopted these computational phantoms for the forthcoming update of organ dose coefficients for internal and external radiation sources (ICRP, 2007). The phantoms are based on medical image data of real people and are consistent with the information given in *Publication 89* (ICRP, 2002) on the reference anatomical and physiological parameters for both male and female subjects. The reference voxel models were constructed after modifying the voxel models (Golem and Laura) of two individuals whose body height and mass closely resembled the reference data. The organ masses of both models were adjusted to the ICRP data on the adult Reference Male and Reference Female, without significantly altering their realistic anatomy. The report describes the methods used for this process and the characteristics of the resulting voxel phantoms. Furthermore, to illustrate the uses of these phantoms, conversion coefficients for some external and internal exposures are also included.

(b) The numerical data representing the phantoms are contained on an electronic data storage medium (CD-ROM) that accompanies the printed publication. One of the aims of this report is to assist those who wish to implement the phantoms for their own calculations.

(c) Chapter 1 summarises the main reasons for constructing these phantoms – voxel phantoms being the state of the art, and the necessity for compliance with the anatomical characteristics of the Reference Male and Reference Female given in *Publication 89* (ICRP, 2002). Chapter 2 summarises the specifications of the computational phantoms with respect to external dimensions and the source and target regions that are required. Chapter 3 characterises the previously segmented voxel models (Golem and Laura) that are the origins of the reference phantoms. Chapter 4 sketches the modifications that had to be applied to these models to create voxel models of the Reference Male and Reference Female. Chapter 5 is a description of the resulting reference computational phantoms of the Reference Male and Reference Female. Finally, Chapter 6 indicates their applications and highlights their limitations.

(d) The phantoms' technical descriptions are contained in a series of annexes that form the larger part of this publication.

(e) Annex A presents a list of the individually segmented organs/structures (identification list), together with the assigned media, densities, masses, containing boxes, and centres of mass.

(f) Annex B presents a list of the phantom media and their elemental compositions.

(g) Annex C is a list of the source regions, together with their typically used acronyms and the identification numbers that make up these source regions, and Annex D presents the respective data for the target regions.

(h) In Annex E, distributions are given of the thickness of tissue shielding selected organs from the front, back, left, right, top, and bottom; these distributions are presented in graphical form.

(i) In Annex F, chord-length distributions between selected pairs of source and target organs are presented in graphical form.

(j) Annex G presents selected transverse, sagittal, and coronal slice images of both reference computational phantoms.

(k) Furthermore, to illustrate the uses of these phantoms, graphical illustrations of conversion coefficients for some external and internal exposures are included in Annexes H–L. A comprehensive set of recommended values will be published in separate reports.

(l) In Annex H, some selected organ dose conversion coefficients for external exposure to monoenergetic photons are presented.

(m) Annex I presents some selected organ dose conversion coefficients for external exposure to monoenergetic neutrons.

(n) In Annex J, some selected organ dose conversion coefficients are presented for external exposure to helium ions.

(o) In Annexes K and L, specific absorbed fractions are given for selected source and target region pairs for monoenergetic photons and electrons, respectively.

(p) Annex M summarises the contents of the CD-ROM containing the phantom numerical data.

References

ICRP, 2002. Basic anatomical and physiological data for use in radiological protection: reference values. ICRP Publication 89. Ann. ICRP 32(3–4).

ICRP, 2007. The 2007 Recommendations of the International Commission on Radiological Protection. ICRP Publication 103. Ann. ICRP 37(2–4).

GLOSSARY

Absorbed dose, D

The fundamental dose quantity given by:

$$D = \frac{\mathrm{d}\bar{\varepsilon}}{\mathrm{d}m}$$

where $\mathrm{d}\bar{\varepsilon}$ is the mean energy imparted to matter of mass $\mathrm{d}m$ by ionising radiation. The SI unit for absorbed dose is joule per kilogramme (J/kg), and its special name is gray (Gy).

Active (bone) marrow

Active marrow is haematopoietically active and gets its red colour from the large numbers of erythrocytes (red blood cells) being produced. Active bone marrow serves as a target tissue for radiogenic risk of leukaemia.

Bone marrow

Bone marrow is a soft, highly cellular tissue that occupies the cylindrical cavities of long bones and the cavities within the trabecular bone of the vertebrae, ribs, sternum, and the flat bones of the cranium and pelvis. Total bone marrow consists of a sponge-like, reticular, connective tissue framework called 'stroma', myeloid (blood-cell-forming) tissue, fat cells, small accumulations of lymphatic tissue, and numerous blood vessels and sinusoids. There are two types of bone marrow: active (red) and inactive (yellow). See 'Active (bone) marrow' and 'Inactive (bone) marrow'.

Cortical (bone) marrow

The marrow contained in the medullary cavities in the shafts of the long bones.

Dose coefficient

Used as a generic term for coefficients relating a dose quantity to another physical quantity, both for internal and external radiation exposure. In internal dosimetry, a typical dose coefficient is the dose per unit intake of a radioactive substance; in external dosimetry, these are dose conversion coefficients.

Dose equivalent, H

The product of D and Q at a point in tissue, where D is the absorbed dose and Q is the quality factor for the specific radiation at this point, thus:

$$H = DQ$$

The unit of dose equivalent is joule per kilogramme (J/kg), and its special name is sievert (Sv).

Effective dose, E

The tissue-weighted sum of the equivalent doses in all specified tissues and organs of the body, given by the expression:

$$E = \sum_{T} w_T \sum_{R} w_R D_{T,R} \text{ or } E = \sum_{T} w_T H_T$$

where H_T or w_R $D_{T,R}$ is the equivalent dose in a tissue or organ, T, and w_T is the tissue weighting factor. The unit for the effective dose is the same as for absorbed dose (J/kg), and its special name is sievert (Sv).

Endosteum (or endosteal tissue)

A 50-μm-thick layer covering the surfaces of the bone trabeculae in regions of trabecular spongiosa and the cortical surfaces of the medullary cavities of the shafts of all long bones. It serves as the target tissue for radiogenic bone cancer. In contrast to previous assumptions, recent studies have indicated that the cells at risk for bone cancer induction are localised out to 50 μm (previously assumed: 10 μm) from both the trabecular surfaces and interior cortical surfaces of the medullary cavities, but not within the Haversian canals of cortical bone.

Equivalent dose, H_T

The dose in a tissue or organ T given by:

$$H_T = \sum_{R} w_R D_{T,R}$$

where $D_{T,R}$ is the mean absorbed dose from radiation R in a tissue or organ T, and w_R is the radiation weighting factor. Since w_R is dimensionless, the unit for the equivalent dose is the same as for absorbed dose (J/kg), and its special name is sievert (Sv).

Fluence, Φ

The quotient of dN by da, where dN is the number of particles incident on a sphere of cross-sectional area da, thus:

$$\Phi = \frac{\mathrm{d}N}{\mathrm{d}a}$$

The use of a sphere of cross-sectional area da is to express the fact that the area da is considered to be perpendicular to the direction of each particle regardless of its spatial orientation.

Identification (ID) number
Number assigned unequivocally to each individually segmented organ/tissue.

Inactive (bone) marrow
In contrast to the active marrow, the inactive marrow is haematopoietically inactive, i.e. does not directly support haematopoiesis. It gets its yellow colour from fat cells, which occupy most of the space of the yellow bone marrow framework.

Marrow cellularity
The fraction of bone marrow volume in a given bone that is haematopoietically active. Age- and bone-site-dependent reference values for marrow cellularity are given in Table 41 of *Publication 70* (ICRP, 1995).

Red (bone) marrow
See 'Active (bone) marrow'.

Reference Male and Reference Female (Reference Individual)
An idealised male or female with characteristics defined by the Commission for the purpose of radiological protection, and with the anatomical and physiological characteristics defined in the report of the ICRP Task Group on Reference Man (ICRP, 2002).

Reference Person
An idealised person for whom the organ or tissue equivalent doses are calculated by averaging the corresponding doses of the Reference Male and Reference Female. The equivalent doses of the Reference Person are used for calculation of the effective dose by multiplying these doses by the corresponding tissue weighting factors.

Reference phantom
Computational phantoms for the human body (male and female voxel phantoms based on medical imaging data) with the anatomical and physiological characteristics defined in the report of the ICRP Task Group on Reference Man (ICRP, 2002).

Reference value
Standardised value of a parameter recommended by the Commission. Examples are the standardised set of anatomical and physiological parameters for radiation protection purposes summarised in *Publication 89* (ICRP, 2002).

Response function

Function representing the absorbed dose in a target region per unit particle fluence in the region, derived using models of the microscopic structure of the target region geometry, and the transport of the secondary ionising radiations in those regions.

Source region, S_i

An anatomical region within the reference phantom which contains the radionuclide following its intake. The region may be an organ, a tissue, the contents of the gastrointestinal tract or urinary bladder, or the surfaces of tissues in the skeleton, the alimentary tract, or the respiratory tract.

Specific absorbed fraction

The fraction of energy emitted as a specified radiation type in a source region, S, that is absorbed per unit mass of target tissue, T. The unit for the specific absorbed fraction is per kilogram (/ kg).

Target region, T_i

Anatomical region within the body (reference phantom) in which radiation is absorbed. The region may be an organ or a specified tissue in the gastrointestinal tract, urinary bladder, skeleton, or respiratory tract.

Tissue weighting factor, w_T

The factor by which the equivalent dose in a tissue or organ T is weighted to represent the relative contribution of that tissue or organ to the total health detriment resulting from uniform irradiation of the body (ICRP, 1991). It is weighted such that:

$$\sum_T w_T = 1$$

Trabecular (bone) marrow

The marrow contained in the spongiosa regions of all bones.

Voxel phantom

Computational anthropomorphic phantom based on medical tomographic images in which the anatomy is described by small three-dimensional volume elements (voxels) specifying the organ or tissue to which they belong.

Yellow (bone) marrow

See 'Inactive (bone) marrow'.

References

ICRP, 1991. 1990 Recommendations of the International Commission on Radiological Protection. ICRP Publication 60. Ann. ICRP 21(1–3).

ICRP, 1995. Basic anatomical and physiological data for use in radiological protection: the skeleton. ICRP Publication 70. Ann. ICRP 25(2).

ICRP, L., 2002. Basic anatomical and physiological data for use in radiological protection: reference values. ICRP Publication 89. Ann. ICRP 32(3–4).

1. INTRODUCTION

(1) Phantoms simulating the human body or parts thereof play a central role in radiation dosimetry, either as physical phantoms for practical measurements or as computational models (ICRU, 1992).

(2) Computational phantoms (or mathematical models) of the human body are used to evaluate the energy deposition in organs resulting from internal and external radiation exposures. Traditionally, these phantoms have been based upon mathematical expressions representing planes, and cylindrical, conical, elliptical, and spherical surfaces that describe the shape and position of idealised body organs. This type of phantom was developed at the Oak Ridge National Laboratory (Fisher and Snyder, 1967, 1968; Snyder et al., 1969, 1978; Cristy, 1980; Cristy and Eckerman, 1987) for the Medical Internal Radiation Dose (MIRD) Committee of the Society of Nuclear Medicine. From the original adult MIRD phantom, several paediatric phantoms were derived to represent infants and children of various ages (Cristy, 1980). For these models, the organ masses and volumes were in accordance with the ICRP data of former Reference Man (ICRP, 1975). As an improvement to these hermaphrodite models, separate male and female adult mathematical models called 'Adam' and 'Eva' were introduced by Kramer et al. (1982). Subsequently, four models representing the adult female, non-pregnant and at three stages of pregnancy, were developed by Stabin et al. (1995).

(3) As an extension and improvement to these earlier models, various groups have developed a new type of anatomical phantom during the last two decades, so-called 'tomographic' or 'voxel' models. Voxel phantoms are anatomical models based on computed tomography, magnetic resonance, or other images obtained from high-resolution scans of a single individual and, thus, offer a more realistic replication of human anatomy. They consist of a large number of volume elements (voxels) and are the most detailed representation of human anatomy at the present time (Zankl et al., 1988; Zubal et al., 1994, 1996; Dimbylow, 1996; Caon et al., 1999; Xu et al., 2000; Zankl and Wittmann, 2001; Petoussi-Henss et al., 2002; Zaidi and Xu, 2007). Voxel phantoms can be used for a wide spectrum of applications where the simulation of human anatomy is required. Until now, they have been used for the simulation of exposures due to ionising or electromagnetic radiation with the emphasis on radiation protection. However, being derived from a specific individual, these models do not represent the average Caucasian man or woman as defined by *Publication 23* (ICRP, 1975) and *Publication 89* (ICRP, 2002).

(4) Various authors have shown that the organ shapes of the MIRD-type phantoms present an over-simplification, having an influence on the energy distribution, which – for some cases – deviates systematically from that calculated for voxel models (Jones, 1996; Smith et al., 2000; Chao et al., 2001; Kinase et al., 2003; Zankl et al., 2003; Kramer et al., 2004). For external radiation, the parameters influencing the organ doses are mainly depth of the organ below the body surface, exterior shape of the trunk, and trunk diameter relative to the incoming radiation beam (Jones, 1997; Chao et al., 2001; Zankl et al., 2002; Kramer et al., 2004; Schlattl et al.,

2007). For internal dosimetry, the influencing parameters are the relative position of source and target organs (for penetrating radiations subject to so-called cross-fire), and organ mass (for non-penetrating radiations) (Jones, 1998; Smith et al., 2000; Chao and Xu, 2001; Zankl et al., 2003).

(5) Following the 2007 Recommendations (ICRP, 2007), the purpose of this document is to introduce the official computational models representing the adult Reference Male and Reference Female. These phantoms will be used by ICRP in establishing radiation protection guidance, e.g. effective dose coefficients (see Fig. 1.1) and other secondary dosimetric quantities.

(6) Similar activities in deriving standard phantoms were performed by Dimbylow (Dimbylow, 1996), who adjusted a segmented magnetic resonance imaging whole-body data set to yield a phantom (NORMAN) with body mass and height as well as organ masses in agreement with the reference values from *Publication 23* (ICRP, 1975). Recently, more efforts have been made to build standard human models (Zankl et al., 2005; Kramer et al., 2006), where the individual organ masses and densities also conform to the values of *Publication 70* (ICRP, 1995) and *Publication 89* (ICRP, 2002). The phantoms presented in this document have been developed by the Task Group on Dose Calculations (DOCAL) of ICRP Committee 2 in collaboration with the Helmholtz Zentrum München – German Research Centre for Environmental Health (formerly: GSF – National Research Centre for Environment and Health), and the International Commission on Radiation Units and Measurements (ICRU). The following chapters describe the specifications that these phantoms had to meet, their construction, their main characteristics, and their limitations. Finally, an overview of their potential applications and intended use is given.

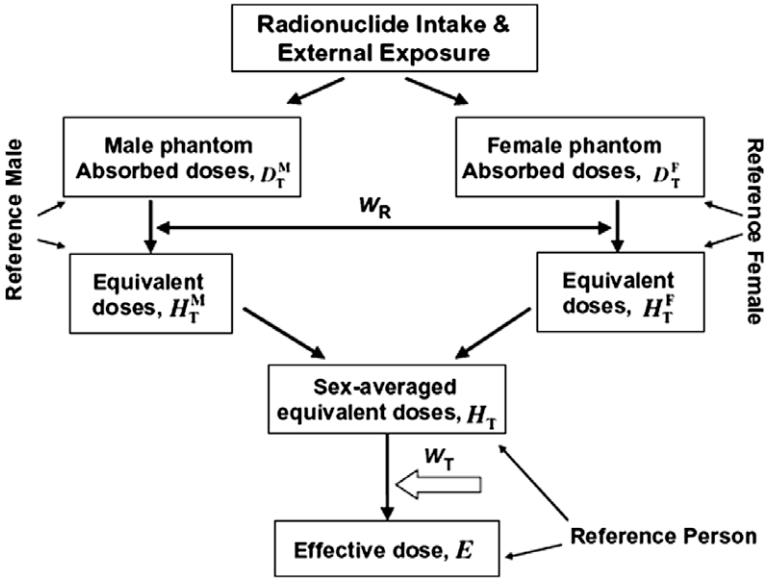

Fig. 1.1. Schematic for calculation of effective dose using sex-specific reference phantoms.

1.1. References

Caon, M., Bibbo, G., Pattison, J., 1999. An EGS4-ready tomographic computational model of a fourteen-year-old female torso for calculating organ doses from CT examinations. Phys. Med. Biol. 44, 2213–2225.

Chao, T.C., Xu, X.G., 2001. Specific absorbed fractions from the image-based VIP-Man body model and EGS4-VLSI Monte Carlo code: internal electron emitters. Phys. Med. Biol. 46, 901–927.

Chao, T.C., Bozkurt, A., Xu, X.G., 2001. Conversion coefficients based on the VIP-Man anatomical model and EGS4-VLSI code for external monoenergetic photons from 10 keV to 10 MeV. Health Phys. 81, 163–183.

Cristy, M., 1980. Mathematical Phantoms Representing Children of Various Ages for Use in Estimates of Internal Dose. ORNL Report TM-367. Oak Ridge National Laboratory, Oak Ridge, TN.

Cristy, M., Eckerman, K.F., 1987. Specific Absorbed Fractions of Energy at Various Ages from Internal Photon Sources. Part I: Methods. ORNL Report TM-8381/V1. Oak Ridge National Laboratory, Oak Ridge, TN.

Dimbylow, P.J., 1996. The development of realistic voxel phantoms for electromagnetic field dosimetry. In: Dimbylow, P.J. (Ed.), Workshop on Voxel Phantom Development. National Radiological Protection Board, Chilton, UK, pp. 1–7.

Fisher, H.L., Snyder, W.S., 1967. Distribution of Dose in the Body from a Source of Gamma Rays Distributed Uniformly in an Organ. ORNL-4168. Oak Ridge National Laboratory, Oak Ridge, TN.

Fisher, H.L., Snyder, W.S., 1968. Distribution of dose in the body from a source of gamma rays distributed uniformly in an organ. First International Congress on Radiation Protection, Oxford, pp. 1473–1486.

ICRP, 1975. Reference Man: Anatomical, Physiological and Metabolic Characteristics. ICRP Publication 23. Pergamon Press, Oxford.

ICRP, 1995. Basic anatomical and physiological data for use in radiological protection: the skeleton. ICRP Publication 70. Ann. ICRP 25(2).

ICRP, 2002. Basic anatomical and physiological data for use in radiological protection: reference values. ICRP Publication 89. Ann. ICRP 32(3–4).

ICRP, 2007. The 2007 Recommendations of the International Commission on Radiological Protection. ICRP Publication 103. Ann. ICRP 37(2–4).

ICRU, 1992. Phantoms and Computational Models in Therapy, Diagnosis and Protection. ICRU Report 48. International Commission on Radiation Units and Measurements, Bethesda, MD.

Jones, D.G., 1996. The use of a realistic voxel phantom in the calculation of organ doses due to external x or gamma rays. In: Dimbylow, P.J. (Ed.), Workshop on Voxel Phantom Development. National Radiological Protection Board, Chilton, UK, pp. 90–97.

Jones, D.G., 1997. A realistic anthropomorphic phantom for calculating organ doses arising from external photon irradiation. Radiat. Prot. Dosim. 72, 21–29.

Jones, D.G., 1998. A realistic anthropomorphic phantom for calculating specific absorbed fractions of energy deposited from internal gamma emitters. Radiat. Prot. Dosim. 79, 411–414.

Kinase, S., Zankl, M., Kuwabara, J., et al., 2003. Evaluation of specific absorbed fractions in voxel phantoms using Monte Carlo simulation. Radiat. Prot. Dosim. 105, 557–563.

Kramer, R., Zankl, M., Williams, G., et al., 1982. The Calculation of Dose from External Photon Exposures Using Reference Human Phantoms and Monte Carlo Methods. Part I: The Male (Adam) and Female (Eva) Adult Mathematical Phantoms. GSF-Report S-885. GSF – National Research Center for Environment and Health, Neuherberg.

Kramer, R., Vieira, J.W., Khoury, H.J., et al., 2004. MAX meets ADAM: a dosimetric comparison between a voxel-based and a mathematical model for external exposure to photons. Phys. Med. Biol. 49, 887–910.

Kramer, R., Khoury, H.J., Vieira, J.W., et al., 2006. MAX06 and FAX06: update of two adult human phantoms for radiation protection dosimetry. Phys. Med. Biol. 51, 3331–3346.

Petoussi-Henss, N., Zankl, M., Fill, U., et al., 2002. The GSF family of voxel phantoms. Phys. Med. Biol. 47, 89–106.

Schlattl, H., Zankl, M., Petoussi-Henss, N., 2007. Organ dose conversion coefficients for voxel models of the reference male and female from idealized photon exposures. Phys. Med. Biol. 52, 2123–2145.

Smith, T., Petoussi-Henss, N., Zankl, M., 2000. Comparison of internal radiation doses estimated by MIRD and voxel techniques for a 'family' of phantoms. Eur. J. Nucl. Med. 27, 1387–1398.

Snyder, W.S., Ford, M.R., Warner, G.G., et al., 1969. Estimates of absorbed fractions for monoenergetic photon sources uniformly distributed in various organs of a heterogeneous phantom. MIRD Pamphlet No. 5. J. Nucl. Med. 10(Suppl. 3) 46–51.

Snyder, W.S., Ford, M.R., Warner, G.G., 1978. Estimates of Specific Absorbed Fractions for Monoenergetic Photon Sources Uniformly Distributed in Various Organs of a Heterogeneous Phantom. MIRD Pamphlet No. 5, Revised. Society of Nuclear Medicine, New York.

Stabin, M.G., Watson, E., Cristy, M., et al., 1995. Mathematical Models and Specific Absorbed Fractions of Photon Energy in the Nonpregnant Adult Female and at the End of Each Trimester of Pregnancy. ORNL Report TM-12907. Oak Ridge National Laboratory, Oak Ridge, TN.

Xu, X.G., Chao, T.C., Bozkurt, A., 2000. VIP-MAN: an image-based whole-body adult male model constructed from color photographs of the Visible Human Project for multi-particle Monte Carlo calculations. Health Phys. 78, 476–486.

Zaidi, H., Xu, X.G., 2007. Computational anthropomorphic models of the human anatomy: the path to realistic Monte Carlo modeling in radiological sciences. Ann. Rev. Biomed. Eng. 9, 471–500.

Zankl, M., Veit, R., Williams, G., et al., 1988. The construction of computer tomographic phantoms and their application in radiology and radiation protection. Radiat. Environ. Biophys. 27, 153–164.

Zankl, M., Wittmann, A., 2001. The adult male voxel model 'Golem' segmented from whole body CT patient data. Radiat. Environ. Biophys. 40, 153–162.

Zankl, M., Fill, U., Petoussi-Henss, N., et al., 2002. Organ dose conversion coefficients for external photon irradiation of male and female voxel models. Phys. Med. Biol. 47, 2367–2385.

Zankl, M., Petoussi-Henss, N., Fill, U., et al., 2003. The application of voxel phantoms to the internal dosimetry of radionuclides. Radiat. Prot. Dosim. 105, 539–548.

Zankl, M., Becker, J., Fill, U., et al., 2005. GSF male and female adult voxel models representing ICRP Reference Man – the present status. In: The Monte Carlo Method: Versatility Unbounded in a Dynamic Computing World. American Nuclear Society, LaGrange Park, IL.

Zubal, I.G., Harrell, C.R., Smith, E.O., et al., 1994. Computerized three-dimensional segmented human anatomy. Med. Phys. 21, 299–302.

Zubal, I.G., Harrell, C.R., Smith, E.O., et al., 1996. Two dedicated software, voxel-based, anthropomorphic (torso and head) phantoms. In: Dimbylow, P.J. (Ed.), Workshop on Voxel Phantom Development. National Radiological Protection Board, Chilton, UK, pp. 105–111.

2. SPECIFICATIONS OF THE COMPUTATIONAL PHANTOMS

(7) The voxel phantoms for calculations of energy deposition in body organs and tissues (so-called 'target regions') following the 2007 Recommendations (ICRP, 2007) should accommodate all organs and tissues that are relevant to the assessment of human exposure to ionising radiation for radiation protection purposes. These target regions are: active ('red') bone marrow, adrenals, brain, breast, colon, endosteal tissue (formerly called 'bone surfaces'), extrathoracic (ET) airways, eye (lens), gall bladder, heart, kidneys, liver, lungs, lymphatic nodes, muscle, oesophagus, oral mucosa, ovaries, pancreas, prostate, salivary glands, skin, small intestine, spleen, stomach, testes, thymus, thyroid, urinary bladder, and uterus. Furthermore, additional target regions have been identified in the Human Respiratory Tract Model (ICRP, 1994) and Human Alimentary Tract Model (ICRP, 2006). These target regions include: alveolar-interstitium, basal cells of anterior and posterior nasal passages and pharynx, basal cells of bronchi, lymph nodes of ET and thoracic region, secretory cells of bronchi and bronchioles, and tongue and tonsils.[1]

(8) When radioactive material is incorporated into the body, those organs, tissues, and body regions where radionuclides reside or pass through become source regions that irradiate other (target) regions. Many regions are both source and target regions. Additional source regions are located in the alimentary and respiratory tracts, as well as in the skeleton. Certain individual anatomical regions have to be considered differently depending on the rate with which the material passes through or is cleared from them. These additional source regions include: oral cavity, teeth surfaces, teeth volumes, oesophagus (fast, slow), stomach content, small intestine content, right colon (content, wall), left colon (content, wall), rectosigmoid colon (content, wall), gall bladder content, urinary bladder content, nasal passages (anterior and posterior surfaces), pharynx, sequestered ET_2 region, bronchi (fast, slow, bound, sequestered), bronchi, bronchioles (fast, slow, bound, sequestered), blood vessels (head, trunk, legs, and arms), cortical bone (surface, volume), trabecular bone (surface, volume), and inactive ('yellow') bone marrow.

(9) Due to the limited resolution (in the range of millimetres) of the tomographic data used to construct the voxel phantoms, and the very small dimensions of some source and target tissues (tens of micrometres), not all tissues could be segmented directly. Therefore, for some source and target tissues, 'surrogate' regions had to be found or correction factors have to be applied to the calculated doses. These limitations of the phantoms are discussed in more detail in Section 5.4.

(10) To enable the application of the reference computational phantoms for dosimetry in nuclear medicine by ICRP Committee 3 and others, further features were introduced: (1) left and right components of organ pairs were identified

[1] Many of the regions from the ICRP Human Respiratory Tract Model and Human Alimentary Tract Model are included in the computational phantoms for the purpose of photon and neutron dosimetry alone. For irradiation by internalised beta-particle and alpha-particle emitters, more spatially refined and localised anatomical models are used to assess absorbed fractions for these radiation types.

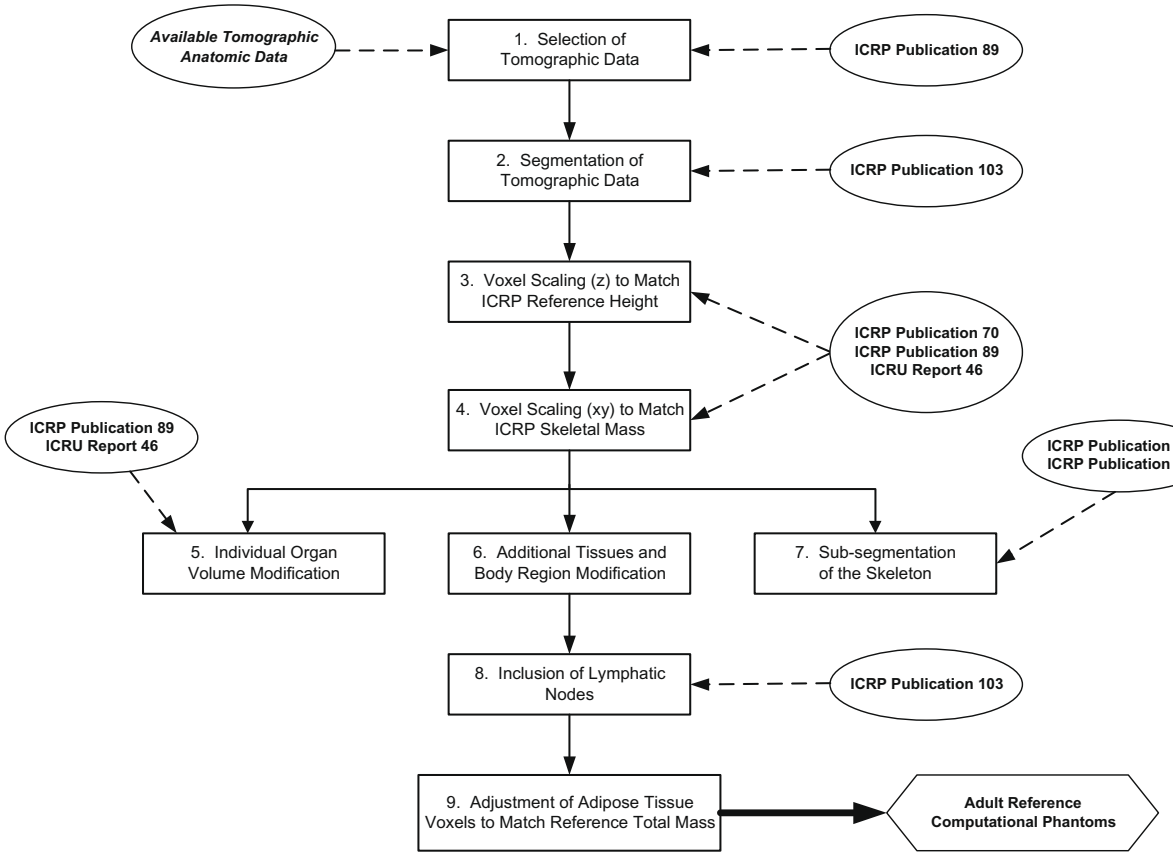

Fig. 2.1. Schematic for constructing computational phantoms representing the adult Reference Male and Reference Female.

separately; and (2) in the kidneys, the renal cortex, medulla, and pelvis were identified separately.

(11) A list of all organs, tissues, and regions that were defined and have been assigned an individual organ identification number is given in Annex A. Annex B is a list of different tissue types of which the organs and tissues consist, and their elemental compositions. Annex C presents a list of all source organs and regions, together with the organ identification numbers by which they are represented. Annex D gives this information for the target organs and tissues.

(12) Since the tomographic data used to create the phantoms were acquired while the individuals were in a supine posture, it is obvious that the anatomy of the resulting voxel models also corresponds to this posture. That means that – due to the fact that the forces of gravity act differently in standing and lying postures – the abdomen is flatter than in a standing person, the abdominal organs are shifted upwards towards the chest, and the lungs are compressed. Furthermore, the curvature of the spine is slightly different from that seen in a standing person. Correcting for these effects would mean the necessity for extensive modifications in organ positioning in the body. On the other hand, although this effect is qualitatively obvious, there is little quantitative information on the amount of positional changes of individual organs, since no comparable examinations of the same person in different positions are usually available. A study on the effects of posture on organ doses per unit activity intake for eight radionuclides with different biokinetic behaviour revealed only moderate dose differences for the main organs (i.e. those contributing to the effective dose with the highest tissue weighting factors) for a person in upright and supine postures (Sato et al., 2007; Sato and Endo, 2008). A similar study for external photon exposure showed agreement of the organ dose conversion coefficients for a supine person and an upright person within 2–20% for photon energies above 50 keV (Sato et al., 2008). Thus, it is concluded that the dosimetric impact of the person's position is limited, and the organ position of the voxel models in the supine position is acceptable for the applications intended.

(13) Being derived from specific individuals, most models to date do not represent the average Caucasian man or woman as defined by *Publication 23* (ICRP, 1975) and *Publication 89* (ICRP, 2002). The method and principles applied to construct computational phantoms representing the adult Reference Male and Reference Female (ICRP, 2002, 2007) and the data that were used during this process are outlined in Fig. 2.1 and will be described in the following chapters.

2.1. References

ICRP, 1975. Reference Man: Anatomical, Physiological and Metabolic Characteristics. ICRP Publication 23. Pergamon Press, Oxford.

ICRP, 1994. Human respiratory tract model for radiological protection. ICRP Publication 66. Ann. ICRP 24(1–3).

ICRP, 2002. Basic anatomical and physiological data for use in radiological protection: reference values. ICRP Publication 89. Ann. ICRP 32(3–4).

ICRP, 2006. Human alimentary tract model for radiological protection. ICRP Publication 100. Ann. ICRP 36(1–2).

ICRP, 2007. The 2007 Recommendations of the International Commission on Radiological Protection. ICRP Publication 103. Ann. ICRP 37(2–4).

Sato, K., Noguchi, H., Emoto, Y., et al., 2007. Japanese adult male voxel phantom constructed on the basis of CT images. Radiat. Prot. Dosim. 123, 337–344.

Sato, K., Endo, A., 2008. Analysis of effects of posture on organ doses by internal photon emitters using voxel phantoms. Phys. Med. Biol. 53, 4555–4572.

Sato, K., Endo, A., Saito, K., 2008. Dose Conversion Coefficients Calculated Using a Series of Adult Japanese Voxel Phantoms Against External Photon Exposures. JAEA-Data/Code 2008-016. Japan Atomic Energy Agency, Tokai-mura.

3. SELECTION AND SEGMENTATION OF TOMOGRAPHIC DATA

(14) In order to construct voxel models representing the adult Reference Male and Reference Female (ICRP, 2002, 2007), appropriate tomographic data sets were used as starting points, i.e. individuals with external dimensions close to the reference values, so that the required modifications remained moderate, and the problem of distorting the anatomical relations was minimal (Step 1 of Fig. 2.1).

3.1. Tomographic data for the male

(15) A whole-body clinical computed tomography image set of a 38-year-old individual with height 176 cm and mass slightly below 70 kg (Reference Male: 176 cm and 73 kg) was selected for construction of the male reference computational phantom. The individual, who suffered from leukaemia and had to undergo whole-body irradiation, did not have obvious signs of illness that would appear in the image data. The person was lying supine with the arms parallel alongside the body. The data set consisted of 220 slices of 256 x 256 pixels. The original voxel size was 8 mm in height with an in-plane resolution of 2.08 mm, resulting in a voxel volume of 34.6 mm^3.

(16) In total, 122 individual objects were segmented (67 of these being bones or bone groups), including many – but not all – of the organs and tissues later identified in the ICRP characterisation of the anatomical reference data (ICRP, 2002). Segmentation refers to the process by which individual pixels in an image slice are given organ identification numbers instead of their original Hounsfield numbers (image pixel intensity). As the image slice refers to a certain anatomical thickness, each pixel also defines a volume element or voxel. The collection of all voxels with the same identification number defines a certain organ or tissue. The whole body is, thus, represented by a three-dimensional array of voxels that is arranged in columns, rows, and slices. The identification number of the organ to which the voxel belongs is stored at each array position (Step 2 of Fig. 2.1).

(17) One of the tissues that could not be segmented from image data of the given resolution was the bone marrow, which is contained in small cavities in the trabecular bone that are much smaller than the voxel size (in the order of a few hundred micrometres) (ICRP, 1995). Therefore, no attempt has been made to identify substructures of each individually segmented bone or group of bones, with the exception of cortical bone and trabecular spongiosa.

(18) Due to the limited resolution of the image data (slice thickness 8 mm), it was difficult to identify small structures, such as blood vessels which are much smaller than the large main vessels in the trunk. Therefore, only a rather small proportion of the blood pool could be segmented. Furthermore, since no cartilage had been considered in the original segmented model, and due to the limited dosimetric importance of this tissue, only limited effort towards its supplementary segmentation was exerted.

(19) For the segmentation, commercial equipment dedicated to image processing purposes was used (Kontron Bildanalyse, MIPRON, Eching, Germany). The software tools used were grey value thresholding and morphological operations on binary images. The result of segmentation was the voxel phantom known as 'Golem' (Zankl and Wittmann, 2001).

3.2. Tomographic data for the female

(20) The female reference computational phantom was based on the computed tomography scan of a 43-year-old individual with height 167 cm and mass 59 kg (Reference Female: 163 cm and 60 kg), performed at a relatively high resolution preparatory to whole-body irradiation for the treatment of leukaemia. The data set consisted of 174 slices of 5-mm width (head and trunk) and 43 slices of 20-mm width (legs), each with 256 x 256 pixels. From the 20-mm-slice images, intermediate slices of 5-mm thickness were obtained by interpolation. The resulting data set consisted of 346 slices. The voxel size was then 5 mm in height with an in-plane resolution of 1.875 mm, resulting in a voxel volume of 17.6 mm^3. The patient was lying on her hands, and at the time of scanning, one shoulder was positioned higher than the other. In total, 88 objects were segmented, and the number of different bone sites was 19 (Step 2 of Fig. 2.1).

(21) The segmentation of this voxel phantom was performed with a commercial software package (Biomedical Image Resource, Analyze AVW, Rochester, MN, USA). The segmentation tools used were grey value thresholding, region growing, and manual segmentation involving Bezier spline functions that could be inherited from slice to slice, and adjusted to the actual organ outlines by moving their control points. The resulting voxel phantom was called 'Laura' (Zankl et al., 2005).

3.3. References

ICRP, 1995. Basic anatomical and physiological data for use in radiological protection: the skeleton. ICRP Publication 70. Ann. ICRP 25(2).

ICRP, 2002. Basic anatomical and physiological data for use in radiological protection: reference values. ICRP Publication 89. Ann. ICRP 32(3–4).

ICRP, 2007. The 2007 Recommendations of the International Commission on Radiological Protection. ICRP Publication 103. Ann. ICRP 37(2–4).

Zankl, M., Wittmann, A., 2001. The adult male voxel model 'Golem' segmented from whole body CT patient data. Radiat. Environ. Biophys. 40, 153–162.

Zankl, M., Becker, J., Fill, U., et al., 2005. GSF male and female adult voxel models representing ICRP Reference Man – the present status. In: The Monte Carlo Method: Versatility Unbounded in a Dynamic Computing World. American Nuclear Society, LaGrange Park, IL.

4. MODIFICATIONS OF SEGMENTED IMAGES TO CREATE REFERENCE COMPUTATIONAL PHANTOMS

(22) In order to create the reference computational phantoms from the two individual segmented data sets, the following steps were followed: (1) adjustment of the body height and the skeleton mass of the original model to the reference values by voxel scaling (Steps 3 and 4 of Fig. 2.1); (2) adjustment of the organ masses to the reference values by adding or subtracting the required number of organ voxels (Step 5 of Fig. 2.1); and (3) adjustment of the whole-body mass to the reference values by adding or subtracting an appropriate number of adipose tissue voxels (Step 9 of Fig. 2.1).

(23) It was the intention to keep the modifications to the skeleton shape to a minimum in order to preserve the 'frame' of the body. However, it was necessary to increase the size of the skull because otherwise it was not possible for both models to accommodate the entire reference brain mass within the skull. The segmented male had a noticeably narrow head, and other organs in the head were also small compared with the reference values. Therefore, it was decided to increase the size of all voxels of the entire head and then resample this volume with the smaller voxel size of the rest of the body. Thus, the male reference phantom has a greater number of head voxels than Golem. For the female reference phantom, only the skull size was increased; the interior surface voxels of the skull were replaced by brain, and an additional layer of skull voxels was added at the exterior surface. In order not to lose a layer of the surrounding tissues, this had to be preceded by an outward movement of the surrounding muscle, adipose tissue, and skin voxels. Furthermore, an outward movement of the ribs (as would occur during breathing) was necessary to accommodate the liver. This was done while the thicknesses of tissues covering the ribs – muscle, adipose tissue, and skin – remained the same.

4.1. Voxel scaling

(24) Apart from these unavoidable modifications of the shape of the skeleton, the volume of the skeleton was adjusted to the reference value by voxel scaling. Since Golem's body height corresponded to the reference value, the original voxel height was kept unmodified. Laura was taller than the Reference Female, so the voxel height for the female reference computational phantom was reduced from 5.0 to 4.84 mm (Step 2 of Fig. 2.1). After the mentioned moderate changes to the skulls of both phantoms, the numbers of segmented skeleton voxels were 211,427 and 378,204 for the male and female reference phantoms, respectively. Table 4.1 shows the volumes of the skeletons of Reference Male and Reference Female as derived from the reference mass data from *Publication 89* (ICRP, 2002) and mass density data of ICRU Report 46 (ICRU, 1992).

Table 4.1. Reference mass values (ICRP, 2002), mass density values (ICRU, 1992), and volumes derived for various constituents of the skeleton of the Reference Male and Reference Female.

	Mass (g)		Mass density (g/cm^3)	Volume (cm^3)	
	Male	Female		Male	Female
Mineral bone	5500	4000	1.92	2860	2080
Cortical bone	4400	3200		2290	1670
Trabecular bone	1100	800		570	420
Cartilage	1100	900	1.10	1000	820
Active bone marrow	1170	900	1.03	1140	870
Inactive bone marrow	2480	1800	0.98	2530	1840
Miscellaneous	200	160	1.03	190	160
Total	10,450	7760	1.35	7730	5770

(25) From these values and the segmented skeleton voxel numbers, voxel volumes of 36.54 and 15.25 mm^3 for the male and female reference computational phantoms, respectively, were evaluated, simply by dividing the volume values aimed at by the respective numbers of skeleton voxels for both phantoms. The in-plane voxel resolution for each phantom was then derived as the square root of the in-plane voxel area (derived by dividing the voxel volume by the voxel height). This resulted in voxel in-plane resolutions of 2.137 mm for the male and 1.775 mm for the female reference computational phantoms. Compared with the original voxel sizes of Golem and Laura, this corresponds to an increase of 5.6% in voxel volume for the male reference computational phantom and a decrease of 13.2% for the female reference computational phantom (Step 3 of Fig. 2.1).

4.2. Individual organ volume modifications

(26) A software package, 'VolumeChange', was developed to modify the organs of the original voxel models in volume, location, and shape (Becker et al., 2007). It uses the programming language IDL ('Interactive Data Language'), and identifies each organ by its surface voxels, i.e. all voxels having at least one neighbour that does not belong to the same organ. The volumes, and consequently masses, are then modified by shifting surface voxels – inward for decreasing and outward for increasing the respective volume.

(27) VolumeChange is not a segmentation tool and does not solve the problem of laborious and very time-consuming segmentation. Only existing voxel models (and organs) can be edited; however, this task can be completed in a couple of days. Furthermore, every organ modification can be easily visualised, together with its effect on the surrounding tissues, checked, or reversed; this supports the anatomical realism and reproducibility of the modified model.

(28) Having overcome the initial difficulties with skull sizes as described above, the individual organs were adjusted one-by-one to the respective reference values, beginning with those that were larger than reference size in order to make room for those that had to be enlarged. Some very fine structures could not be adjusted exactly to the reference values, due to limitations of voxel resolution and visibility. For most

organs, however, a very close approximation of the reference values could be achieved. The only limitation then was due to the fact that each organ has to consist of an integer number of voxels. That means that the resulting volumes may deviate from the desired value by, at most, half a voxel volume, i.e. approximately 18.3 mm^3 for the male reference computational phantom and 7.6 mm^3 for the female reference computational phantom (Step 5 of Fig. 2.1).

4.3. Additional organ and body region modifications

(29) In an additional attempt to improve the models, further anatomical details were segmented in the reference computational phantoms, going back to the original computed tomography images (Step 6 of Fig. 2.1). Some effort was made to identify additional blood vessels, which was especially demanding for the male phantom due to the relatively large slice thickness resulting in decreased recognition of very fine structures. Inside the lungs, larger blood vessels were also segmented, as well as an increased amount of bronchi; thus, the reference computational phantoms have inhomogeneous lungs in contrast to Golem and Laura. The rest of the lung volume was then assigned a homogeneous tissue, the density of which was selected such that the whole mass of the lungs, including the blood, corresponds to its reference value.

(30) The individual whose medical image data were used to construct the female reference computational phantom was lying on her hands during the computed tomography scan. In order to avoid shielding of the body by the arms for posterior irradiation, the arms had to be shifted to the sides. At the height of the fingertips, movement of the left hand by 71 pixels to the left and movement of the right hand by 68 pixels to the right was necessary to separate the hands from the trunk. To preserve the realistic geometry of the shoulders and create smooth transitions for the sideward movement, the upper two slices of the arms were moved by just one pixel, the next two slices by two pixels, and so on. Where the hands had been, the trunk shape showed indentations that had to be removed. Therefore, a smooth body contour was drawn manually instead of the indented one in these slices, and this was then filled by adipose tissue. Similarly, a small indentation at the bottom of the trunk of the male phantom, due to one of the arms, had to be removed.

(31) After adjusting the masses of the organs to their reference values, the internal anatomy was fixed. At this stage, lymphatic nodes were incorporated. Since these tissues could not be identified on the medical images, they were drawn manually at locations specified in anatomical textbooks (Brash and Jamieson, 1943; Möller and Reif, 1993, 1997; GEO kompakt, 2005). Although only part of the lymphatic tissue reference mass could thus be introduced, the distribution throughout the body and the higher concentration at specified locations, such as in the groins and axillae, and to some extent the hollows of the knees, crooks of the arms, etc., was correctly mirrored (Step 8 of Fig. 2.1).

(32) The final step was to adjust the whole-body masses to 73 and 60 kg for the male and female reference computational phantoms, respectively. In both cases, the whole-body masses were lower than the reference values, so the body had to

be 'wrapped' with additional layers of adipose tissue (Step 9 of Fig. 2.1). Towards the end of this procedure, small iterations had to be made, since each modification of the number of adipose tissue voxels resulted in small changes to the skin mass, because the number of body surface voxels was modified. Finally, the whole-body masses were adjusted to the reference values within 0.01 g.

(33) Due to representing a thickness of several millimetres, the top and bottom slices of the segmented phantoms contain not only skin, but also other structures of the head and the feet, such as adipose (residual) tissue, muscle, and bone. To make sure that all surface voxels are skin, additional slices were added at the top of the head and the bottom of the feet with voxels that cover the segmented structures of the neighbouring slices. These are additional voxels, not included in the reference height and mass, and were assigned a separate identification number (141, called 'skin at top and bottom' in Annex A). It is at the discretion of the user and will depend on the situation under consideration whether or not these additional slices are actually used in a dose calculation. A simple way to neglect them is to assign air instead of skin as the medium for this identification number. For these organ and body region modifications, two different software tools were used (Biomedical Image Resource, Analyze AVW, Rochester, MN, USA; Becker et al., 2007).

4.4. Sub-segmentation of the skeleton

(34) The skeleton is composed of cortical bone, trabecular bone, active (red) and inactive (yellow) bone marrow, cartilage, teeth, and miscellaneous skeletal tissues (periosteum and blood vessels). A sub-region of the bone marrow, 50 μm from the bone surfaces, is further defined as the endosteal tissues. The dimensions of internal structures of most of these tissues are in the order of micrometres and therefore smaller than the resolution of a normal computed tomography scan (order of millimetres); thus, these volumes could not be segmented. However, the gross spatial distributions of the source and target volumes were represented as realistically as possible for the given voxel resolution (Zankl et al., 2007). For this purpose, the skeleton was divided into the 19 bones and bone groups for which individual data on red bone marrow content and marrow cellularity are given in *Publication 70* (ICRP, 1995). These bones are: upper halves of humeri, lower halves of humeri, lower arm bones (ulnae and radii), wrists and hand bones, clavicles, cranium, upper halves of femora, lower halves of femora, lower leg bones (tibiae, fibulae, and patellae), ankles and foot bones, mandible, pelvis (os coxae), ribs, scapulae, cervical spine, thoracic spine, lumbar spine, sacrum, and sternum. These were then sub-segmented into an outer shell of cortical bone and the enclosed spongiosa part of the bone. The long bones contain a medullary cavity as a third component, which is enclosed by cortical bone. This sub-division resulted in 44 different identification numbers in the skeleton: two – cortical bone and spongiosa – for each of the 19 bones mentioned above, and a medullary cavity for each of the six long bones (upper and lower half of humeri, lower arm bones, upper and lower half of femora, and lower leg bones). Furthermore, the amount of cartilage that could be identified on the computed tomography images and could, thus, be segmented directly was attributed to four body parts – head,

trunk, arms, and legs. Hence, the skeleton covers a total of 48 individual identification numbers (Step 7 of Fig. 2.1).

(35) The total volume of each bone results directly from the number of segmented voxels and the voxel volume. The cortical shell around the spongiosa was chosen to be one voxel layer; the cortical bone at the long bones' shafts is thicker, and its thickness was adjusted such that the total cortical bone volume is in agreement with the reference value. For each of the 19 bones and bone groups, the spongiosa is composed of various proportions of trabecular bone, red marrow, and yellow marrow. Furthermore, the additional volumes of 'miscellaneous' tissues (ICRP, 2002) and the non-segmented cartilage had to be accommodated in the skeleton; for practicability, these were merged within the spongiosa volume of all skeletal sites.

(36) The volume of red marrow in each of the 19 bones and bone groups can be calculated from the reference values of the total amount of red marrow (ICRP, 1995, 2002) and its percentage distribution among individual bones as given in *Publication 70* (ICRP, 1995) and *Publication 89* (ICRP, 2002) based on earlier data of Cristy (Cristy, 1981). The bone marrow cellularity (Cristy, 1981; ICRP, 1995) in an individual bone gives the volume proportion of the entire marrow in this bone that is still haematopoietically active, i.e. the red bone marrow fraction. From this value, the total bone marrow volume in that bone can be calculated. This method permits evaluation of the volume of yellow marrow from the red bone marrow volume for all those bones with a cellularity that is non-zero. Of course, for those bones with zero cellularity, the yellow marrow content cannot be estimated by this method. Therefore, the difference remaining between the total inactive marrow volume (ICRP, 1995,2002) and that assigned to individual bones using the non-zero cellularity values was distributed among those bones that do not contain red bone marrow. These are the lower halves of humeri and femora, the lower arm and leg bones, and the hand and foot bones. A portion of the remaining yellow bone marrow is contained within the segmented medullary cavities of the lower halves of humeri and femora, and the lower arm and leg bones; the rest was attributed to the spongiosa regions of all zero-cellularity bones in relation to their respective volumes. Accordingly, each of the 19 bones or bone groups has its own unique bone-specific spongiosa composition. The masses of red and yellow bone marrow in each bone (group) are given in Table 4.2, together with the masses of the endosteal tissue.

(37) For some bones, e.g. the sternum of the male reference computational phantom, and the sacrum and sternum of the female reference computational phantom, the total bone marrow volume that is required to accommodate the reference volumes of red and yellow bone marrow (ICRP, 1995) is only marginally less than the segmented total volume of these bones. Consequently, there was not enough space left in these bones for an enclosing cortical shell. Cortical bone voxels around the sternum were, therefore, segmented in only a few slices of both models. Although it would have been possible to spare a few voxels to accommodate a small amount of cortical bone around the female phantom's sacrum, this option was abandoned in order not to exceed the reference value of 1666.7 cm^3 for the total cortical bone volume. Similarly, in the ribs of both models, the space for cortical bone was limited. Only the larger portions are enclosed in a cortical shell; smaller parts – especially

Table 4.2 Masses of red marrow, yellow marrow, and endosteum in the 19 bones and bone groups of the reference computational phantoms.

Bone	Mass (g)					
	Male			Female		
	RBM	YBM	Endosteum *	RBM	YBM	Endosteum *
Humeri, upper half	26.9	76.8	9.6	20.7	59.1	7.3
Humeri, lower half	0.0	73.0	11.5	0.0	55.0	8.5
Ulnae and radii	0.0	131.8	16.4	0.0	93.0	12.1
Wrists and hand bones	0.0	83.7	12.5	0.0	47.5	7.1
Clavicles	9.4	18.1	2.5	7.2	13.9	1.9
Cranium	88.9	138.0	83.4	68.4	106.2	64.2
Femora, upper half	78.4	223.8	44.2	60.3	172.1	34.2
Femora, lower half	0.0	344.0	48.5	0.0	169.3	24.0
Tibiae, fibulae and patellae	0.0	516.2	92.4	0.0	469.9	84.5
Ankles and foot bones	0.0	304.6	42.2	0.0	176.2	24.4
Mandible	9.4	14.5	2.0	7.2	11.2	1.6
Pelvis (os coxae)	205.2	211.5	51.7	157.5	162.3	39.7
Ribs	188.7	77.0	29.8	144.9	59.1	22.9
Scapulae	32.8	50.9	9.8	25.2	39.1	7.6
Cervical spine	45.6	18.6	11.5	35.1	14.3	8.8
Thoracic spine	188.7	77.0	26.9	144.9	59.1	20.6
Lumbar spine	143.9	58.7	23.4	110.7	45.1	18.0
Sacrum	115.8	47.2	20.6	89.1	36.3	15.8
Sternum	36.3	14.8	5.5	27.9	11.4	4.3
Total	1170	2480.2	544.4	899.1	1800.1	407.5

RBM, red bone marrow; YBM, yellow bone marrow.

* Bolch et al. (2007).

those with a large surface-to-volume ratio – are not given a cortical shell. This difficulty was encountered since reference masses and volumes had to be accommodated at the assigned voxel size.

(38) The segmented cortical bone has the reference mass of *Publication 89* (ICRP, 2002), and although no direct segmentation of the trabecular bone and active and inactive marrow in the spongiosa was possible at the given voxel resolution, the volume and composition of the spongiosa is such that all skeletal constituents (mineral bone, cartilage, active and inactive marrow, and miscellaneous tissues) are incorporated in the skeleton at their reference masses as given in Table 4.1.

4.5. References

Becker, J., Zankl, M., Petoussi, N., 2007. A software tool for modification of human voxel models used for application in radiation protection. Phys. Med. Biol. 52, N195–N205.

Bolch, W.E., Shah, A.P., Watchman, C.J., Jokisch, D.W., Patton, P.W., Rajon, D.A., Zankl, M., Petoussi-Henss, N., Eckerman, K.F., 2007. Skeletal absorbed fractions for electrons in the adult male: considerations of a revised 50-μm definition of the bone endosteum. Radiat. Prot. Dosim. 127, 169–173.

Brash, J.C., Jamieson, E.B., 1943. Cunningham's Text-book of Anatomy. Oxford University Press, New York.

Cristy, M., 1981. Active bone marrow distribution as a function of age in humans. Phys. Med. Biol. 26, 389–400.

GEO kompakt, 2005. Das Wunder Mensch. Gruner+Jahr, Hamburg.

ICRP, 1995. Basic anatomical and physiological data for use in radiological protection: the skeleton. ICRP Publication 70. Ann. ICRP 25(2).

ICRP, 2002. Basic anatomical and physiological data for use in radiological protection: reference values. ICRP Publication 89. Ann. ICRP 32(3–4).

ICRU, 1992. Photon, Electron, Proton and Neutron Interaction Data for Body Tissues. ICRU Report 46. International Commission on Radiation Units and Measurements, Bethesda, MD.

Möller, T.B., Reif, E., 1993. Taschenatlas der Schnittbildanatomie – Computertomographie und Kernspintomographie. Band II: Thorax, Abdomen, Becken. Georg Thieme Verlag, Stuttgart.

Möller, T.B., Reif, E., 1997. Taschenatlas der Schnittbildanatomie – Computertomographie und Kernspintomographie. Band I: Kopf, Hals, Wirbelsäule, Gelenke. Georg Thieme Verlag, Stuttgart.

Zankl, M., Eckerman, K.F., Bolch, W.E., 2007. Voxel-based models representing the male and female ICRP reference adult – the skeleton. Radiat. Prot. Dosim. 127, 174–186.

5. DESCRIPTION OF THE ADULT REFERENCE COMPUTATIONAL PHANTOMS

5.1. Main characteristics of the phantoms

(39) The orientation of the three-dimensional voxel array (arranged in columns, rows, and slices) describing the computational phantom is as follows. The columns correspond to the x co-ordinates, the rows correspond to the y co-ordinates, and the slices correspond to the z co-ordinates. Column numbers increase from right to left, row numbers increase from front to back, and slice numbers increase from the toes up to the vertex of the body.

(40) The main characteristics of the adult male and female reference computational phantoms are summarised in Table 5.1.

(41) Table 5.2 shows a list of source and target regions of the two phantoms, their segmented volumes, and resulting masses. For comparison, the reference masses (ICRP, 2002) are also shown.

5.2. The skeleton

5.2.1. Source regions

(42) For internal sources in the skeleton, the following source regions have to be considered: cortical bone (surface or volume), trabecular bone (surface or volume), and cortical and trabecular bone marrow. As in previous calculations for internal photon and neutron sources (Cristy and Eckerman, 1987a), no distinction is made between surface and volume sources in cortical and trabecular bone. The results from the respective volume sources will be applied to estimate values for the surface sources.

(43) A cortical bone volume has been segmented separately in most of the 19 bones and bone groups of the skeleton (for exceptions, see Para. 37), so the entirety of these segmented voxels can be directly used to sample a uniform source distribution.

Table 5.1 Main characteristics of the adult male and female reference computational phantoms.

Property	Male	Female
Height (m)	1.76	1.63
Mass (kg)	73.0	60.0
Number of tissue voxels	1,946,375	3,886,020
Slice thickness (voxel height, mm)	8.0	4.84
Voxel in-plane resolution (mm)	2.137	1.775
Voxel volume (mm^3)	36.54	15.25
Number of columns	254	299
Number of rows	127	137
Number of slices	220 (+2)*	346 (+2)*

* Additional slices of skin at the top and bottom as discussed in the text (Para. 33).

Table 5.2 List of source and target regions, their segmented volumes, and resulting masses compared with the reference masses (ICRP, 2002).

Organ	Male			Female		
	Volume (cm^3)	Mass (g)	Reference mass (g)	Volume (cm^3)	Mass (g)	Reference mass (g)
Adrenals	13.6	14.0	14	12.6	13.0	13
Blood (segmented vessels)*	973.7	1032.1	5600	807.4	855.8	4100
Brain	1381.0	1450.0	1450	1238.1	1300.0	1300
Breast	25.6	25.0	25	511.9	500.0	500
Eyes	14.3	15.0	15	14.3	15.0	15
Eye lenses	0.4	0.4	0.4	0.4	0.4	0.4
Gall bladder	66.0	68.0	68	54.3	56.0	56
Gall bladder wall	13.5	13.9	10	9.9	10.2	8
Gall bladder contents	52.5	54.1	58	44.4	45.8	48
Gastro-intestinal tract						
Stomach wall	144.2	150.0	150	134.6	140.0	140
Stomach contents	240.4	250.0	250	221.2	230.0	230
Small intestine wall	625.0	650.0	650	576.9	600.0	600
Small intestine contents	336.6	350.0	350	269.2	280.0	280
Right colon wall	144.2	150.0	150	139.4	145.0	145
Right colon contents	144.3	150.0	150	153.8	160.0	160
Left colon wall	144.2	150.0	150	139.4	145.0	145
Left colon contents	72.1	75.0	75	76.9	80.0	80
Recto-sigmoid colon wall	67.3	70.0	70	67.3	70.0	70
Sigmoid colon contents	72.1	75.0	75	76.9	80.0	80
Heart	795.4	840.0	840	587.2	620.0	620
Heart wall	314.3	330.0	330	238.1	250.0	250
Heart contents (blood)	481.1	510.0	510	349.1	370.0	370
Kidneys	295.3	310.0	310	261.9	275.0	275
Liver	1714.3	1800.0	1800	1333.3	1400.0	1400
Lungs	2891.3	1200.0	1200	2300.8	950.0	950
Lymphatic tissue†	134.0	138.0	730	76.8	79.1	600
Muscle tissue	27,619.0	29,000.0	29,000	16,666.7	17,500.0	17,500
Oesophagus	38.8	40.0	40	34.0	35.0	35
Ovaries				10.6	11.0	11
Pancreas	133.3	140.0	140	114.3	120.0	120
Pituitary gland	0.6	0.6	0.6	0.6	0.6	0.6
Prostate	16.5	17.0	17			
Residual (adipose) tissue	21,535.2	20,458.4	18,200	24,838.3	23,596.4	22,500
Salivary glands	82.5	85.0	85	68.0	70.0	70
Skin	3420.2	3728.0	3300	2496.8	2721.5	2300
Skeleton	7725.3	10,450.0	10,450	5767.4	7760.1	7760
Cortical bone‡	2291.7	4400.0	4400	1666.7	3200.0	3200
Trabecular bone§	572.9	1100.0	1100	416.7	800.0	800
Cartilage¶	1000.0	1100.0	1100	818.2	900.0	900
Active marrow§	1135.9	1170.0	1170	872.9	899.1	900
Inactive marrow¶	2530.6	2480.0	2480	1836.8	1800.1	1800
Miscellaneous§	194.2	200.0	200	155.3	160.0	160
Spleen	144.2	150.0	150	125.0	130.0	130
Teeth	18.2	50.0	50	14.6	40.0	40

Table 5.2 (*continued*)

Organ	Male			Female		
	Volume (cm^3)	Mass (g)	Reference mass (g)	Volume (cm^3)	Mass (g)	Reference mass (g)
Testes	33.7	35.0	35			
Thymus	24.3	25.0	25	19.4	20.0	20
Thyroid	19.2	20.0	20	16.4	17.0	17
Tongue	69.5	73.0	73	57.1	60.0	60
Tonsils	2.9	3.0	3	2.9	3.0	3
Ureters	15.5	16.0	16	14.6	15.0	15
Urinary bladder wall	48.1	50.0	50	38.5	40.0	40
Urinary bladder contents	192.3	200.0		192.3	200.0	
Uterus				77.7	80.0	80
Total body	71,109.9	73,000.0	73,000	59,258.0	60,000.0	60,000

Some of the reference values (e.g. blood and lymphatic tissue) duplicate other mass information and are, thus, not additive.

[*] Segmented blood vessels vs total blood (partly included in the organs).

[†] Segmented lymph nodes vs 'fixed' lymphatic tissue including lymphatic ducts and lymph.

[‡] Segmented directly.

[§] Incorporated in spongiosa regions.

[¶] Partly segmented directly and partly incorporated in spongiosa regions.

(44) As described above, trabecular bone is one of the constituents that make up the spongiosa. Therefore, the entirety of the segmented spongiosa voxels of all bones serves as the volume which can be sampled for particle emissions. However, since the relative amount of trabecular bone in the spongiosa varies between individual bones and bone groups, the source should not simply be assumed to be homogeneously distributed; for Monte Carlo radiation transport calculations, the variation of trabecular bone concentration should be used, e.g. either to determine the probability of a starting point being selected, or to assign bone-specific initial 'statistical weights' to the particles starting in the spongiosa volumes of various regions of the skeleton.

(45) For cortical marrow, medullary cavities have been segmented in the shafts of the long bones, so the entirety of these segmented voxels can be directly used to sample a uniform source distribution. In the adult models considered here, the medullary cavities only contain yellow marrow.

(46) The trabecular marrow is the marrow situated in the spongiosa. Consequently, the same particle source sampling principle as for the trabecular bone should be applied for the trabecular marrow, now considering the bone-specific relative bone marrow content (red and yellow marrow).

5.2.2. Target regions

(47) The skeletal target tissues of interest are the red bone marrow and the endosteal tissues (formerly called 'bone surfaces'). Since the dimensions of the marrow cavities and the endosteal layer lining these cavities (assumed thickness: 50 μm) are clearly finer than the resolution of a normal computed tomography scan, they

could not be directly segmented and had to be incorporated in the spongiosa volumes, as discussed. However, in contrast to the source volumes described above, it is not sufficient to consider the bone-specific relative amounts of these tissues in the spongiosa. The reason is that secondary equilibrium between the mineral bone and soft tissue components of the spongiosa does not exist; secondary particles are primarily released from mineral bone into the soft tissues during photon interactions, and these cause a dose enhancement in red bone marrow and endosteum compared with the mean dose in the spongiosa volume (Spiers, 1969; King and Spiers, 1985). Therefore, in skeletal dosimetry, specific techniques have to be applied, such as the use of correction factors (e.g. Zankl et al., 2002; Schlattl et al., 2007) or fluence-to-dose response functions that are multiplied with the particle fluence inside specific bone regions to give the dose quantities of interest to the target tissues (Cristy and Eckerman, 1987b).

5.3. Blood

(48) It was not possible to segment the entire blood pool of the body; only the larger vessels could be identified on the computed tomography images, especially for the male where the slice thickness was greater and therefore partial volume effects blurred the boundaries. The larger part of the blood volume is situated in the small vessels and capillaries inside most of the organs, and it was not possible to segment models of the intra-organ vasculature (aside from some major vessels within the lungs). On the other hand, the elemental compositions listed in *Publication 89* (ICRP, 2002) and ICRU Report 46 (ICRU, 1992) are exclusive of blood and thus are only relevant to the organ parenchyma. The blood content in each organ was, therefore, considered by including a blood portion in the elemental tissue composition of each organ. This distribution of the blood among the individual organs was again taken from *Publication 89* (ICRP, 2002) for the male and female phantom separately.

(49) The following expression was used to assign blood-inclusive elemental compositions to all phantom tissues. For example, the percentage by mass of hydrogen in the liver of the reference phantom would be calculated as:

$$(\%H)_{liver}^{phantom} = \frac{(\%H)_{liver}^{ICRU46}\left(m_{liver}^{ICRP89} - m_{blood-in-liver}\right) + (\%H)_{blood}^{ICRU46}\left(m_{blood-in-liver}\right)}{m_{liver}^{ICRP89}} \quad (1)$$

$$\text{with} \quad m_{blood-in-liver} = \left(m_{total-blood}^{ICRP89}\right)\left(f_{liver}^{total-blood}\right)_{Section\ 7.7.2\ of\ ICRP89} \quad (2)$$

where $(\%H)_{liver}^{phantom}$ is the percentage by mass of hydrogen in the liver of the phantom, $(\%H)_{liver}^{ICRU46}$ is the percentage by mass of hydrogen in the liver parenchyma as given in ICRU Report 46 (ICRU, 1992), m_{liver}^{ICRP89} is the reference mass of the liver (ICRP, 2002), $m_{blood\text{-}in\text{-}liver}$ is the mass of blood in the liver of the phantom, $(\%H)_{blood}^{ICRU46}$ is the percentage by mass of hydrogen in blood, $m_{total-blood}^{ICRP89}$ is the reference mass of the total blood pool, and $f_{liver}^{total-blood}$ is the fraction of the total blood volume that is contained in the liver.

(50) A table of the percentage distribution of the entire blood volume in individual organs is given in Section 7.7.2 of *Publication 89* (ICRP, 2002). The amount of blood can, thus, be evaluated for the large majority of organs. The liver, as an example, contains 10% of the blood volume; i.e. 0.53 l (or 560 g) for the male reference computational phantom and 0.39 l (or 410 g) for the female reference computational phantom. Expressions similar to Eq. (1) are applied in the data given in Annex B for the tissue compositions of the reference computational phantoms inclusive of organ blood content.

5.4. Limitations due to image resolution

(51) In addition to the skeletal source and target tissues, other regions could not be fully segmented in the reference computational phantoms, or could not be adjusted to their reference masses at the given voxel resolution due to their small size or complex structure.

(52) The ET airways are represented by an entire voxel layer lining the airways of nose, larynx, and pharynx. This does not mirror their small dimension of only a few micrometres thickness, but locates them at their correct anatomical position. The same holds for the trachea.

(53) The bronchi were not followed down more than the very first generations of branching. Small volumes of bronchial tissues were segmented to greater depths in the lungs, although not connected by a tree-like structure.

(54) The bronchioles are too small to be segmented in a voxel phantom. These form the rest of the lungs as homogeneous tissue with a density that is the average of the higher density bronchiolar tissue and included air.

(55) The skin is represented by a voxel layer, wrapping the phantoms' exterior. This renders it a thickness of 2.137 mm for the male reference computational phantom and 1.775 mm for the female reference computational phantom. The total skin masses of 3728.0 g for the male phantom and 2721.5 g for the female phantom thus derived are 13% and 18% higher than the reference values of 3300 g and 2300 g, respectively. Using the skin density of approximately 1.1 g/cm^3 and the reference body surface area of 1.90 m^2 for the male and 1.66 m^2 for the female, the reference skin thickness (epidermis and dermis) can be assumed to be approximately 1.6 mm and 1.3 mm for the adult male and female, respectively.

(56) The cartilage was only partly segmented due to its distributed nature and low contrast in the original images.

(57) In both reference computational phantoms, the gall bladder wall mass is higher than its reference value. The gall bladder is a small organ and, at the given voxel resolution, the number of wall voxels was not sufficient to encompass the volume of its contents. The entire mass of both the wall and contents was assigned the reference value, and the enclosing voxel layer represents the gall bladder wall.

(58) The residual tissue voxels of the reference computational phantoms were assigned as adipose tissue with the number of residual tissue voxels adjusted to permit matching of the reference total body mass for each phantom. Through this method, matching of reference adipose tissue masses was approximately achieved.

(59) The finite voxel resolution of the two reference computational phantoms limits their application to short-ranged radiations such as beta and alpha particles. For example, for assessing depth doses in the tissues of the respiratory airways of the Human Respiratory Tract Model (ICRP, 1994) or the walls of the stomach, small intestine, or colon of the Human Alimentary Tract Model (ICRP, 2006), the corresponding organs presented in these phantoms make these calculations impossible. Supplemental stylised or fine-resolution voxel tissue models must thus be used to compile absorbed fraction data relevant to particulate radiations in the body. However, in most cases, photon and neutron absorbed doses to these same tissues may be taken from radiation transport simulations in the reference computational phantoms directly or through surrogate tissue assignment.

5.5. References

Cristy, M., Eckerman, K.F., 1987a. Specific Absorbed Fractions of Energy at Various Ages from Internal Photon Sources. Part VII: Adult Male. ORNL Report TM-8381/V7. Oak Ridge National Laboratory, Oak Ridge, TN.

Cristy, M., Eckerman, K.F., 1987b. Specific Absorbed Fractions of Energy at Various Ages from Internal Photon Sources. Part I: Methods. ORNL Report TM-8381/V1. Oak Ridge National Laboratory, Oak Ridge, TN.

ICRP, 1994. Human respiratory tract model for radiological protection. ICRP Publication 66. Ann. ICRP 24(1–3).

ICRP, 2002. Basic anatomical and physiological data for use in radiological protection: reference values. ICRP Publication 89. Ann. ICRP 32(3–4).

ICRP, 2006. Human alimentary tract model for radiological protection. ICRP Publication 100. Ann. ICRP 36(1–2).

ICRU, 1992. Photon, Electron, Proton and Neutron Interaction Data for Body Tissues. ICRU Report 46. International Commission on Radiation Units and Measurements, Bethesda, MD.

King, S.D., Spiers, F.W., 1985. Photoelectron enhancement of the absorbed dose from X rays to human bone marrow: experimental and theoretical studies. Br. J. Radiol. 58, 345–356.

Schlattl, H., Zankl, M., Petoussi-Henss, N., 2007. Organ dose conversion coefficients for voxel models of the reference male and female from idealized photon exposures. Phys. Med. Biol. 52, 2123–2145.

Spiers, F.W., 1969. Beta Particle Dosimetry in Trabecular Bone. University of Utah Press, Salt Lake City, UT.

Zankl, M., Fill, U., Petoussi-Henss, N., et al., 2002. Organ dose conversion coefficients for external photon irradiation of male and female voxel models. Phys. Med. Biol. 47, 2367–2385.

6. APPLICATIONS AND LIMITATIONS OF THE REFERENCE COMPUTATIONAL PHANTOMS

(60) The phantoms presented in this document are the official computational models representing the adult Reference Male and Reference Female. These reference computational models are based on computed tomographic data of real people and, hence, represent digital three-dimensional representations of human anatomy. They are defined to enable calculations of the protection quantities – organ and tissue equivalent dose and effective dose – from exposure to ionising radiation. ICRP will publish recommended values for dose coefficients for both internal and external exposures using the male and female adult reference computational phantoms. These documents will include specific absorbed fractions for particles relevant to internal exposures, and dose conversion coefficients for external radiation fields.

(61) It should be clear that although these phantoms have organ masses of reference values, they still have individual organ topology reflecting the tomographic data used in their construction. Obviously, both models cannot represent real individuals, and thus they should not be used to assess doses for specific individuals. While the reference computational phantoms were created for the purpose of deriving radiological protection quantities, it is acknowledged that the phantoms may have broader applications. However, the specific limitations related to their intended application have to be kept in mind.

SUPPLEMENTARY DATA

Supplementary data associated with this article can be found, in the online version, at doi:10.1016/j.icrp.2009.07.004.

ANNEX A. ID LISTINGS, MEDIUM, DENSITY, MASS, MINIMUM/ MAXIMUM COLUMNS, ROWS AND SLICES OCCUPIED BY EACH ORGAN/TISSUE (CONTAINING RECTANGULAR PRISM), AND ORGAN CENTRES OF MASS

(A 1) Table A.1 lists the organ identification (ID) number, medium, density, and mass of each organ/tissue. The organ ID is the number stored in the voxel array at the positions of those voxels belonging to the respective organ/tissue. For the purpose of radiation transport calculations, a material composition has to be assigned to the organs/tissues. The 'medium' numbers given here refer to the elemental compositions of Annex B.

(A 2) Furthermore, for each organ, a rectangular prism (box) containing the organ (minimum/maximum columns, rows, and slices occupied by the organ/tissue) is given to facilitate the sampling of internal sources; finally, the organ's centre of mass (in terms of voxels as well as co-ordinates) is also given (Tables A.2 and A.3).

(A 3) The orientation of the three-dimensional voxel array describing the computational phantom is as follows. The columns correspond to the x co-ordinates, the rows correspond to the y co-ordinates, and the slices correspond to the z co-ordinates.

(A 4) Column numbers increase from right to left, row numbers increase from front to back, and slice numbers increase from the toes up to the vertex of the body.

Table A.1 ID listings, medium, density, and mass of each organ/tissue.

Organ ID	Organ/tissue	Medium	Density* (g/cm^3)	Mass (g)	
				Male	Female
	Adrenals:				
1	Adrenal, left	43	1.030	7.00	5.73
2	Adrenal, right	43	1.030	7.00	7.27
	Airways (and mouth):				
3	Anterior nasal passage (ET_1)	45	1.030†	11.03	4.32
4	Posterior nasal passage down to larynx (ET_2)	45	1.030†	28.41	14.29
5	Oral mucosa, tongue	29	1.050	30.73	18.45
6	Oral mucosa, lips and cheeks	29	1.050	5.10	4.00
7	Trachea	45	1.030	10.01	7.99
8	Bronchi	45	1.030†	66.31	8.69
	Blood vessels:				
9	Blood vessels, head	28	1.060	0.85	6.06
10	Blood vessels, trunk	28	1.060	271.93	242.38
11	Blood vessels, arms	28	1.060	15.72	43.24
12	Blood vessels, legs	28	1.060	83.04	92.64
	Bones:				
	Arm bones:				
	Humeri, upper half:				
13	Humeri, proximal end, cortical bone	2	1.920	135.26	112.60
14	Humeri, upper half, spongiosa	3	‡	184.86	111.90
15	Humeri, upper half, medullary cavity	22	0.980	33.48	19.89
	Humeri, lower half:				
16	Humeri, lower half, cortical	2	1.920	128.03	102.21
17	Humeri, lower half, spongiosa	4	‡	59.73	52.78
18	Humeri, lower half, medullary cavity	23	0.980	37.13	20.55
	Ulnae and radii:				
19	Ulnae and radii, cortical	2	1.920	270.80	155.14
20	Ulnae and radii, spongiosa	5	‡	181.91	91.24
21	Ulnae and radii, medullary cavity	24	0.980	22.67	33.59
	Wrists and hand bones:				
22	Wrists and hand bones, cortical	2	1.920	179.74	104.08
23	Wrists and hand bones, spongiosa	6	‡	139.59	72.84
	Clavicles:				
24	Clavicles, cortical	2	1.920	47.78	32.50
25	Clavicles, spongiosa	7	‡	53.06	40.45
	Cranium:				
26	Cranium, cortical	2	1.920	562.85	403.60
27	Cranium, spongiosa	8	‡	451.06	417.09
	Leg bones:				
	Femora, upper half:				
28	Femora, upper half, cortical	2	1.920	261.68	247.75
29	Femora, upper half, spongiosa	9	‡	472.05	225.05
30	Femora, upper half, medullary cavity	22	0.980	25.78	39.51
	Femora, lower half:				
31	Femora, lower half, cortical	2	1.920	294.09	232.47
32	Femora, lower half, spongiosa	10	‡	438.57	174.67
33	Femora, lower half, medullary cavity	23	0.980	80.89	55.43
	Tibiae, fibulae, and patellae:				
34	Tibiae, fibulae, and patellae, cortical	2	1.920	531.35	618.85

Table A.1 (*continued*)

Organ ID	Organ/tissue	Medium	Density* (g/cm^3)	Mass (g)	
				Male	Female
35	Tibiae, fibulae, and patellae, spongiosa	11	‡	729.38	586.52
36	Tibiae, fibulae, and patellae, medullary cavity	25	0.980	78.67	87.65
	Ankles and foot bones:				
37	Ankles and foot bones, cortical	2	1.920	232.56	171.75
38	Ankles and foot bones, spongiosa	12	‡	507.78	270.35
	Mandible:				
39	Mandible, cortical	2	1.920	76.12	44.94
40	Mandible, spongiosa	13	‡	73.90	34.67
	Pelvis:				
41	Pelvis, cortical	2	1.920	398.62	259.84
42	Pelvis, spongiosa	14	‡	681.18	445.07
	Ribs:				
43	Ribs, cortical	2	1.920	365.16	162.87
44	Ribs, spongiosa	15	‡	520.06	258.96
	Scapulae:				
45	Scapulae, cortical	2	1.920	221.13	120.45
46	Scapulae, spongiosa	16	‡	192.21	96.87
	Spine:				
	Cervical spine:				
47	Cervical spine, cortical	2	1.920	102.92	70.88
48	Cervical spine, spongiosa	17	‡	73.55	72.81
	Thoracic spine:				
49	Thoracic spine, cortical	2	1.920	286.58	203.78
50	Thoracic spine, spongiosa	18	‡	335.34	252.56
	Lumbar spine:				
51	Lumbar spine, cortical	2	1.920	186.19	154.62
52	Lumbar spine, spongiosa	19	‡	302.07	261.28
	Sacrum:				
53	Sacrum, cortical	2	1.920	109.23	0.00
54	Sacrum, spongiosa	20	‡	173.51	140.44
	Sternum:				
55	Sternum, cortical	2	1.920	9.89	1.67
56	Sternum, spongiosa	21	‡	56.31	47.41
	Cartilage:				
57	Cartilage, head	26	1.100	15.96	15.78
58	Cartilage, trunk	26	1.100	88.67	313.61
59	Cartilage, arms	26	1.100	5.91	98.51
60	Cartilage, legs	26	1.100	34.73	222.61
61	Brain	32	1.050§	1450.00	1300.00
	Breast:				
62	Breast, left, adipose tissue	49	0.950	7.50	150.01
63	Breast, left, glandular tissue	48	1.020	4.99	100.00
64	Breast, right, adipose tissue	49	0.950	7.50	150.01
65	Breast, right, glandular tissue	48	1.020	4.99	100.00
	Eyes:				
66	Eye lens, left	34	1.050¶	0.19	0.21
67	Eye bulb, left	34	1.050¶	7.29	7.30
68	Eye lens, right	34	1.050¶	0.19	0.19

(*continued on next page*)

Table A.1 (*continued*)

Organ ID	Organ/tissue	Medium	Density* (g/cm^3)	Mass (g)	
				Male	Female
69	Eye bulb, right	34	1.050¶	7.33	7.30
	Gall bladder:				
70	Gall bladder wall	45	1.030	13.92	10.24
71	Gall bladder contents	45	1.030	54.08	45.75
	Gastrointestinal tract:				
72	Stomach wall	36	1.040**	149.99	140.00
73	Stomach contents	51	1.040**	250.01	230.00
74	Small intestine wall	37	1.040**	650.00	599.99
75	Small intestine contents	51	1.040**	350.02	280.01
76	Ascending colon wall	38	1.040**	89.99	90.00
77	Ascending colon contents	51	1.040**	55.02	100.01
78	Transverse colon wall, right	38	1.040**	60.00	55.00
79	Transverse colon contents, right	51	1.040**	95.00	59.99
80	Transverse colon wall, left	38	1.040**	60.00	55.00
81	Transverse colon contents, left	51	1.040**	40.01	30.01
82	Descending colon wall	38	1.040**	89.99	90.00
83	Descending colon contents	51	1.040**	35.00	50.00
84	Sigmoid colon wall	38	1.040**	40.01	45.01
85	Sigmoid colon contents	51	1.040**	74.97	79.99
86	Rectum wall	38	1.040**	29.98	24.99
	Heart:				
87	Heart wall	33	1.050§	329.98	250.00
88	Heart contents (blood)	28	1.060	510.01	370.01
	Kidneys:				
	Kidney, left:				
89	Kidney, left, cortex	35	1.050§	107.12	104.63
90	Kidney, left, medulla	35	1.050§	38.25	37.37
91	Kidney, left, pelvis	35	1.050§	7.63	7.48
	Kidney, right:				
92	Kidney, right, cortex	35	1.050§	109.92	87.87
93	Kidney, right, medulla	35	1.050§	39.25	31.38
94	Kidney, right, pelvis	35	1.050§	7.87	6.28
95	Liver	30	1.050¶	1800.01	1400.00
	Lungs:				
	Lung, left				
96	Lung, left, blood	28	1.060	79.01	59.22
97	Lung, left, tissue	50	‡	477.74	376.78
	Lung, right				
98	Lung, right, blood	28	1.060	71.54	42.27
99	Lung, right, tissue	50	‡	580.08	471.74
	Lymphatic nodes:				
100	Lymphatic nodes, ET airways	47	1.030	2.26	1.34
101	Lymphatic nodes, thoracic airways	47	1.030	6.40	3.86
102	Lymphatic nodes, head	47	1.030	5.98	2.58
103	Lymphatic nodes, trunk	47	1.030	104.40	57.66
104	Lymphatic nodes, arms	47	1.030	7.83	3.90
105	Lymphatic nodes, legs	47	1.030	11.10	9.80
	Muscle tissue:				
106	Muscle, head	29	1.050	1217.81	401.97

Table A.1 (*continued*)

Organ ID	Organ/tissue	Medium	Density* (g/cm^3)	Mass (g)	
				Male	Female
107	Muscle, trunk	29	1.050	15,006.82	8518.22
108	Muscle, arms	29	1.050	2750.53	1524.87
109	Muscle, legs	29	1.050	10,024.97	7054.94
110	Oesophagus (wall)	44	1.030	40.01	34.99
	Ovaries:				
111	Ovary, left	42	1.040**	n.a.	5.50
112	Ovary, right	42	1.040**	n.a.	5.50
113	Pancreas	31	1.050¶	140.00	120.01
114	Pituitary gland	45	1.030	0.60	0.60
115	Prostate	46	1.030	17.01	n.a.
	Residual tissue:				
116	Residual tissue, head	49	0.950	1048.51	886.07
117	Residual tissue, trunk	49	0.950	12,370.04	11,803.12
118	Residual tissue, arms	49	0.950	1643.47	2042.40
119	Residual tissue, legs	49	0.950	5396.47	8864.84
	Salivary glands:				
120	Salivary glands, left	45	1.030	42.49	34.99
121	Salivary glands, right	45	1.030	42.49	35.01
	Skin:				
122	Skin, head	27	1.090	291.34	173.39
123	Skin, trunk	27	1.090	1465.21	1004.12
124	Skin, arms	27	1.090	639.03	469.52
125	Skin, legs	27	1.090	1332.43	1074.43
126	Spinal cord	45	1.030	36.62	18.63
127	Spleen	39	1.040**	149.99	130.00
128	Teeth	1	2.750	50.04	40.01
	Testes:				
129	Testis, left	42	1.040**	17.48	n.a.
130	Testis, right	42	1.040**	17.52	n.a.
131	Thymus	45	1.030	24.99	19.99
132	Thyroid	40	1.040**	19.99	17.00
133	Tongue (inner part)	29	1.050	42.28	41.55
134	Tonsils	45	1.030	3.01	3.00
	Ureters:				
135	Ureter, left	45	1.030	8.51	7.51
136	Ureter, right	45	1.030	7.49	7.49
137	Urinary bladder wall	41	1.040**	50.01	40.00
138	Urinary bladder contents	52	1.040**	200.00	200.00
139	Uterus/cervix	46	1.030	n.a.	80.01
140	Air inside body	53	0.001293	0.20	0.05
141	Skin at top and bottom	27	1.090	154.3	28.42

ET, extrathoracic; n.a., not applicable.

* From ICRU Report 46 (ICRU, 1992).

† Density of trachea.

‡ Mass density different for male and female phantoms (see Paras 29 and 36).

§ Arithmetic mean of the densities of brain, heart, and kidneys.

¶ Arithmetic mean of the densities of eyes, liver, and pancreas.

** Arithmetic mean of the densities of stomach, small intestine, large intestine, ovaries, spleen, testes, thyroid, and urinary bladder.

Table A.2 ID listings, rectangular prism (box) containing the organ (minimum/maximum columns, rows, and slices occupied by each organ/tissue), and organs' centres of mass (in terms of voxels as well as co-ordinates) for the adult male reference computational phantom.

Organ ID	Organ/tissue	Rectangular prism						Centre of mass					
		Column		Row		Slice		Voxels			Co-ordinates (cm)		
		Min	Max	Min	Max	Min	Max	x	y	z	x	y	z
1	Adrenal, left	142	167	79	98	155	156	153.70	88.98	155.20	32.86	19.02	124.10
2	Adrenal, right	91	111	77	94	154	155	101.90	86.59	154.00	21.78	18.50	123.20
3	Anterior nasal passage (ET_1)	124	138	2	27	204	210	128.90	13.30	205.40	27.55	2.84	164.30
4	Posterior nasal passage down to larynx (ET_2)	118	140	22	57	190	209	128.80	44.98	201.10	27.53	9.61	160.90
5	Oral mucosa, tongue	121	140	19	52	198	202	129.50	37.99	200.60	27.67	8.12	160.50
6	Oral mucosa, lips and cheeks	115	144	15	43	201	202	129.20	26.89	201.00	27.62	5.75	160.80
7	Trachea	124	134	46	76	179	190	128.60	63.11	183.80	27.48	13.49	147.00
8	Bronchi	78	186	33	96	165	178	135.40	60.37	172.00	28.93	12.90	137.60
9	Blood vessels, head	109	155	56	69	192	203	127.10	65.05	195.60	27.17	13.90	156.50
10	Blood vessels, trunk	39	222	25	118	104	190	129.10	67.76	151.30	27.59	14.48	121.10
11	Blood vessels, arms	5	243	68	120	118	172	130.80	96.61	148.00	27.95	20.65	118.40
12	Blood vessels, legs	51	191	46	114	13	103	122.50	94.22	58.15	26.19	20.14	46.52
13	Humeri, upper half, cortical	29	224	55	93	168	186	127.50	74.97	176.10	27.25	16.02	140.90
14	Humeri, upper half, spongiosa	36	222	56	80	177	186	131.50	68.31	181.50	28.10	14.60	145.20
15	Humeri, upper half, medullary cavity	31	222	70	92	168	176	120.20	80.80	171.80	25.68	17.27	137.40
16	Humeri, lower half, cortical	16	231	80	116	149	167	116.70	94.86	158.30	24.95	20.27	126.60
17	Humeri, lower half, spongiosa	17	230	93	115	149	156	112.40	101.00	151.30	24.01	21.57	121.00
18	Humeri, lower half, medullary cavity	28	223	82	102	157	167	125.50	92.06	161.60	26.83	19.68	129.30
19	Ulnae and radii, cortical	4	245	93	117	116	148	125.00	104.30	131.90	26.71	22.29	105.50
20	Ulnae and radii, spongiosa	5	244	94	116	116	148	124.20	104.00	137.30	26.54	22.24	109.90
21	Ulnae and radii, medullary cavity	7	241	95	114	122	138	118.50	104.30	130.20	25.32	22.28	104.10
22	Wrists and hand bones, cortical	4	253	86	125	97	115	128.60	103.40	106.20	27.49	22.09	84.99
23	Wrists and hand bones, spongiosa	5	252	87	124	97	115	127.90	102.60	107.20	27.33	21.93	85.76
24	Clavicles, cortical	57	208	49	81	181	189	131.40	61.25	184.60	28.08	13.09	147.70
25	Clavicles, spongiosa	58	207	50	80	181	189	132.10	62.35	184.90	28.23	13.33	147.90
26	Cranium, cortical	93	161	11	110	203	221	126.60	61.03	210.30	27.05	13.04	168.30
27	Cranium, spongiosa	94	159	18	109	203	221	125.80	63.96	212.60	26.89	13.67	170.10
28	Femora, upper half, cortical	52	196	54	90	91	118	123.90	71.39	104.20	26.48	15.26	83.36
29	Femora, upper half, spongiosa	53	195	55	89	97	118	123.50	72.83	110.40	26.40	15.57	88.28
30	Femora, upper half, medullary cavity	67	180	61	74	91	96	124.10	66.60	92.98	26.51	14.23	74.39
31	Femora, lower half, cortical	72	176	56	92	63	90	123.40	68.29	75.87	26.38	14.59	60.70
32	Femora, lower half, spongiosa	74	173	57	91	63	76	123.00	71.72	66.40	26.29	15.33	53.12
33	Femora, lower half, medullary cavity	75	173	60	73	77	90	124.40	65.29	82.18	26.60	13.95	65.74

Table A.2 (*continued*)

Organ ID	Organ/tissue	Rectangular prism						Centre of mass					
		Column		Row		Slice		Voxels			Co-ordinates (cm)		
		Min	Max	Min	Max	Min	Max	x	y	z	x	y	z
34	Tibiae, fibulae, and patellae, cortical	69	177	48	110	14	68	123.20	85.79	40.52	26.33	18.34	32.42
35	Tibiae, fibulae, and patellae, spongiosa	70	176	49	109	14	68	123.20	83.10	44.83	26.32	17.76	35.86
36	Tibiae, fibulae, and patellae, medullary cavity	86	160	79	95	25	46	121.90	86.67	36.12	26.05	18.52	28.90
37	Ankles and foot bones, cortical	60	186	6	121	3	13	125.90	70.09	7.31	26.91	14.98	5.85
38	Ankles and foot bones, spongiosa	61	185	7	120	3	13	125.70	77.69	8.31	26.87	16.60	6.64
39	Mandible, cortical	100	158	16	62	194	205	129.70	41.15	199.30	27.72	8.79	159.40
40	Mandible, spongiosa	101	157	17	61	194	205	130.80	37.48	198.20	27.96	8.01	158.60
41	Pelvis, cortical	55	194	39	108	109	135	123.00	73.15	121.80	26.29	15.63	97.45
42	Pelvis, spongiosa	56	193	40	107	109	135	122.70	73.19	121.30	26.21	15.64	97.06
43	Ribs, cortical	63	192	20	112	152	187	126.00	87.81	169.90	26.93	18.77	135.90
44	Ribs, spongiosa	61	193	20	111	144	187	126.20	75.03	164.90	26.97	16.04	131.90
45	Scapulae, cortical	41	216	58	122	168	187	124.80	95.86	179.80	26.66	20.49	143.80
46	Scapulae, spongiosa	42	215	59	121	168	187	125.80	88.90	181.80	26.89	19.00	145.50
47	Cervical spine, cortical	111	149	56	93	189	203	130.10	68.99	195.40	27.80	14.74	156.30
48	Cervical spine, spongiosa	112	148	57	92	189	203	130.00	68.31	195.30	27.77	14.60	156.20
49	Thoracic spine, cortical	109	155	67	115	152	188	126.30	94.04	169.40	27.00	20.10	135.50
50	Thoracic spine, spongiosa	110	154	68	114	152	188	126.30	90.00	168.00	27.00	19.23	134.40
51	Lumbar spine, cortical	102	146	64	110	132	151	124.20	85.47	140.60	26.55	18.27	112.50
52	Lumbar spine, spongiosa	103	145	65	109	132	151	124.50	80.64	140.50	26.60	17.23	112.40
53	Sacrum, cortical	94	153	67	114	116	132	121.80	94.86	125.70	26.03	20.27	100.60
54	Sacrum, spongiosa	95	152	68	113	116	132	122.10	88.71	127.40	26.09	18.96	101.90
55	Sternum, cortical	112	147	44	53	180	181	128.70	48.46	180.00	27.50	10.36	144.00
56	Sternum, spongiosa	114	146	25	52	161	182	130.00	39.08	173.10	27.78	8.35	138.50
57	Cartilage, head	120	144	6	60	191	208	130.30	44.12	194.10	27.85	9.43	155.30
58	Cartilage, trunk	57	203	23	119	110	190	125.60	76.34	140.20	26.85	16.32	112.20
59	Cartilage, arms	10	235	93	115	100	148	136.00	101.20	115.70	29.06	21.62	92.57
60	Cartilage, legs	73	172	40	116	4	62	124.30	84.63	41.40	26.56	18.09	33.12
61	Brain	95	158	23	105	204	220	126.00	66.44	212.00	26.93	14.20	169.60
62	Breast, left, adipose tissue	166	189	20	32	165	167	177.00	26.14	165.60	37.83	5.59	132.40
63	Breast, left, glandular tissue	172	188	21	29	165	167	179.60	24.47	165.60	38.39	5.23	132.50
64	Breast, right, adipose tissue	69	93	18	30	165	167	80.92	24.36	165.60	17.29	5.21	132.40
65	Breast, right, glandular tissue	71	87	18	27	165	167	79.13	22.43	165.60	16.91	4.79	132.50
66	Eye lens, left	143	146	22	23	209	209	143.90	22.30	208.50	30.75	4.77	166.80
67	Eye bulb, left	140	149	22	30	208	210	143.60	25.84	208.60	30.69	5.52	166.90
68	Eye lens, right	114	117	21	22	209	209	115.10	21.30	208.50	24.60	4.55	166.80
69	Eye bulb, right	110	120	21	29	208	210	114.00	24.93	208.60	24.36	5.33	166.80
70	Gall bladder wall	82	120	36	67	151	156	99.73	53.01	152.90	21.31	11.33	122.30
71	Gall bladder contents	83	119	37	66	151	156	98.56	52.41	152.70	21.06	11.20	122.20

(*continued on next page*)

Table A.2 (*continued*)

Organ ID	Organ/tissue	Rectangular prism						Centre of mass					
		Column		Row		Slice		Voxels			Co-ordinates (cm)		
		Min	Max	Min	Max	Min	Max	x	y	z	x	y	z
72	Stomach wall	116	177	24	86	150	162	152.20	49.18	156.30	32.53	10.51	125.00
73	Stomach contents	120	174	27	83	151	162	154.70	51.21	157.00	33.07	10.94	125.60
74	Small intestine wall	73	179	34	95	121	158	131.80	56.54	137.50	28.17	12.08	110.00
75	Small intestine contents	76	177	37	92	122	158	140.90	58.39	144.30	30.10	12.48	115.40
76	Ascending colon wall	72	97	43	77	129	147	82.69	61.56	138.80	17.67	13.16	111.10
77	Ascending colon contents	75	94	46	74	131	147	82.97	61.33	139.80	17.73	13.11	111.90
78	Transverse colon wall, right	78	126	23	69	144	150	100.40	39.20	146.70	21.46	8.38	117.40
79	Transverse colon contents, right	80	126	25	67	144	150	99.78	39.52	147.40	21.32	8.45	117.90
80	Transverse colon wall, left	127	182	25	54	144	154	153.20	35.77	147.50	32.73	7.65	118.00
81	Transverse colon contents, left	127	180	28	48	145	153	150.30	36.02	148.20	32.12	7.70	118.60
82	Descending colon wall	166	189	43	77	132	158	177.40	58.49	146.70	37.91	12.50	117.30
83	Descending colon contents	169	186	46	74	132	158	178.00	59.49	150.00	38.04	12.71	120.00
84	Sigmoid colon wall	108	178	39	103	120	131	144.20	68.37	123.30	30.83	14.61	98.67
85	Sigmoid colon contents	110	177	40	101	120	131	149.30	64.38	124.50	31.91	13.76	99.60
86	Rectum wall	107	130	79	101	116	119	120.00	90.79	117.20	25.65	19.40	93.73
87	Heart wall	111	174	31	88	163	178	138.50	59.50	168.30	29.59	12.72	134.60
88	Heart contents (blood)	113	171	34	86	164	177	141.00	58.10	167.70	30.13	12.42	134.10
89	Kidney, left, cortex	142	177	72	97	144	155	160.10	84.32	150.00	34.21	18.02	120.00
90	Kidney, left, medulla	149	172	76	93	145	155	160.30	84.37	150.10	34.27	18.03	120.10
91	Kidney, left, pelvis	151	166	79	88	146	154	158.00	82.63	149.80	33.77	17.66	119.90
92	Kidney, right, cortex	77	111	68	95	144	154	92.28	82.66	148.90	19.72	17.67	119.10
93	Kidney, right, medulla	82	106	71	91	144	154	92.55	82.61	148.90	19.78	17.66	119.20
94	Kidney, right, pelvis	89	103	76	88	146	152	95.15	80.78	149.00	20.33	17.26	119.20
95	Liver	65	156	21	104	146	165	97.26	59.14	157.10	20.79	12.64	125.70
96	Lung, left, blood	141	181	52	103	164	185	156.30	87.47	170.50	33.40	18.69	136.40
97	Lung, left, tissue	135	188	29	107	159	185	163.10	73.93	171.50	34.86	15.80	137.20
98	Lung, right, blood	76	117	44	100	165	184	101.50	82.44	170.90	21.68	17.62	136.70
99	Lung, right, tissue	68	138	24	107	159	185	97.90	69.19	171.30	20.92	14.79	137.10
100	Lymphatic nodes, ET airways	125	137	43	56	190	197	131.20	48.38	193.80	28.04	10.34	155.00
101	Lymphatic nodes, thoracic airways	109	156	46	86	169	190	128.40	69.90	178.80	27.44	14.94	143.00
102	Lymphatic nodes, head	94	164	27	97	191	204	130.70	65.76	197.40	27.93	14.05	157.90
103	Lymphatic nodes, trunk	58	196	25	107	104	190	132.10	61.46	147.70	28.23	13.13	118.20
104	Lymphatic nodes, arms	33	223	84	107	139	172	126.80	91.06	154.10	27.11	19.46	123.30
105	Lymphatic nodes, legs	86	158	47	112	51	103	123.20	86.01	74.79	26.32	18.38	59.84
106	Muscle, head	92	163	13	108	191	221	130.30	62.47	198.80	27.85	13.35	159.00
107	Muscle, trunk	18	233	11	123	101	190	124.60	77.19	142.70	26.62	16.50	114.10
108	Muscle, arms	3	252	66	121	98	172	121.30	99.37	143.20	25.92	21.24	114.60

Table A.2 (*continued*)

Organ ID	Organ/tissue	Rectangular prism						Centre of mass					
		Column		Row		Slice		Voxels			Co-ordinates (cm)		
		Min	Max	Min	Max	Min	Max	x	y	z	x	y	z
109	Muscle, legs	47	201	2	123	2	103	122.70	80.50	66.47	26.23	17.20	53.18
110	Oesophagus (wall)	123	143	55	85	161	193	132.00	72.58	175.00	28.20	15.51	140.00
111	Ovary, left	n.a.	n.a.	n.a.	n.a.	n.a.	n.a.	n.a.	n.a.	n.a.	n.a.	n.a.	n.a.
112	Ovary, right	n.a.	n.a.	n.a.	n.a.	n.a.	n.a.	n.a.	n.a.	n.a.	n.a.	n.a.	n.a.
113	Pancreas	100	156	46	71	149	154	124.60	57.21	151.30	26.63	12.23	121.10
114	Pituitary gland	127	131	53	58	208	209	128.30	55.38	207.90	27.42	11.83	166.40
115	Prostate	117	130	68	84	111	115	123.20	72.91	112.60	26.33	15.58	90.07
116	Residual tissue, head	86	169	2	112	191	221	128.20	62.97	204.90	27.40	13.46	163.90
117	Residual tissue, trunk	15	237	8	126	97	190	126.00	74.63	142.40	26.92	15.95	113.90
118	Residual tissue, arms	2	253	62	126	96	172	126.30	100.10	140.80	26.99	21.40	112.70
119	Residual tissue, legs	34	209	2	123	2	103	121.80	83.43	69.83	26.04	17.83	55.87
120	Salivary glands, left	134	165	29	70	194	207	155.00	56.75	200.10	33.13	12.13	160.00
121	Salivary glands, right	92	129	29	67	194	207	103.50	55.78	200.20	22.12	11.92	160.10
122	Skin, head	85	170	1	113	191	221	128.00	62.29	205.70	27.35	13.31	164.50
123	Skin, trunk	14	238	7	127	97	190	125.20	74.60	145.80	26.75	15.94	116.70
124	Skin, arms	1	254	61	127	96	172	124.80	100.90	136.60	26.67	21.56	109.30
125	Skin, legs	33	210	1	124	2	103	123.10	82.35	56.27	26.30	17.60	45.02
126	Spinal cord	123	134	67	104	147	203	127.20	86.93	176.20	27.18	18.58	140.90
127	Spleen	143	187	69	105	154	163	169.10	87.37	158.50	36.14	18.67	126.80
128	Teeth	116	143	16	43	201	202	129.20	28.34	201.00	27.62	6.06	160.80
129	Testis, left	126	135	39	62	97	103	129.10	49.35	99.98	27.58	10.55	79.99
130	Testis, right	118	125	41	66	97	103	122.30	51.49	99.85	26.15	11.00	79.88
131	Thymus	120	139	48	61	177	184	130.00	54.36	180.60	27.78	11.62	144.50
132	Thyroid	115	145	52	67	185	190	130.70	58.92	186.40	27.94	12.59	149.10
133	Tongue (inner part)	123	139	20	51	199	201	130.10	37.83	199.60	27.80	8.08	159.70
134	Tonsils	120	136	55	61	204	204	128.00	57.55	203.50	27.35	12.30	162.80
135	Ureter, left	127	159	57	80	124	149	138.00	68.62	136.80	29.49	14.67	109.50
136	Ureter, right	103	118	58	74	124	146	109.90	66.04	134.60	23.48	14.11	107.70
137	Urinary bladder wall	106	144	47	83	115	123	124.30	63.54	118.30	26.55	13.58	94.62
138	Urinary bladder contents	108	142	49	81	115	123	124.30	63.99	118.90	26.57	13.68	95.14
139	Uterus/cervix	n.a.	n.a.	n.a.	n.a.	n.a.	n.a.	n.a.	n.a.	n.a.	n.a.	n.a.	n.a.
140	Air inside body	82	185	3	88	165	213	129.00	45.90	199.40	27.56	9.81	159.50
141	Skin at top and bottom	60	189	8	88	1	222	122.80	54.05	74.43	26.24	11.55	59.55

ET, extrathoracic; n.a., not applicable.

Table A.3 ID listings, rectangular prism (box) containing the organ (minimum/maximum columns, rows, and slices occupied by each organ/tissue), and organs' centres of mass (in terms of voxels as well as co-ordinates) for the adult female reference computational phantom.

Organ ID	Organ/tissue	Rectangular prism						Centre of mass					
		Column		Row		Slice		Voxels			Co-ordinates (cm)		
		Min	Max	Min	Max	Min	Max	x	y	z	x	y	z
1	Adrenal, left	157	169	69	91	244	246	162.10	80.92	244.50	28.77	14.36	118.30
2	Adrenal, right	121	136	80	100	240	243	129.90	90.10	240.30	23.06	15.99	116.30
3	Anterior nasal passage (ET_1)	148	157	6	31	315	322	152.60	15.94	317.40	27.08	2.83	153.60
4	Posterior nasal passage down to larynx (ET_2)	140	162	21	67	303	322	151.00	54.70	313.30	26.81	9.71	151.70
5	Oral mucosa, tongue	140	164	27	59	308	315	151.50	43.59	311.30	26.89	7.74	150.70
6	Oral mucosa, lips and cheeks	130	175	19	47	311	314	151.70	29.70	311.90	26.92	5.27	151.00
7	Trachea	144	154	58	88	281	303	148.70	74.02	291.00	26.40	13.14	140.80
8	Bronchi	105	182	72	103	263	280	152.50	88.36	273.80	27.06	15.68	132.50
9	Blood vessels, head	124	178	63	73	306	320	149.90	68.23	312.20	26.60	12.11	151.10
10	Blood vessels, trunk	42	225	25	112	170	305	152.10	73.00	243.50	27.00	12.96	117.80
11	Blood vessels, arms	18	283	67	128	191	280	151.90	104.70	239.20	26.97	18.58	115.80
12	Blood vessels, legs	96	200	46	126	29	169	147.70	98.91	105.80	26.21	17.56	51.21
13	Humeri, upper half, cortical	49	248	58	102	266	299	147.80	82.21	280.90	26.24	14.59	136.00
14	Humeri, upper half, spongiosa	50	247	59	87	284	299	152.60	73.14	291.50	27.09	12.98	141.10
15	Humeri, upper half, medullary cavity	54	243	73	98	266	285	140.10	86.15	276.30	24.88	15.29	133.70
16	Humeri, lower half, cortical	32	268	90	128	235	269	151.30	107.20	251.90	26.86	19.03	121.90
17	Humeri, lower half, spongiosa	33	267	104	127	235	250	153.70	113.20	241.00	27.28	20.09	116.60
18	Humeri, lower half, medullary cavity	43	254	93	114	246	269	140.60	104.10	256.80	24.96	18.48	124.30
19	Ulnae and radii, cortical	18	285	103	129	189	243	153.30	115.20	215.50	27.22	20.45	104.30
20	Ulnae and radii, spongiosa	19	284	104	128	189	243	156.30	116.60	218.90	27.74	20.70	106.00
21	Ulnae and radii, medullary cavity	22	280	107	122	198	229	145.20	113.00	213.10	25.77	20.06	103.10
22	Wrists and hand bones, cortical	10	293	112	131	164	192	163.70	121.20	179.40	29.06	21.51	86.81
23	Wrists and hand bones, spongiosa	11	292	113	130	164	192	160.70	120.30	182.70	28.53	21.35	88.42
24	Clavicles, cortical	70	225	55	83	285	303	148.60	67.13	292.90	26.37	11.92	141.70
25	Clavicles, spongiosa	71	224	56	82	285	303	147.70	67.62	293.10	26.22	12.00	141.90
26	Cranium, cortical	113	189	6	111	313	346	151.10	54.92	329.20	26.82	9.75	159.30
27	Cranium, spongiosa	114	188	7	110	313	346	151.00	57.84	332.30	26.81	10.27	160.80
28	Femora, upper half, cortical	68	232	57	87	150	188	147.40	70.97	165.80	26.17	12.60	80.24
29	Femora, upper half, spongiosa	69	231	58	86	170	188	148.50	71.62	178.70	26.35	12.71	86.49
30	Femora, upper half, medullary cavity	79	217	65	78	150	169	146.20	69.82	159.20	25.94	12.39	77.08
31	Femora, lower half, cortical	84	211	63	93	110	149	147.70	73.18	132.00	26.21	12.99	63.88
32	Femora, lower half, spongiosa	93	201	67	92	110	126	145.50	77.82	116.00	25.83	13.81	56.16
33	Femora, lower half, medullary cavity	89	206	65	80	127	149	144.30	71.31	135.80	25.61	12.66	65.73

Table A.3 (*continued*)

Organ ID	Organ/tissue	Rectangular prism						Centre of mass					
		Column		Row		Slice		Voxels			Co-ordinates (cm)		
		Min	Max	Min	Max	Min	Max	x	y	z	x	y	z
34	Tibiae, fibulae, and patellae, cortical	84	211	56	114	25	114	145.40	91.58	73.42	25.81	16.26	35.53
35	Tibiae, fibulae, and patellae, spongiosa	85	210	57	113	25	113	145.60	90.06	76.40	25.85	15.99	36.98
36	Tibiae, fibulae, and patellae, medullary cavity	101	193	83	102	42	92	147.40	92.73	67.60	26.17	16.46	32.72
37	Ankles and foot bones, cortical	99	201	25	127	4	24	147.80	77.33	14.47	26.24	13.73	7.00
38	Ankles and foot bones, spongiosa	100	200	26	126	5	27	147.50	85.58	17.19	26.19	15.19	8.32
39	Mandible, cortical	121	184	21	68	304	322	151.90	44.63	311.40	26.96	7.92	150.70
40	Mandible, spongiosa	122	183	22	60	304	322	152.00	41.18	310.00	26.98	7.31	150.00
41	Pelvis, cortical	78	222	38	110	174	213	149.90	73.91	192.80	26.60	13.12	93.31
42	Pelvis, spongiosa	79	221	39	109	174	212	149.40	75.72	192.90	26.52	13.44	93.38
43	Ribs, cortical	87	218	37	123	227	299	148.00	97.97	271.30	26.28	17.39	131.30
44	Ribs, spongiosa	86	219	34	122	227	298	149.30	85.90	263.00	26.50	15.25	127.30
45	Scapulae, cortical	54	240	62	128	272	303	146.80	100.90	289.90	26.06	17.91	140.30
46	Scapulae, spongiosa	55	239	63	127	273	303	147.40	93.67	292.50	26.16	16.63	141.60
47	Cervical spine, cortical	132	171	61	108	298	319	149.50	78.80	307.50	26.54	13.99	148.80
48	Cervical spine, spongiosa	133	170	62	107	298	319	149.70	76.37	307.90	26.57	13.56	149.00
49	Thoracic spine, cortical	129	169	74	128	242	297	147.30	103.30	268.30	26.15	18.34	129.90
50	Thoracic spine, spongiosa	130	168	75	127	242	297	147.40	99.17	266.70	26.16	17.60	129.10
51	Lumbar spine, cortical	119	181	61	114	208	241	149.00	84.80	223.20	26.44	15.05	108.00
52	Lumbar spine, spongiosa	120	180	62	113	208	241	149.00	79.86	222.50	26.44	14.18	107.70
53	Sacrum, cortical	n.a.	n.a.	n.a.	n.a.	n.a.	n.a.	n.a.	n.a.	n.a.	n.a.	n.a.	n.a.
54	Sacrum, spongiosa	118	182	66	126	183	207	149.40	96.55	201.20	26.52	17.14	97.38
55	Sternum, cortical	136	164	53	62	284	284	150.40	56.69	283.50	26.69	10.06	137.20
56	Sternum, spongiosa	137	165	38	63	250	287	150.80	49.51	272.50	26.76	8.79	131.90
57	Cartilage, head	121	183	10	94	306	327	151.30	53.80	311.70	26.86	9.55	150.80
58	Cartilage, trunk	48	248	30	128	170	305	150.00	77.61	230.10	26.62	13.78	111.40
59	Cartilage, arms	10	292	76	131	164	281	173.70	112.90	234.60	30.83	20.05	113.50
60	Cartilage, legs	75	221	29	127	4	169	145.60	88.19	77.71	25.84	15.65	37.61
61	Brain	116	185	11	107	316	345	150.80	60.72	332.20	26.77	10.78	160.80
62	Breast, left, adipose tissue	157	225	21	62	257	285	189.80	35.98	271.20	33.68	6.39	131.20
63	Breast, left, glandular tissue	167	219	21	57	263	276	194.70	36.44	268.70	34.56	6.47	130.10
64	Breast, right, adipose tissue	78	150	20	59	257	285	114.10	36.28	270.80	20.25	6.44	131.10
65	Breast, right, glandular tissue	84	134	20	55	262	275	108.70	34.37	267.40	19.29	6.10	129.40
66	Eye lens, left	168	172	17	18	322	323	169.80	17.04	322.00	30.14	3.02	155.80
67	Eye bulb, left	163	177	13	26	322	325	169.60	18.68	323.10	30.10	3.32	156.40
68	Eye lens, right	134	137	16	17	322	323	135.00	16.00	322.00	23.96	2.84	155.80
69	Eye bulb, right	129	143	12	25	322	325	135.40	18.03	323.00	24.04	3.20	156.30
70	Gall bladder wall	117	162	44	82	238	245	138.60	64.27	240.80	24.60	11.41	116.60
71	Gall bladder contents	118	161	45	81	238	245	138.70	64.67	240.80	24.61	11.48	116.50

(*continued on next page*)

Table A.3 (*continued*)

Organ ID	Organ/tissue	Rectangular prism						Centre of mass					
		Column		Row		Slice		Voxels			Co-ordinates (cm)		
		Min	Max	Min	Max	Min	Max	x	y	z	x	y	z
72	Stomach wall	149	211	35	95	229	256	182.80	58.77	242.10	32.45	10.43	117.20
73	Stomach contents	153	208	39	92	229	256	186.40	64.54	245.20	33.08	11.46	118.70
74	Small intestine wall	107	208	37	118	187	244	156.60	62.29	211.90	27.80	11.06	102.60
75	Small intestine contents	111	204	41	114	187	244	159.60	63.39	215.00	28.33	11.25	104.10
76	Ascending colon wall	95	132	37	77	195	231	110.20	55.70	211.10	19.55	9.89	102.20
77	Ascending colon contents	98	129	40	74	195	231	110.00	55.43	210.70	19.53	9.84	102.00
78	Transverse colon wall, right	105	152	38	63	208	228	126.70	47.76	214.90	22.49	8.48	104.00
79	Transverse colon contents, right	107	151	41	61	208	228	125.60	48.34	215.70	22.29	8.58	104.40
80	Transverse colon wall, left	152	201	36	63	209	223	176.00	48.19	213.90	31.24	8.55	103.50
81	Transverse colon contents, left	152	197	40	60	209	223	176.20	48.02	213.70	31.27	8.52	103.50
82	Descending colon wall	160	210	39	76	192	224	192.00	54.31	206.60	34.07	9.64	99.99
83	Descending colon contents	165	207	43	73	192	224	193.00	54.99	207.90	34.26	9.76	100.60
84	Sigmoid colon wall	129	178	42	121	184	192	155.60	90.42	187.90	27.62	16.05	90.92
85	Sigmoid colon contents	132	176	44	119	184	192	155.50	91.73	188.20	27.60	16.28	91.08
86	Rectum wall	135	159	75	102	176	183	147.20	83.90	179.60	26.12	14.89	86.93
87	Heart wall	135	204	42	98	256	280	165.60	67.79	266.60	29.40	12.03	129.10
88	Heart contents (blood)	140	203	48	92	257	277	167.70	68.12	264.80	29.76	12.09	128.20
89	Kidney, left, cortex	161	198	73	103	224	245	180.60	87.79	236.10	32.06	15.58	114.30
90	Kidney, left, medulla	168	196	76	97	225	241	182.10	86.39	232.60	32.32	15.33	112.60
91	Kidney, left, pelvis	170	188	80	95	228	240	179.60	86.21	233.80	31.88	15.30	113.20
92	Kidney, right, cortex	99	136	69	100	224	239	117.10	82.30	232.10	20.78	14.61	112.40
93	Kidney, right, medulla	103	131	71	96	224	238	115.40	81.64	230.50	20.49	14.49	111.60
94	Kidney, right, pelvis	112	128	77	88	228	237	119.60	81.34	232.00	21.23	14.44	112.30
95	Liver	89	209	32	116	231	259	126.30	67.87	246.60	22.41	12.05	119.40
96	Lung, left, blood	159	209	60	117	254	293	179.70	98.05	268.90	31.91	17.40	130.20
97	Lung, left, tissue	153	214	43	120	250	294	185.20	87.54	272.10	32.87	15.54	131.70
98	Lung, right, blood	93	145	51	115	255	291	123.60	88.41	268.70	21.93	15.69	130.00
99	Lung, right, tissue	90	202	39	118	252	293	118.50	81.18	270.80	21.03	14.41	131.00
100	Lymphatic nodes, ET airways	140	162	44	65	303	311	150.80	55.61	306.40	26.76	9.87	148.30
101	Lymphatic nodes, thoracic airways	127	178	60	97	267	303	148.70	78.83	284.40	26.39	13.99	137.60
102	Lymphatic nodes, head	117	184	62	98	306	321	150.10	76.43	313.90	26.65	13.57	151.90
103	Lymphatic nodes, trunk	71	224	37	122	170	300	153.40	70.77	236.20	27.22	12.56	114.30
104	Lymphatic nodes, arms	58	246	88	122	230	281	149.30	107.70	250.00	26.50	19.11	121.00
105	Lymphatic nodes, legs	95	199	43	125	93	169	147.00	77.51	137.80	26.09	13.76	66.68
106	Muscle, head	112	189	8	111	306	347	150.90	65.79	316.00	26.79	11.68	152.90
107	Muscle, trunk	37	260	27	133	170	305	150.30	83.00	232.30	26.68	14.73	112.40
108	Muscle, arms	9	293	65	132	164	281	148.00	108.80	234.40	26.27	19.31	113.50

Table A.3 (*continued*)

Organ ID	Organ/tissue	Rectangular prism						Centre of mass					
		Column		Row		Slice		Voxels			Co-ordinates (cm)		
		Min	Max	Min	Max	Min	Max	x	y	z	x	y	z
109	Muscle, legs	64	231	24	129	3	169	145.60	89.37	114.70	25.85	15.86	55.52
110	Oesophagus (wall)	146	167	66	97	253	305	154.20	82.08	278.70	27.37	14.57	134.90
111	Ovary, left	160	172	76	91	180	183	164.90	82.49	181.20	29.28	14.64	87.72
112	Ovary, right	123	134	79	92	184	188	128.20	85.00	185.40	22.75	15.09	89.72
113	Pancreas	115	193	43	79	229	241	153.30	59.58	234.60	27.20	10.58	113.50
114	Pituitary gland	147	156	57	62	324	325	150.50	59.32	324.00	26.72	10.53	156.80
115	Prostate	n.a.	n.a.	n.a.	n.a.	n.a.	n.a.	n.a.	n.a.	n.a.	n.a.	n.a.	n.a.
116	Residual tissue, head	103	198	2	115	306	347	151.00	57.19	322.30	26.80	10.15	156.00
117	Residual tissue, trunk	29	268	19	136	170	305	150.80	84.22	222.90	26.77	14.95	107.90
118	Residual tissue, arms	2	298	62	134	159	281	148.90	109.20	239.20	26.43	19.38	115.80
119	Residual tissue, legs	47	250	18	132	2	169	147.10	90.47	110.00	26.11	16.06	53.24
120	Salivary glands, left	153	188	36	73	306	321	174.40	60.00	313.50	30.96	10.65	151.70
121	Salivary glands, right	115	151	36	74	306	321	127.70	58.73	313.70	22.67	10.42	151.80
122	Skin, head	102	199	1	116	306	347	150.80	59.31	325.40	26.77	10.53	157.50
123	Skin, trunk	28	269	18	137	170	305	150.30	81.00	236.40	26.68	14.38	114.40
124	Skin, arms	1	299	61	135	159	281	151.90	112.10	225.50	26.96	19.90	109.10
125	Skin, legs	46	251	17	133	2	169	146.50	91.08	94.81	26.01	16.17	45.89
126	Spinal cord	145	154	74	112	235	315	147.80	93.96	278.60	26.23	16.68	134.80
127	Spleen	164	213	68	109	240	255	193.90	93.29	247.60	34.42	16.56	119.80
128	Teeth	135	168	21	47	311	314	151.60	32.46	311.90	26.91	5.76	150.90
129	Testis, left	n.a.	n.a.	n.a.	n.a.	n.a.	n.a.	n.a.	n.a.	n.a.	n.a.	n.a.	n.a.
130	Testis, right	n.a.	n.a.	n.a.	n.a.	n.a.	n.a.	n.a.	n.a.	n.a.	n.a.	n.a.	n.a.
131	Thymus	133	167	58	73	279	290	149.40	64.50	285.10	26.52	11.45	138.00
132	Thyroid	135	163	62	73	292	301	148.00	66.43	295.70	26.27	11.79	143.10
133	Tongue (inner part)	141	163	28	58	309	314	151.40	44.72	311.10	26.88	7.94	150.60
134	Tonsils	137	168	45	54	314	316	152.70	49.65	314.50	27.10	8.81	152.20
135	Ureter, left	160	183	61	83	186	237	169.50	69.71	209.30	30.08	12.37	101.30
136	Ureter, right	130	145	62	79	189	237	138.00	68.38	212.40	24.49	12.14	102.80
137	Urinary bladder wall	118	183	35	76	179	190	148.90	53.50	184.10	26.42	9.50	89.09
138	Urinary bladder contents	119	181	37	74	179	190	148.30	52.90	185.10	26.33	9.39	89.60
139	Uterus/cervix	123	172	61	99	177	188	151.60	76.86	183.10	26.91	13.64	88.61
140	Air inside body	124	179	9	102	267	331	150.90	57.08	304.70	26.79	10.13	147.50
141	Skin at top and bottom	96	197	22	80	1	348	139.30	54.33	147.60	24.72	9.64	71.45

ET, extrathoracic; n.a., not applicable.

A.1. Reference

ICRU, 1992b. Photon, Electron, Proton and Neutron Interaction Data for Body Tissues. ICRU Report 46. International Commission on Radiation Units and Measurements, Bethesda, MD.

ANNEX B. LIST OF MEDIA AND THEIR ELEMENTAL COMPOSITIONS

(B 1) For the purpose of radiation transport calculations, each organ/tissue must have a certain material composition. Therefore, a list of media has been defined that are assigned to the various organ IDs (see Table A.1). Table B.1 gives the elemental compositions of the media for the male phantom, and Table B.2 gives those for the female phantom.

Table B.1 List of media, their elemental compositions (percentage by mass), and their densities for the adult male reference computational phantom.

Medium no.		H_1	C_6	N_7	O_8	Na_{11}	Mg_{12}	P_{15}	S_{16}	Cl_{17}	K_{19}	Ca_{20}	Fe_{26}	I_{53}	Density (g/cm)
1	Teeth	2.2	9.5	2.9	42.1		0.7	13.7				28.9			2.750
2	Mineral bone	3.6	15.9	4.2	44.8	0.3	0.2	9.4	0.3			21.3			1.920
3	Humeri, upper half, spongiosa	8.5	28.8	2.6	49.8	0.2	0.1	3.3	0.4	0.2		6.1			1.205
4	Humeri, lower half, spongiosa	9.7	43.9	1.7	38.1	0.2		2.1	0.3	0.1		3.9			1.108
5	Lower arm bones, spongiosa	9.7	43.9	1.7	38.1	0.2		2.1	0.3	0.1		3.9			1.108
6	Hand bones, spongiosa	9.7	43.9	1.7	38.1	0.2		2.1	0.3	0.1		3.9			1.108
7	Clavicles, spongiosa	9.1	34.8	2.4	45.7	0.2		2.6	0.3	0.1		4.8			1.151
8	Cranium, spongiosa	9.0	33.5	2.5	46.7	0.2		2.6	0.3	0.2	0.1	4.9			1.157
9	Femora, upper half, spongiosa	9.4	38.5	2.2	43.0	0.2		2.2	0.3	0.1		4.1			1.124
10	Femora, lower half, spongiosa	9.7	43.9	1.7	38.1	0.2		2.1	0.3	0.1		3.9			1.108
11	Lower leg bones, spongiosa	9.7	43.9	1.7	38.1	0.2		2.1	0.3	0.1		3.9			1.108
12	Foot bones, spongiosa	9.7	43.9	1.7	38.1	0.2		2.1	0.3	0.1		3.9			1.108
13	Mandible, spongiosa	8.3	26.6	2.7	51.1	0.3	0.1	3.6	0.4	0.2		6.7			1.228
14	Pelvis, spongiosa	9.4	36.0	2.5	45.4	0.2		2.1	0.3	0.2	0.1	3.8			1.123
15	Ribs, spongiosa	8.9	29.2	2.9	50.7	0.2		2.6	0.4	0.2	0.1	4.8			1.165
16	Scapulae, spongiosa	8.7	30.9	2.6	48.3	0.2	0.1	3.0	0.4	0.2		5.6			1.183
17	Cervical spine, spongiosa	10.3	40.0	2.7	44.4	0.1		0.7	0.2	0.2	0.1	1.2	0.1		1.050
18	Thoracic spine, spongiosa	9.9	37.6	2.7	45.9	0.1		1.2	0.2	0.2	0.1	2.0	0.1		1.074
19	Lumbar spine, spongiosa	9.5	34.0	2.8	48.0	0.1		1.8	0.3	0.2	0.1	3.2			1.112
20	Sacrum, spongiosa	10.5	41.9	2.7	43.2	0.1		0.4	0.2	0.2	0.1	0.6	0.1		1.031
21	Sternum, spongiosa	10.4	40.9	2.7	43.8	0.1		0.6	0.2	0.2	0.1	0.9	0.1		1.041
22	Humeri and femora, upper halves, medullary cavity	11.5	63.6	0.7	23.9	0.1			0.1	0.1					0.980

(*continued on next page*)

Table B.1 (*continued*)

Medium no.		H_1	C_6	N_7	O_8	Na_{11}	Mg_{12}	P_{15}	S_{16}	Cl_{17}	K_{19}	Ca_{20}	Fe_{26}	I_{53}	Density (g/cm)
23	Humeri and femora, lower halves, medullary cavity	11.5	63.6	0.7	23.9	0.1			0.1	0.1					0.980
24	Lower arm bones, medullary cavity	11.5	63.6	0.7	23.9	0.1			0.1	0.1					0.980
25	Lower leg bones, medullary cavity	11.5	63.6	0.7	23.9	0.1			0.1	0.1					0.980
26	Cartilage	9.6	9.9	2.2	74.4	0.5		2.2	0.9	0.3					1.100
27	Skin	10.0	19.9	4.2	65.0	0.2		0.1	0.2	0.3	0.1				1.090
28	Blood	10.2	11.0	3.3	74.5	0.1		0.1	0.2	0.3	0.2		0.1		1.060
29	Muscle tissue	10.2	14.2	3.4	71.1	0.1		0.2	0.3	0.1	0.4				1.050
30	Liver	10.2	13.0	3.1	72.5	0.2		0.2	0.3	0.2	0.3				1.050
31	Pancreas	10.5	15.5	2.5	70.6	0.2		0.2	0.1	0.2	0.2				1.050
32	Brain	10.7	14.3	2.3	71.3	0.2		0.4	0.2	0.3	0.3				1.050
33	Heart	10.4	13.8	2.9	71.9	0.1		0.2	0.2	0.2	0.3				1.050
34	Eyes	9.7	18.1	5.3	66.3	0.1		0.1	0.3	0.1					1.050
35	Kidneys	10.3	12.4	3.1	73.1	0.2		0.2	0.2	0.2	0.2	0.1			1.050
36	Stomach	10.5	11.4	2.5	75.0	0.1		0.1	0.1	0.2	0.1				1.040
37	Small intestine	10.5	11.3	2.6	75.0	0.1		0.1	0.1	0.2	0.1				1.040
38	Large intestine	10.5	11.3	2.6	75.0	0.1		0.1	0.1	0.2	0.1				1.040
39	Spleen	10.2	11.1	3.3	74.3	0.1		0.2	0.2	0.3	0.2		0.1		1.040
40	Thyroid	10.4	11.7	2.6	74.5	0.2		0.1	0.1	0.2	0.1			0.1	1.040
41	Urinary bladder	10.5	9.6	2.6	76.1	0.2		0.2	0.2	0.3	0.3				1.040
42	Testes	10.6	10.0	2.1	76.4	0.2		0.1	0.2	0.2	0.2				1.040
43	Adrenals	10.4	22.1	2.8	63.7	0.1		0.2	0.3	0.2	0.2				1.030
44	Oesophagus	10.4	21.3	2.9	64.4	0.1		0.2	0.3	0.2	0.2				1.030
45	Gall bladder, pituitary gland, trachea, thymus, tonsils, ureters	10.4	23.1	2.8	62.7	0.1		0.2	0.3	0.2	0.2				1.030
46	Prostate	10.4	23.1	2.8	62.7	0.1		0.2	0.3	0.2	0.2				1.030
47	Lymph	10.8	4.2	1.1	83.1	0.3			0.1	0.4					1.030
48	Breast (mammary gland)	11.2	51.6	1.1	35.8	0.1			0.1	0.1					1.020
49	Adipose tissue	11.4	58.8	0.8	28.7	0.1			0.1	0.1					0.950
50	Lung tissue (compressed lungs)	10.3	10.7	3.2	74.6	0.2		0.2	0.3	0.3	0.2				0.382
51	Gastro-intestinal tract – contents*	10.0	22.2	2.2	64.4	0.1		0.2	0.3	0.1	0.4	0.1			1.040
52	Urine	10.7	0.3	1.0	87.3	0.4		0.1			0.2				1.040
53	Air			80.0	20.0										0.001

* White et al. (1987).

Table B.2 List of media, their elemental compositions (percentage by mass), and their densities for the adult female reference computational phantom.

Medium no.		H_1	C_6	N_7	O_8	Na_{11}	Mg_{12}	P_{15}	S_{16}	Cl_{17}	K_{19}	Ca_{20}	Fe_{26}	I_{53}	Density (g/cm^3)
1	Teeth	2.2	9.5	2.9	42.1		0.7	13.7				28.9			2.750
2	Mineral bone	3.6	15.9	4.2	44.8	0.3	0.2	9.4	0.3			21.3			1.920
3	Humeri, upper half, spongiosa	8.7	36.6	2.5	42.2	0.2	0.1	3.0	0.3	0.1	0.1	6.2			1.185
4	Humeri, lower half, spongiosa	9.6	47.3	1.7	34.1	0.2		2.2	0.2	0.1		4.6			1.117
5	Lower arm bones, spongiosa	9.6	47.3	1.7	34.1	0.2		2.2	0.2	0.1		4.6			1.117
6	Hand bones, spongiosa	9.6	47.3	1.7	34.1	0.2		2.2	0.2	0.1		4.6			1.117
7	Clavicles, spongiosa	8.7	36.1	2.5	42.4	0.2	0.1	3.1	0.3	0.1	0.1	6.4			1.191
8	Cranium, spongiosa	8.1	31.7	2.8	45.1	0.2	0.1	3.7	0.3	0.1	0.1	7.8			1.245
9	Femora, upper half, spongiosa	10.4	49.6	1.8	34.9	0.1		0.9	0.2	0.1	0.1	1.9			1.046
10	Femora, lower half, spongiosa	9.6	47.3	1.7	34.1	0.2		2.2	0.2	0.1		4.6			1.117
11	Lower leg bones, spongiosa	9.6	47.3	1.7	34.1	0.2		2.2	0.2	0.1		4.6			1.117
12	Foot bones, spongiosa	9.6	47.3	1.7	34.1	0.2		2.2	0.2	0.1		4.6			1.117
13	Mandible, spongiosa	8.7	35.7	2.6	42.9	0.2	0.1	3.0	0.3	0.1	0.1	6.3			1.189
14	Pelvis, spongiosa	9.6	40.6	2.5	41.2	0.1		1.8	0.2	0.1	0.1	3.8			1.109
15	Ribs, spongiosa	9.7	38.1	2.8	44.5	0.1		1.4	0.2	0.2	0.1	2.8	0.1		1.092
16	Scapulae, spongiosa	9.4	40.6	2.4	40.4	0.1		2.2	0.2	0.1	0.1	4.5			1.128
17	Cervical spine, spongiosa	9.2	35.1	2.9	45.8	0.1		2.1	0.2	0.2	0.1	4.3			1.135
18	Thoracic spine, spongiosa	9.8	38.6	2.8	44.2	0.1		1.3	0.2	0.2	0.1	2.6	0.1		1.084
19	Lumbar spine, spongiosa	8.8	32.9	3.0	46.6	0.1	0.1	2.6	0.3	0.1	0.1	5.4			1.171
20	Sacrum, spongiosa	10.2	41.0	2.7	43.3	0.1		0.7	0.2	0.2	0.1	1.4	0.1		1.052
21	Sternum, spongiosa	9.9	39.2	2.8	43.9	0.1		1.2	0.2	0.2	0.1	2.3	0.1		1.076
22	Humeri and femora, upper halves, medullary cavity	11.5	63.7	0.7	23.8	0.1			0.1	0.1					0.980
23	Humeri and femora, lower halves, medullary cavity	11.5	63.7	0.7	23.8	0.1			0.1	0.1					0.980
24	Lower arm bones, medullary cavity	11.5	63.7	0.7	23.8	0.1			0.1	0.1					0.980
25	Lower leg bones, medullary cavity	11.5	63.7	0.7	23.8	0.1			0.1	0.1					0.980
26	Cartilage	9.6	9.9	2.2	74.4	0.5		2.2	0.9	0.3					1.100
27	Skin	10.0	19.9	4.2	65.0	0.2		0.1	0.2	0.3	0.1				1.090
28	Blood	10.2	11.0	3.3	74.5	0.1		0.1	0.2	0.3	0.2		0.1		1.060
29	Muscle tissue	10.2	14.2	3.4	71.1	0.1		0.2	0.3	0.1	0.4				1.050
30	Liver	10.2	13.1	3.1	72.4	0.2		0.2	0.3	0.2	0.3				1.050

(*continued on next page*)

Table B.2 (*continued*)

Medium no.		H_1	C_6	N_7	O_8	Na_{11}	Mg_{12}	P_{15}	S_{16}	Cl_{17}	K_{19}	Ca_{20}	Fe_{26}	I_{53}	Density (g/cm^3)
31	Pancreas	10.5	15.7	2.4	70.5	0.2		0.2	0.1	0.2	0.2				1.050
32	Brain	10.7	14.4	2.2	71.3	0.2		0.4	0.2	0.3	0.3				1.050
33	Heart	10.4	13.8	2.9	71.9	0.1		0.2	0.2	0.2	0.3				1.050
34	Eyes	9.7	18.3	5.4	66.0	0.1		0.1	0.3	0.1					1.050
35	Kidneys	10.3	12.5	3.1	73.0	0.2		0.2	0.2	0.2	0.2	0.1			1.050
36	Stomach	10.5	11.4	2.5	75.0	0.1		0.1	0.1	0.2	0.1				1.040
37	Small intestine	10.5	11.4	2.5	75.0	0.1		0.1	0.1	0.2	0.1				1.040
38	Large intestine	10.5	11.4	2.5	75.0	0.1		0.1	0.1	0.2	0.1				1.040
39	Spleen	10.3	11.2	3.2	74.3	0.1		0.2	0.2	0.2	0.3				1.040
40	Thyroid	10.4	11.8	2.5	74.5	0.2		0.1	0.1	0.2	0.1			0.1	1.040
41	Urinary bladder	10.5	9.6	2.6	76.1	0.2		0.2	0.2	0.3	0.3				1.040
42	Ovaries	10.5	9.4	2.5	76.6	0.2		0.2	0.2	0.2	0.2				1.040
43	Adrenals	10.4	22.8	2.8	63.0	0.1		0.2	0.3	0.2	0.2				1.030
44	Oesophagus	10.4	22.2	2.8	63.6	0.1		0.2	0.3	0.2	0.2				1.030
45	Gall bladder, pituitary gland, trachea, thymus, tonsils, ureters	10.5	23.5	2.8	62.2	0.1		0.2	0.3	0.2	0.2				1.030
46	Uterus	10.5	28.6	2.5	57.6	0.1		0.2	0.2	0.1	0.2				1.030
47	Lymph	10.8	4.2	1.1	83.1	0.3			0.1	0.4					1.030
48	Breast (mammary gland)	11.4	46.1	0.5	42.0	0.0									1.020
49	Adipose tissue	11.4	58.9	0.7	28.7	0.1			0.1	0.1					0.950
50	Lung tissue (compressed lungs)	10.3	10.7	3.2	74.6	0.2		0.2	0.3	0.3	0.2				0.385
51	Gastro-intestinal tract – contents*	10.0	22.2	2.2	64.4	0.1		0.2	0.3	0.1	0.4	0.1			1.040
52	Urine	10.7	0.3	1.0	87.3	0.4		0.1			0.2				1.040
53	Air			80.0	20.0										0.001

* White et al. (1987).

B.1. Reference

White, D.R., Woodard, H.Q., Hammond, S.M., 1987. Average soft-tissue and bone models for use in radiation dosimetry. Br. J. Radiol. 60, 907–913.

ANNEX C. LIST OF SOURCE REGIONS, ACRONYMS, AND ID NUMBERS

(C 1) Table C.1 establishes a set of acronyms for the source regions for the calculation of specific absorbed fractions. The regions of the Human Alimentary Tract Model (ICRP, 2006) and the Human Respiratory Tract Model (ICRP, 1994) are listed first, followed by the systemic regions. The third column gives the ID numbers in the phantoms that make up the respective region or – if these are too many – a footnote to this table where the sub-division of the region is expanded in detail.

Table C.1. List of source regions, their acronyms, and corresponding ID numbers in the phantoms.

Source region	Acronym	ID number(s)
Oral cavity	O-cavity	5, 6
Oral mucosa	O-mucosa	5, 6
Teeth surface activity	Teeth-S	128
Teeth volume activity	Teeth-V	128
Tongue	Tongue	5, 133*
Tonsils	Tonsils	134
Oesophagus fast	Oesophag-f	110
Oesophagus slow	Oesophag-s	110
Oesophagus wall	Oesophagus	110
Stomach contents	St-cont	73
Stomach wall	St-wall	72
Small intestine contents	SI-cont	75
Small intestine wall	SI-wall	74
Right colon contents	RC-cont	77, 79
Right colon wall	RC-wall	76, 78
Left colon contents	LC-cont	81, 83
Left colon wall	LC-wall	80, 82
Rectosigmoid colon contents	RSig-cont	85
Rectosigmoid colon wall	RSig-wall	84, 86
Surface of anterior nasal passages	ET1-sur	3
Surface of posterior nasal passages + pharynx	ET2-sur	4
Sequestered ET_2 region	ET2-seq	4
Lymph nodes in ET region	LN-ET	100
Bronchi fast	Bronchi-f	7, 8
Bronchi slow	Bronchi-s	7, 8
Bronchi bound	Bronchi-b	7, 8
Bronchi sequestered	Bronchi-q	7, 8
Bronchioles fast	Brchiole-f	97, 99
Bronchioles slow	Brchiole-s	97, 99
Bronchioles bound	Brchiole-b	97, 99
Bronchioles sequestered	Brchiole-q	97, 99
Alveolar-interstitium	AI	97, 99
Lymph nodes in thoracic region	LN-Th	101
Right lung lobe	RLung	98, 99
Left lung lobe	LLung	96, 97
RLung + LLung	Lungs	96–99
Right adrenal gland	RAdrenal	2
Left adrenal gland	LAdrenal	1

(*continued on next page*)

Table C.1 (*continued*)

Source region	Acronym	ID number(s)
RAdrenal + LAdrenal	Adrenals	1, 2
Blood vessels of head	HBlood	9
Blood vessels of trunk	TBlood	10
Blood vessels of arms	ABlood	11
Blood vessels of legs	LBlood	12
Blood in heart	Ht-cont	88
HBlood + TBlood + ABlood + LBlood + Ht-cont + Lung left, blood + Lung right, blood + blood in organs	Blood	†
Cortical bone mineral surface	C-bone-S	‡
Cortical bone mineral volume	C-bone-V	‡
Trabecular bone mineral surface	T-bone-S	§
Trabecular bone mineral volume	T-bone-V	§
Cortical bone marrow	C-marrow	¶
Trabecular bone marrow	T-marrow	**
Brain	Brain	61
Right breast adipose	RBreast-a	64
Right breast glandular	RBreast-g	65
Left breast adipose	LBreast-a	62
Left breast glandular	LBreast-g	63
RBreast-a + RBreast-g	RBreast	64, 65
LBreast-a + LBreast-g	LBreast	62, 63
RBreast-a + LBreast-a	Breast-a	62, 64
RBreast-g + LBreast-g	Breast-g	63, 65
Breast-a + Breast-g	Breast	62–65
Lenses of eye	Eye-lens	66, 68
Gall bladder wall	GB-wall	70
Gall bladder contents	GB-cont	71
Heart wall	Ht-wall	87
Right kidney cortex	RKidney-C	92
Right kidney medulla	RKidney-M	93
Right kidney pelvis	RKidney-P	94
Right kidney C+M+P	RKidney	92–94
Left kidney cortex	LKidney-C	89
Left kidney medulla	LKidney-M	90
Left kidney pelvis	LKidney-P	91
Left kidney C+M+P	LKidney	89–91
RKidney + LKidney	Kidneys	89–94
Liver	Liver	95
Lymph nodes, except LN-ET + LN-Th	Lymph	102–105
Muscle	Muscle	106–109
Right ovary	ROvary	112
Left ovary	LOvary	111
ROvary + LOvary	Ovaries	111, 112
Pancreas	Pancreas	113
Pituitary gland	P-gland	114
Prostate	Prostate	115
Salivary glands	S-glands	120, 121
Skin	Skin	122–125
Spinal cord	Sp-cord	126

Table C.1 (*continued*)

Source region	Acronym	ID number(s)
Spleen	Spleen	127
Testes	Testes	129, 130
Thymus	Thymus	131
Thyroid	Thyroid	132
Ureters	Ureters	135, 136
Urinary bladder wall	UB-wall	137
Urinary bladder contents	UB-cont	138
Uterus/cervix	Uterus	139
Adipose/residual tissue	Adipose	62, 64, 116–119
Total body tissues (total body minus contents of walled organs)	T-body	††
Soft tissue (T-body – mineral bone)	S-tissue	‡‡

* The surface voxels of the tongue have been segmented as 'oral cavity, tongue'. They are considered for both source regions – oral cavity as well as tongue.

† Blood: 9–12, 88, 96, 98, plus blood contained in the organs and tissues.

‡ Cortical bone mineral: 13, 16, 19, 22, 24, 26, 28, 31, 34, 37, 39, 41, 43, 45, 47, 49, 51, 53, 55.

§ Trabecular bone mineral: mineral bone fraction of 14, 17, 20, 23, 25, 27, 29, 32, 35, 38, 40, 42, 44, 46, 48, 50, 52, 54, 56.

¶ Cortical bone marrow: 15, 18, 21, 30, 33, 36.

** Trabecular bone marrow: marrow fraction of 14, 17, 20, 23, 25, 27, 29, 32, 35, 38, 40, 42, 44, 46, 48, 50, 52, 54, 56 (red and yellow marrow).

†† Total body tissues: 1–70, 72, 74, 76, 78, 80, 82, 84, 86–137, 139.

‡‡ Soft tissue: 1–12, 15, 18, 21, 30, 33, 36, 57–70, 72, 74, 76, 78, 80, 82, 84, 86–127, 129–137, 139, plus soft tissue fraction of 14, 17, 20, 23, 25, 27, 29, 32, 35, 38, 40, 42, 44, 46, 48, 50, 52, 54, 56.

C.1. References

ICRP, 1994. Human respiratory tract model for radiological protection. ICRP Publication 66. Ann. ICRP 24(1–3).

ICRP, 2006. Human alimentary tract model for radiological protection. ICRP Publication 100. Ann. ICRP 36(1–2).

ANNEX D. LIST OF TARGET REGIONS, ACRONYMS, AND ID NUMBERS

(D 1) Table D.1 establishes a set of acronyms for the target regions. The organs contributing to effective dose are listed first, followed by the regions of the Human Alimentary Tract Model (ICRP, 2006), the Human Respiratory Tract Model (ICRP, 1994), and the systemic regions. The third column gives the ID numbers in the phantoms that make up the respective tissue or – if these are too many – a footnote to this table where the sub-division of the tissue is expanded in detail.

Table D.1. List of target regions, their acronyms, and corresponding ID numbers in the phantoms.

Target region	Acronym	ID number(s)
Active (red) marrow	R-marrow	*
Colon	Colon	76, 78, 80, 82, 84, 86
RLung + LLung	Lungs	96–99
Stomach wall	St-wall	72
Breast-a + Breast-g	Breast	62–65
ROvary + LOvary	Ovaries	111, 112
Testes	Testes	129, 130
Urinary bladder wall	UB-wall	137
Oesophagus wall	Oesophagus	110
Liver	Liver	95
Thyroid	Thyroid	132
50-μm endosteal region	Endost-BS	†
Brain	Brain	61
Salivary glands	S-glands	120, 121
Skin	Skin	122–125
RAdrenal + LAdrenal	Adrenals	1, 2
ET region	ET	3, 4
Gall bladder wall	GB-wall	70
Heart wall	Ht-wall	87
RKidney + LKidney	Kidneys	89–94
Lymph nodes, except LN-ET + LN-Th	Lymph	102–105
Muscle	Muscle	106–109
Oral mucosa	O-mucosa	5, 6
Pancreas	Pancreas	113
Prostate	Prostate	115
Small intestine wall	SI-wall	74
Spleen	Spleen	127
Thymus	Thymus	131
Uterus/cervix	Uterus	139
Tongue	Tongue	5, 133
Tonsils	Tonsils	134
Right colon wall (ascending + right transverse)	RC-wall	76, 78
Left colon wall (left transverse + descending)	LC-wall	80, 82
Sigmoid colon wall + rectum wall	RSig-wall	84, 86
Basal cells of anterior nasal passages	ET1-bas	3
Basal cells of posterior nasal passages + pharynx	ET2-bas	4
Lymph nodes of ET region	LN-ET	100

(*continued on next page*)

Table D.1 (*continued*)

Target region	Acronym	ID number(s)
Basal cells of bronchi	Bronchi-bas	8
Secretory cells of bronchi	Bronchi-sec	8
Secretory cells of bronchioles	Brchiol-sec	96–99
Alveolar-interstitium	AI	97, 99
Lymph nodes in thoracic region	LN-Th	101
Right lung lobe	RLung	98, 99
Left lung lobe	LLung	96, 97
Right adrenal gland	RAdrenal	2
Left adrenal gland	LAdrenal	1
Right breast adipose	RBreast-a	64
Right breast glandular	RBreast-g	65
Left breast adipose	LBreast-a	62
Left breast glandular	LBreast-g	63
RBreast-a + RBreast-g	RBreast	64, 65
LBreast-a + LBresat-g	LBreast	62, 63
RBreast-a + LBreast-a	Breast-a	62, 64
RBreast-g + LBreast-g	Breast-g	63, 65
Lenses of eye	Eye-lens	66, 68
Right kidney cortex	RKidney-C	92
Right kidney medulla	RKidney-M	93
Right kidney pelvis	RKidney-P	94
Right kidney C+M+P	RKidney	92–94
Left kidney cortex	LKidney-C	89
Left kidney medulla	LKidney-M	90
Left kidney pelvis	LKidney-P	91
Left kidney C+M+P	LKidney	89–91
Right ovary	ROvary	112
Left ovary	LOvary	111
Pituitary gland	P-gland	114
Spinal cord	Sp-cord	126
Ureters	Ureters	135, 136
Adipose/residual tissue	Adipose	62, 64, 116–119

ET, extrathoracic.

[*] Red bone marrow fraction in organ IDs 14, 25, 27, 29, 40, 42, 44, 46, 48, 50, 52, 54, 56.

[†] Endosteum fraction in organ IDs 14, 15, 17, 18, 20, 21, 23, 25, 27, 29, 30, 32, 33, 35, 36, 38, 40, 42, 44, 46, 48, 50, 52, 54, 56.

D.1. References

ICRP, 1994. Human respiratory tract model for radiological protection. ICRP Publication 66. Ann. ICRP 24(1–3).

ICRP, 2006. Human alimentary tract model for radiological protection. ICRP Publication 100. Ann. ICRP 36(1–2).

ANNEX E. DISTRIBUTIONS OF DEPTHS OF SELECTED ORGANS/TISSUES

(E 1) In Figs. E.1–E.13, depth distributions below the body surfaces at the front, back, right, left, bottom, and top are shown for those organs and tissues that contribute to effective dose with specific tissue weighting factors, except the endosteal tissues for which no geometrical representation is available in the reference computational phantoms.

(E 2) The distributions have been evaluated for 10 million points sampled randomly in the organs considered. Due to the curved surface of the body, these depths are not below planar, but below uneven surfaces. They indicate the amount of overlying tissue by which each point of an organ or tissue is shielded from radiation impinging from the front, back, left, right, top, or bottom.

(E 3) Together with the attenuation properties of the overlying tissues and the organ considered, the depth below the surface is a parameter that significantly influences the dose coefficients from external radiation.

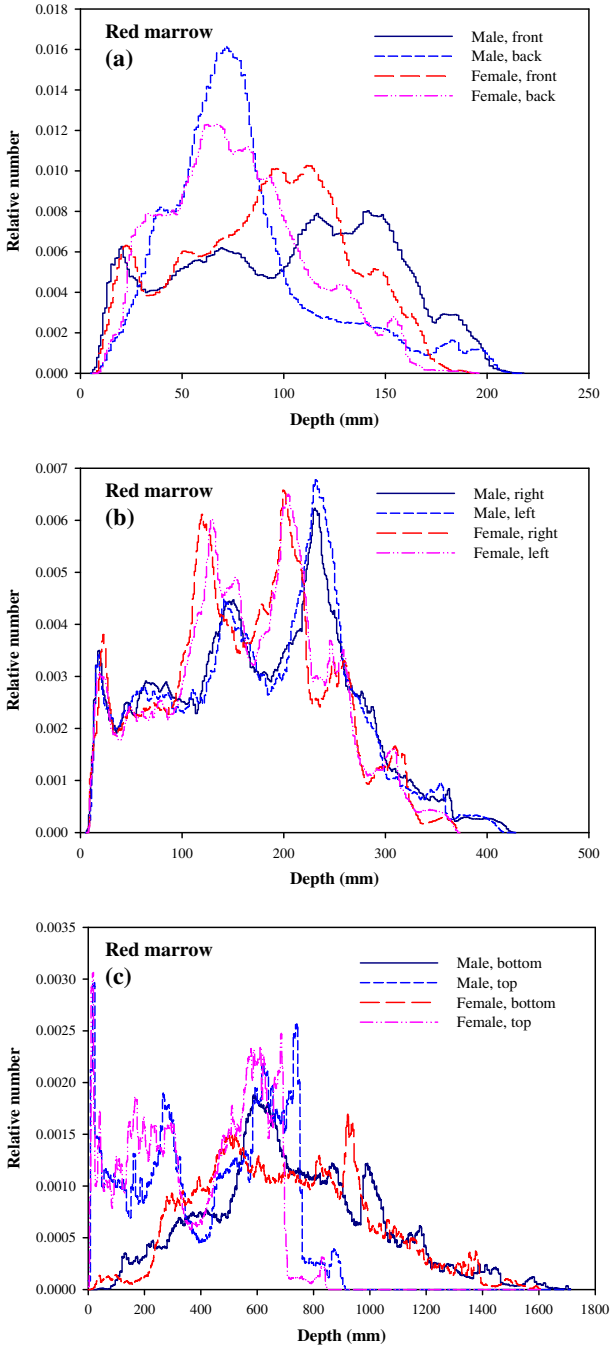

Fig. E.1. Distribution of depths of 10 million randomly sampled points in the red bone marrow below the body surfaces at: (a) front and back, (b) right and left, and (c) bottom and top.

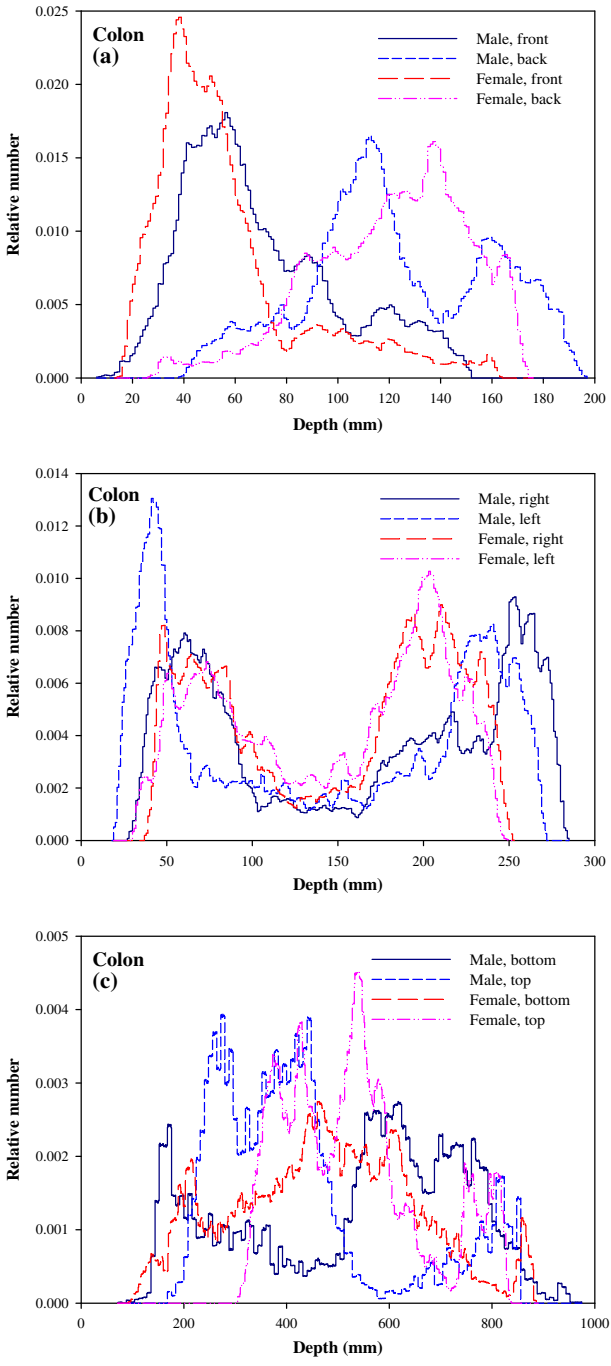

Fig. E.2. Distribution of depths of 10 million randomly sampled points in the colon wall below the body surfaces at: (a) front and back, (b) right and left, and (c) bottom and top.

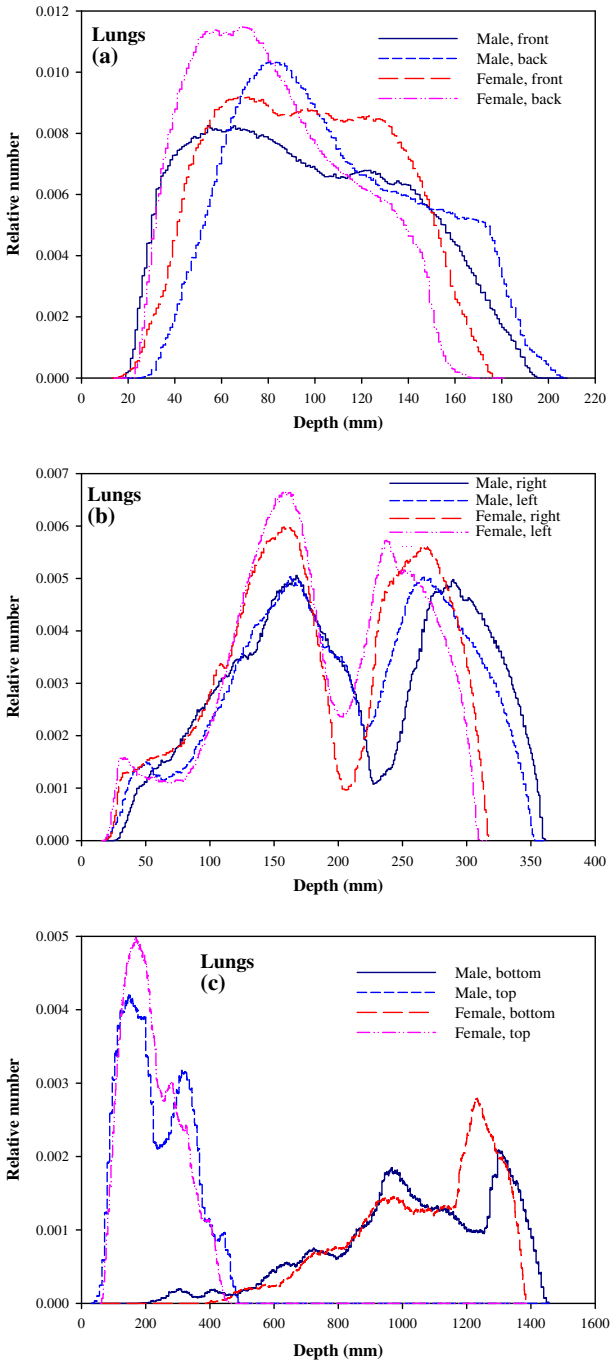

Fig. E.3. Distribution of depths of 10 million randomly sampled points in the lungs below the body surfaces at: (a) front and back, (b) right and left, and (c) bottom and top.

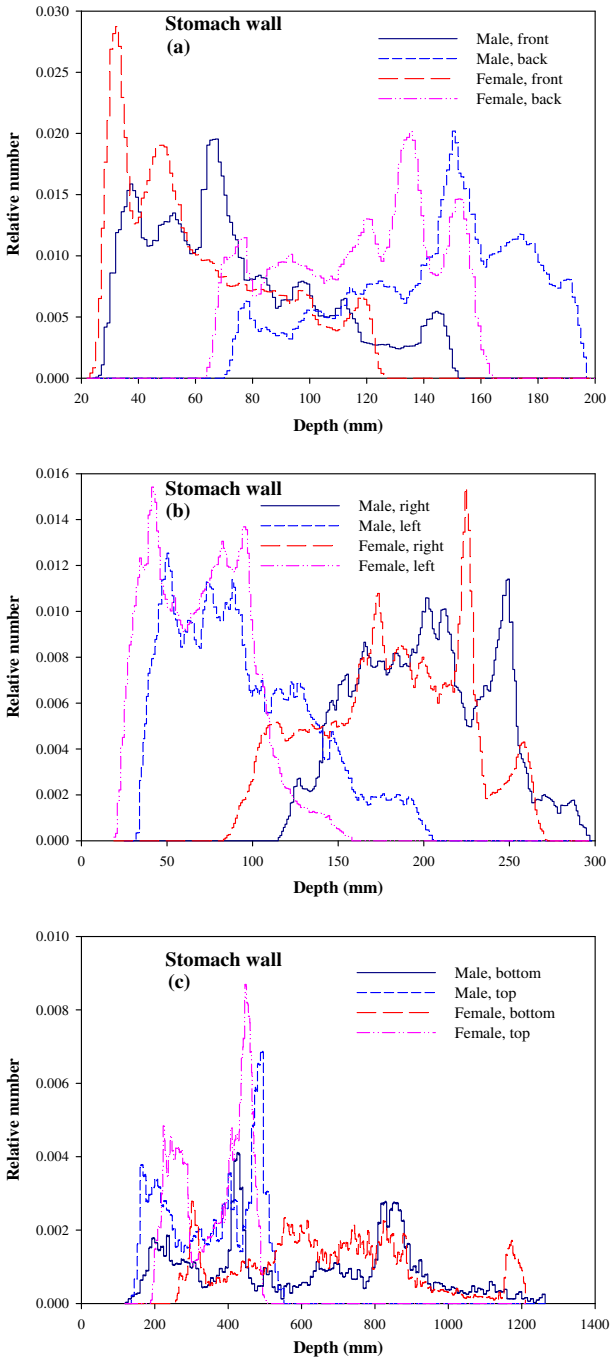

Fig. E.4. Distribution of depths of 10 million randomly sampled points in the stomach wall below the body surfaces at: (a) front and back, (b) right and left, and (c) bottom and top.

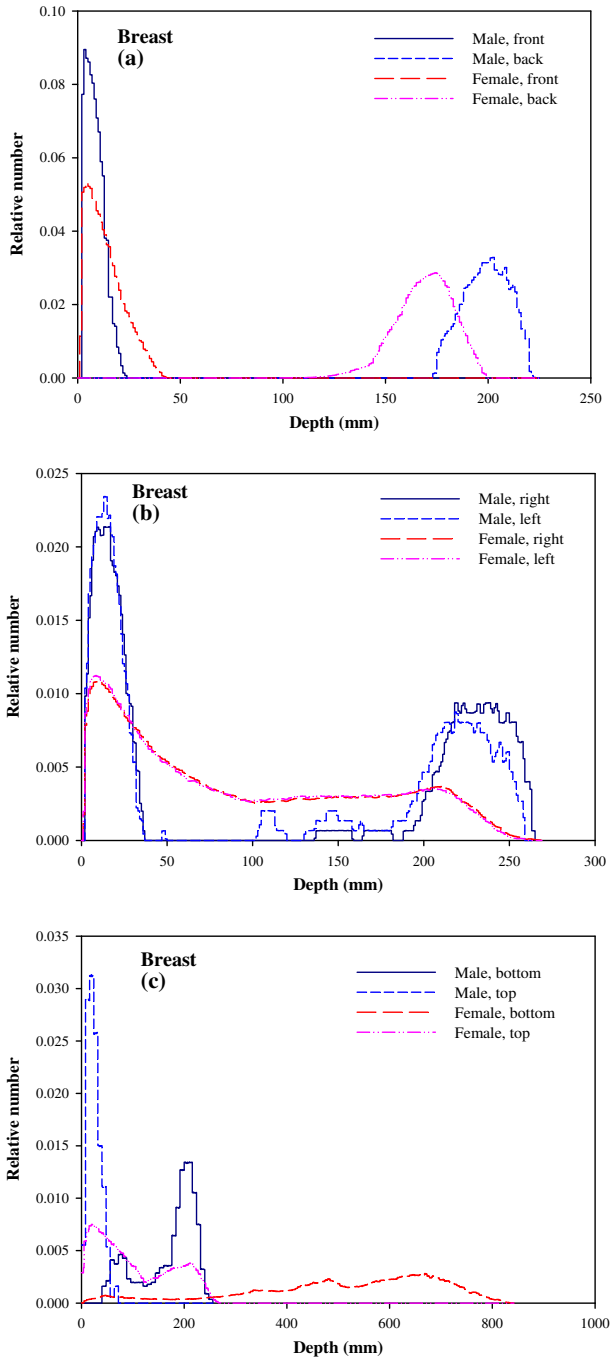

Fig. E.5. Distribution of depths of 10 million randomly sampled points in the breast below the body surfaces at: (a) front and back, (b) right and left, and (c) bottom and top.

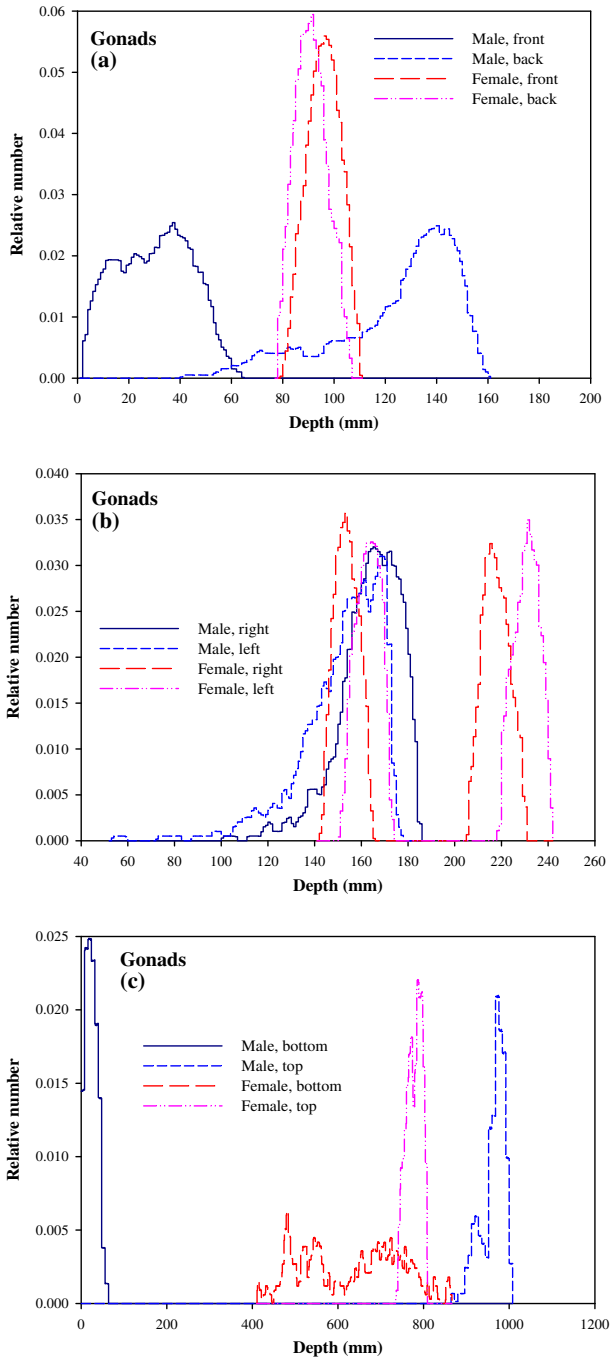

Fig. E.6. Distribution of depths of 10 million randomly sampled points in the gonads below the body surfaces at: (a) front and back, (b) right and left, and (c) bottom and top.

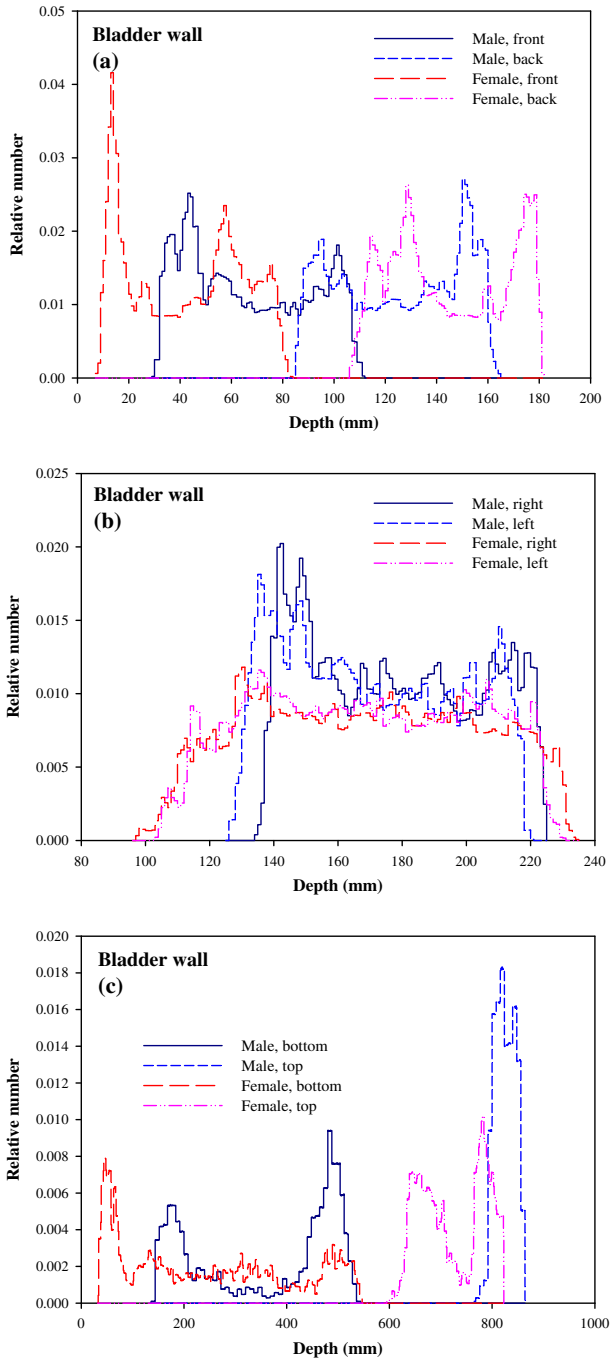

Fig. E.7. Distribution of depths of 10 million randomly sampled points in the urinary bladder wall below the body surfaces at: (a) front and back, (b) right and left, and (c) bottom and top.

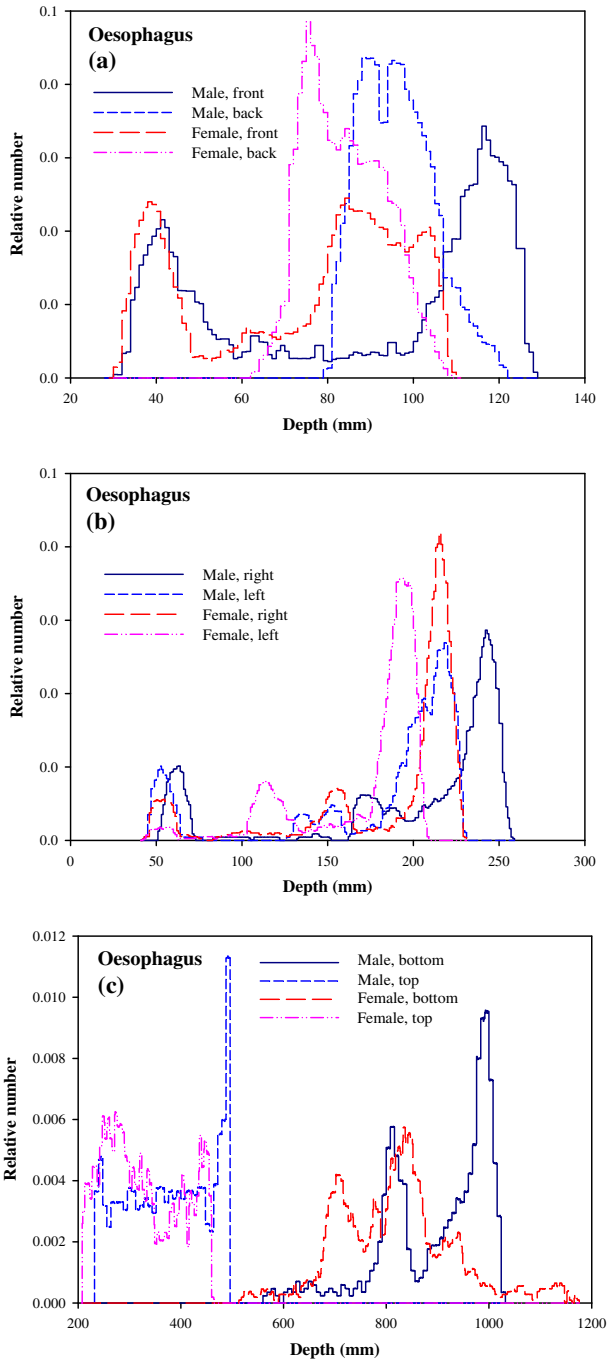

Fig. E.8. Distribution of depths of 10 million randomly sampled points in the oesophagus below the body surfaces at: (a) front and back, (b) right and left, and (c) bottom and top.

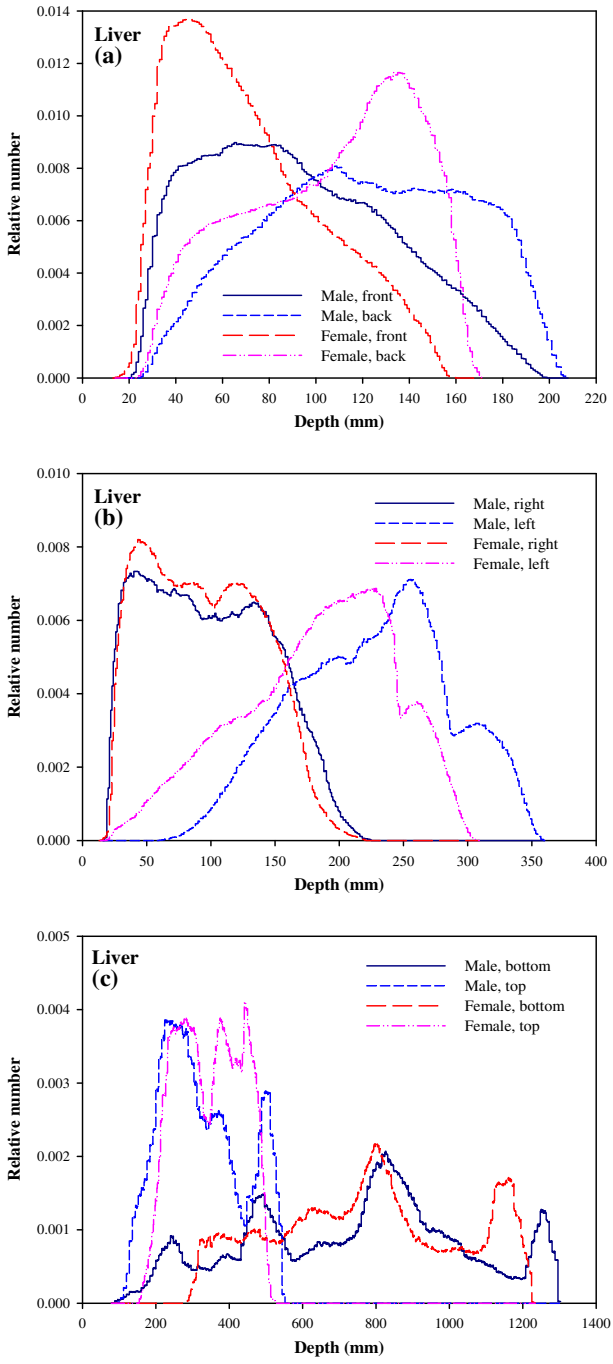

Fig. E.9. Distribution of depths of 10 million randomly sampled points in the liver below the body surfaces at: (a) front and back, (b) right and left, and (c) bottom and top.

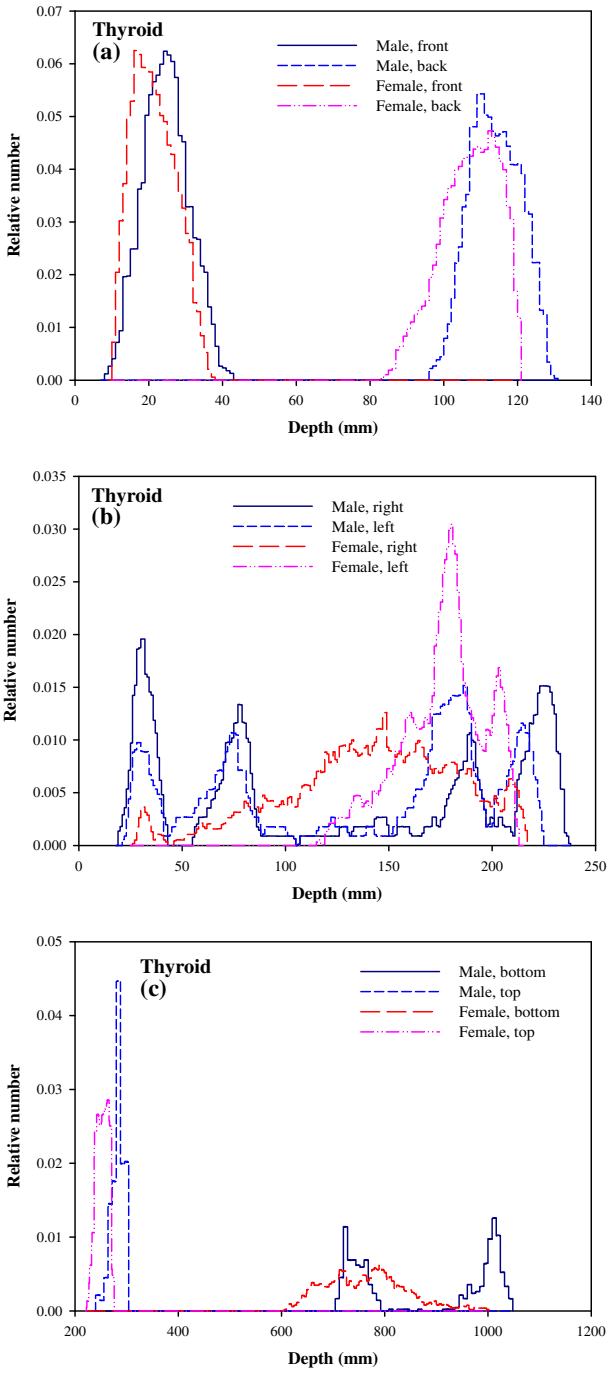

Fig. E.10. Distribution of depths of 10 million randomly sampled points in the thyroid below the body surfaces at: (a) front and back, (b) right and left, and (c) bottom and top.

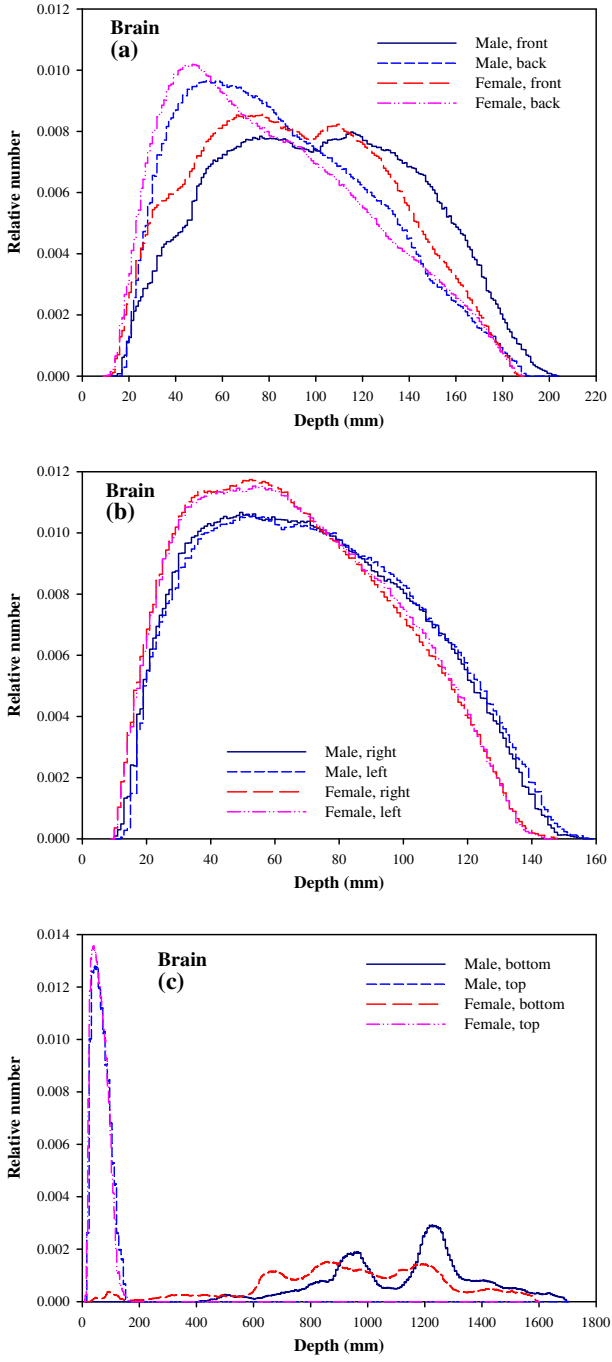

Fig. E.11. Distribution of depths of 10 million randomly sampled points in the brain below the body surfaces at: (a) front and back, (b) right and left, and (c) bottom and top.

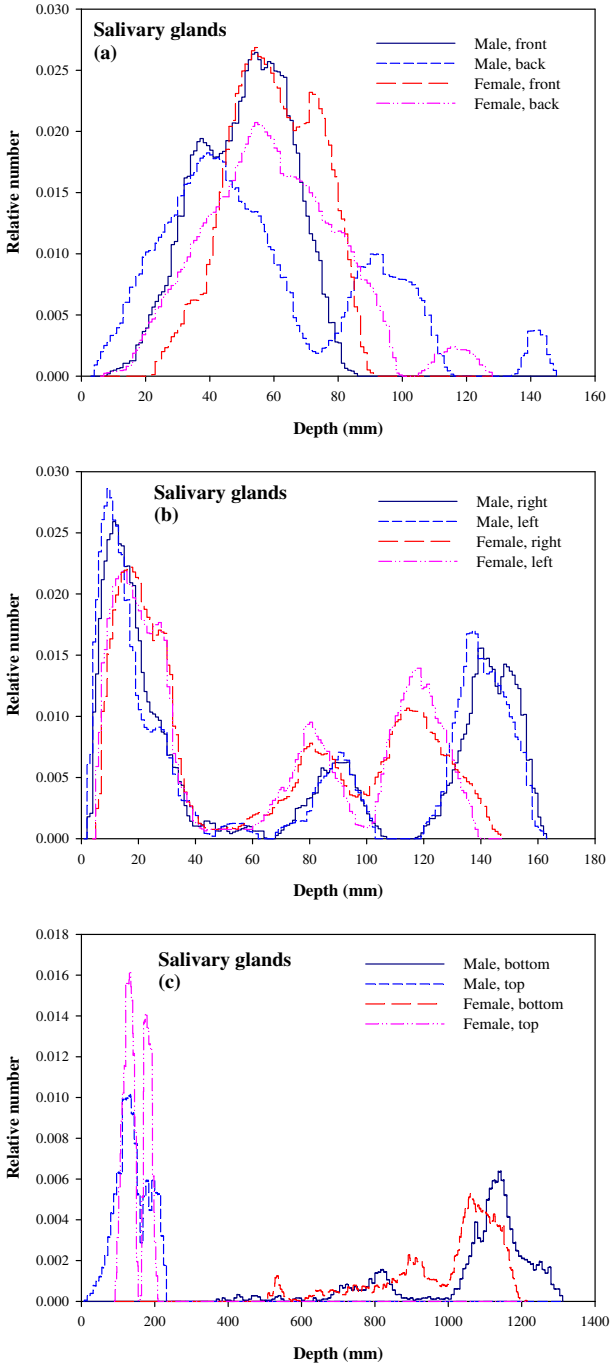

Fig. E.12. Distribution of depths of 10 million randomly sampled points in the salivary glands below the body surfaces at: (a) front and back, (b) right and left, and (c) bottom and top.

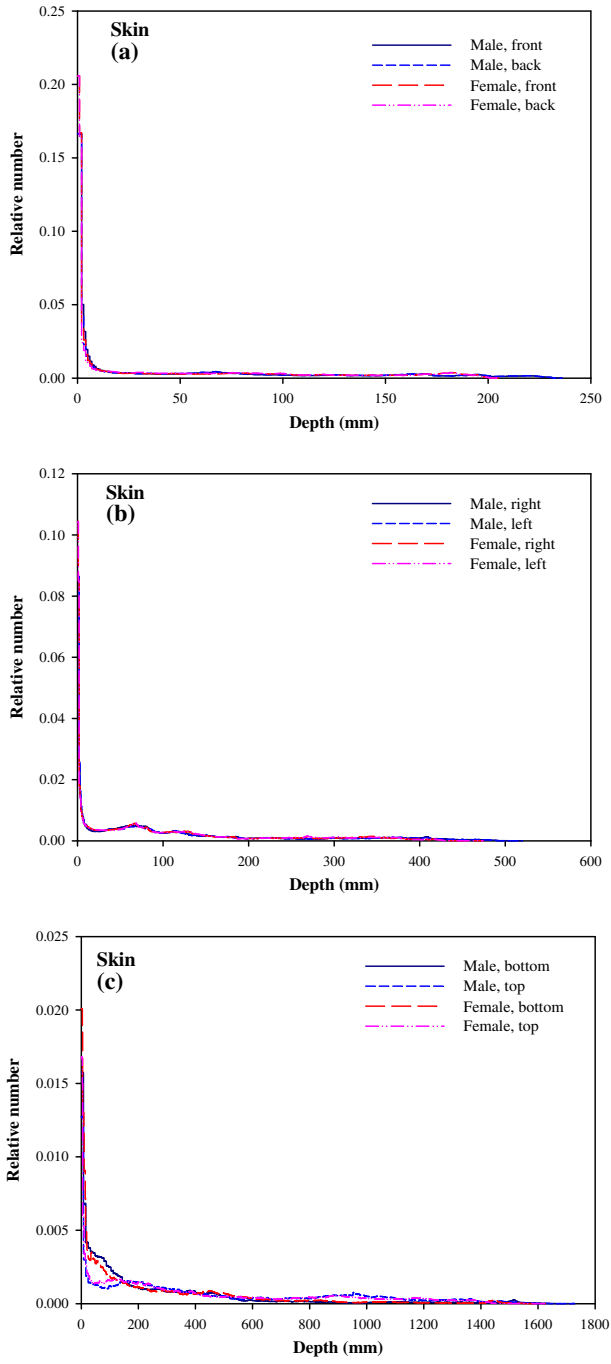

Fig. E.13. Distribution of depths of 10 million randomly sampled points in the skin below the body surfaces at: (a) front and back, (b) right and left, and (c) bottom and top.

ANNEX F. CHORD-LENGTH DISTRIBUTIONS BETWEEN SELECTED ORGAN PAIRS (SOURCE/TARGET TISSUES)

(F 1) In Figs. F.1–F.4, chord-length distributions are shown between mineral bone, liver, lungs, and thyroid as source organs and the target organs red bone marrow, colon wall, lungs, stomach wall, and breast. Ten million point pairs have been sampled randomly in the organs considered, and the distributions of the resulting chord-lengths evaluated.

(F 2) The distance between source and target region is a parameter influencing the specific absorbed fractions in internal dosimetry.

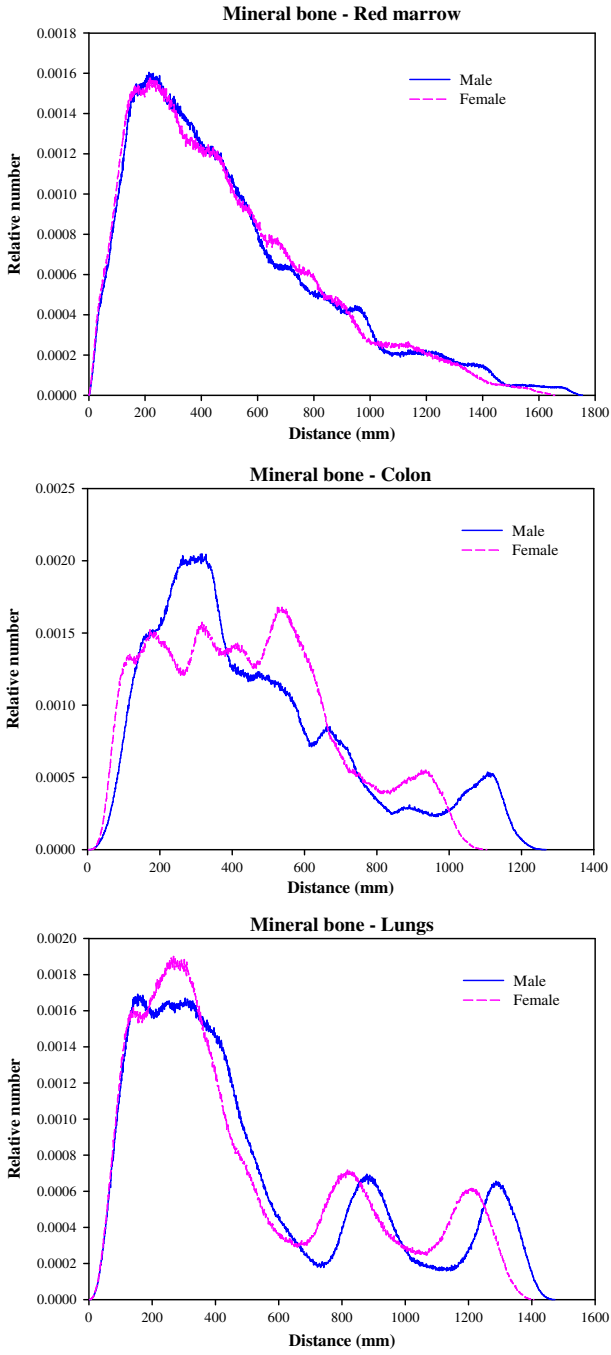

Fig. F.1. Distribution of distances between 10 million randomly sampled point pairs in mineral bone (source region) and red bone marrow, colon, lungs, stomach wall, and breast (target regions).

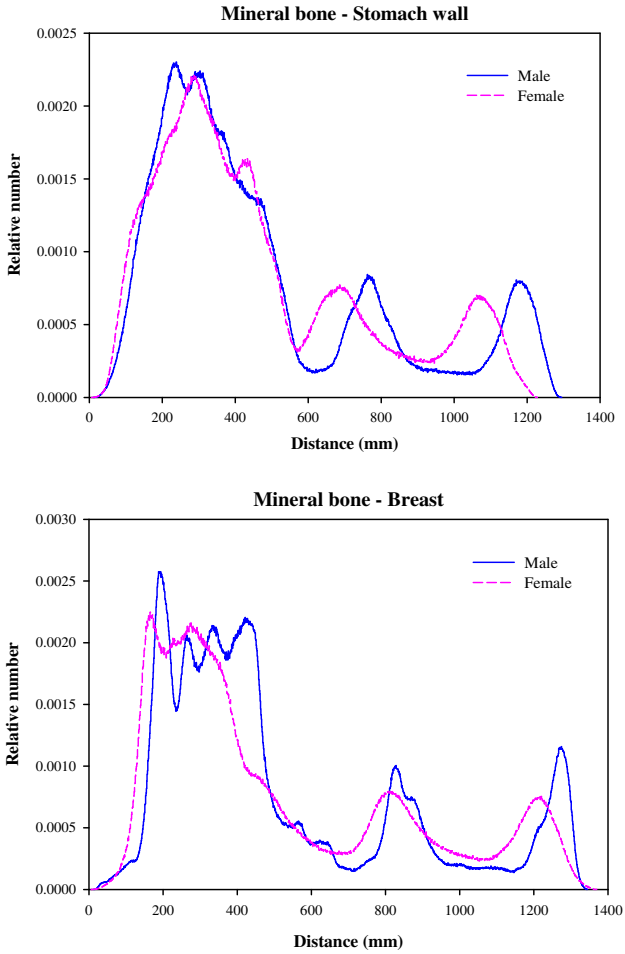

Fig. F.1 *(continued)*

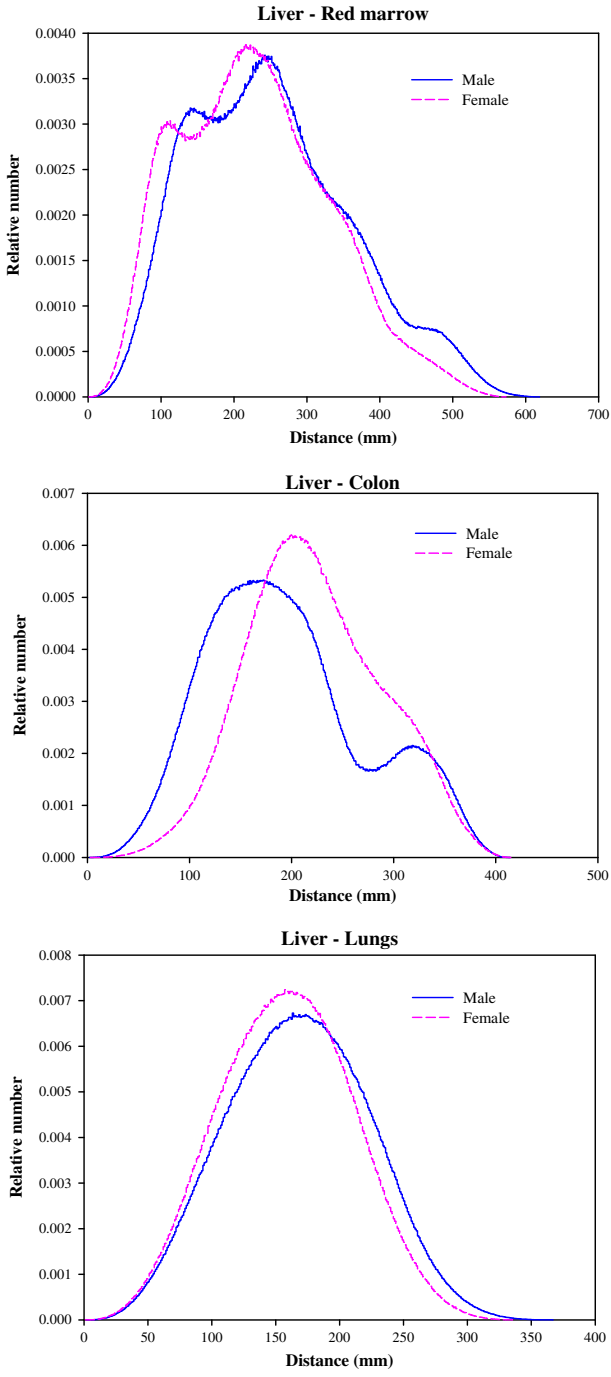

Fig. F.2. Distribution of distances between 10 million randomly sampled point pairs in liver (source region) and red bone marrow, colon, lungs, stomach wall, and breast (target regions).

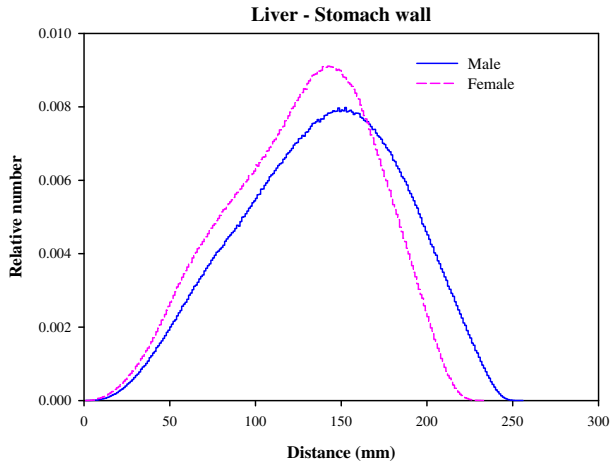

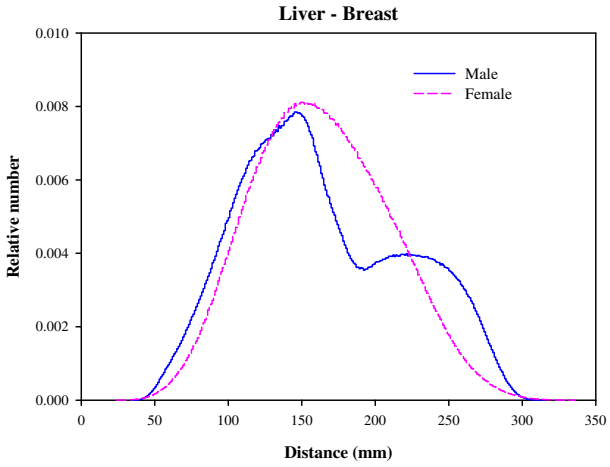

Fig. F.2 *(continued)*

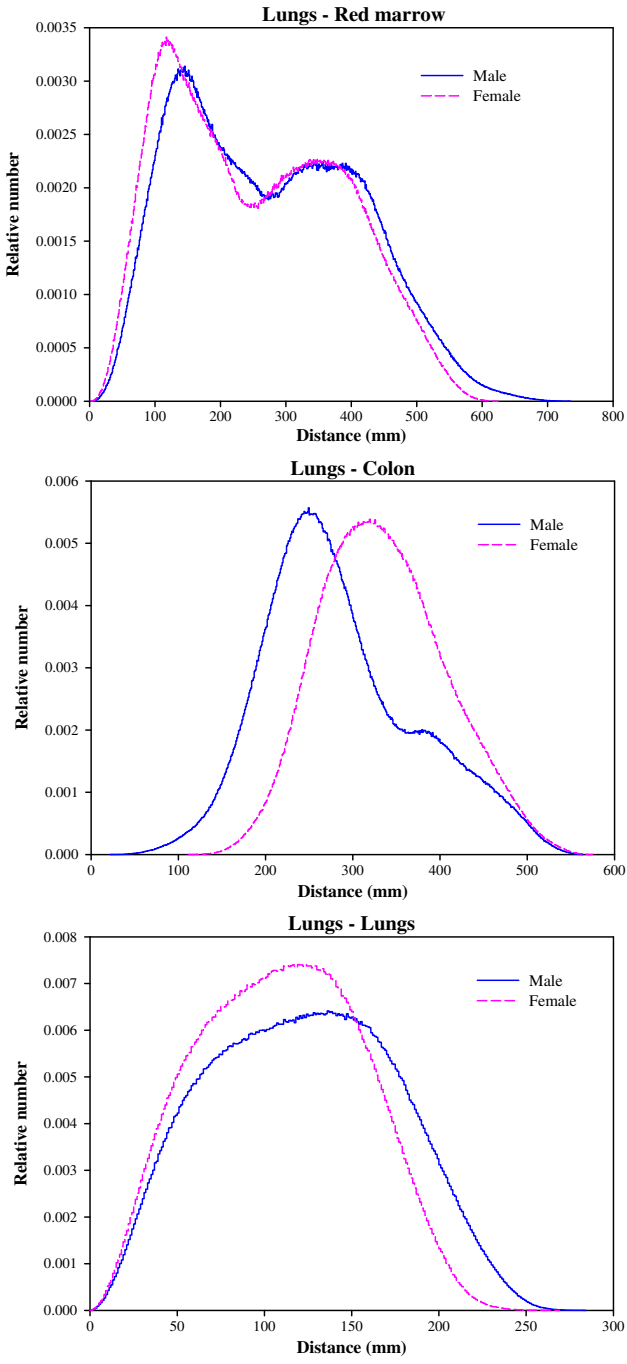

Fig. F.3. Distribution of distances between 10 million randomly sampled point pairs in lungs (source region) and red bone marrow, colon, lungs, stomach wall, and breast (target regions).

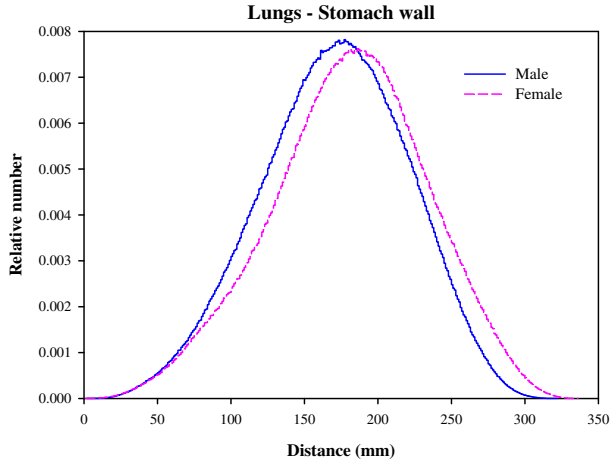

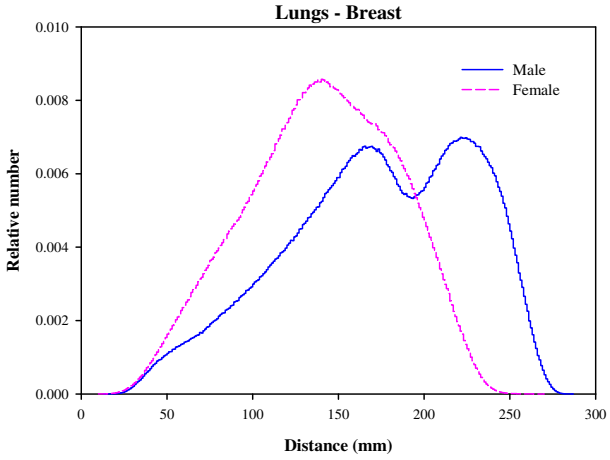

Fig. F.3 *(continued)*

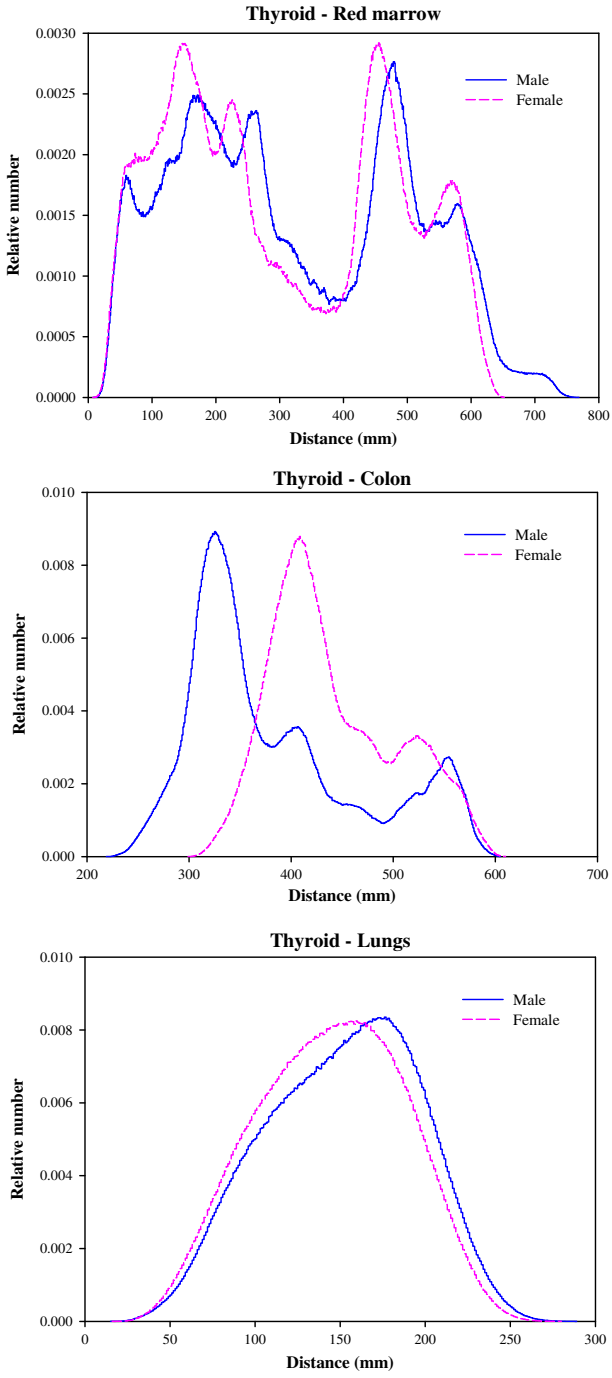

Fig. F.4. Distribution of distances between 10 million randomly sampled point pairs in thyroid (source region) and red bone marrow, colon, lungs, stomach wall, and breast (target regions).

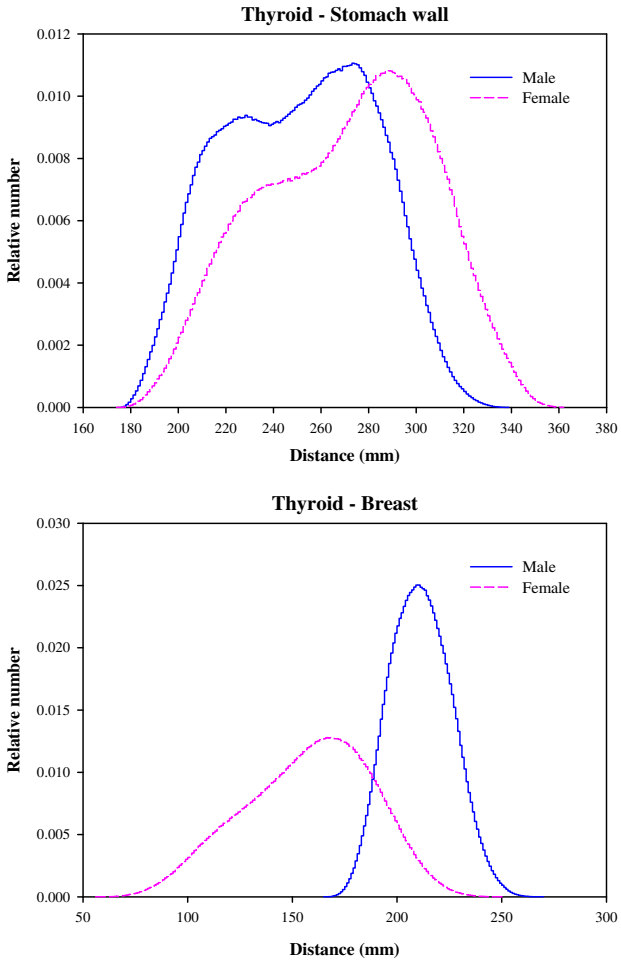

Fig. F.4 *(continued)*

ANNEX G. CROSS-SECTIONAL IMAGES

(G 1) This annex presents selected cross-sectional images of both reference computational phantoms. The cross-sectional images are presented in three different orientations, i.e. transverse, coronal, and sagittal. Each cross-sectional image presents a planar 'cut' through the three-dimensional voxel array describing the computational phantom. The transverse images show the columns (x co-ordinates) and rows (y co-ordinates) at a specific slice (z co-ordinate); the coronal images show the columns and slices at a specific row; and the sagittal images show the rows and slices at a specific column.

(G 2) The green lines indicate the location of single organs as given in the legend. The yellow lines (appearing as a coordinate cross in the figures) indicate the location of the images in the other orientations. In the transversal images, the vertical yellow line indicates the location of the sagittal image, and the horizontal yellow line indicates the location of the coronal image.

G.1. Images of the male reference computational phantom

G.1.1. Transverse (axial) images

Slice no. 147

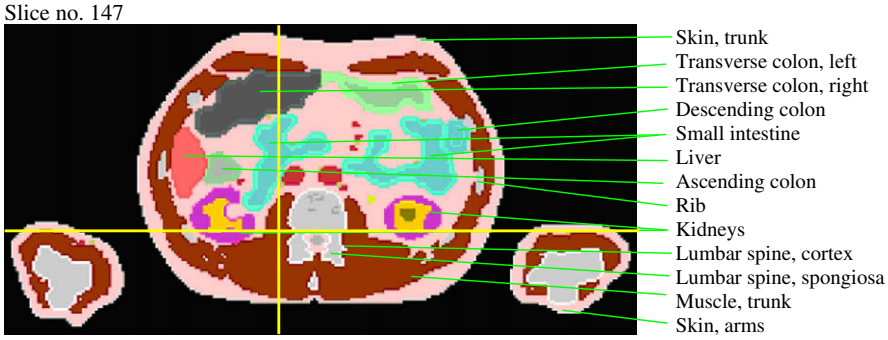

Slice no. 158

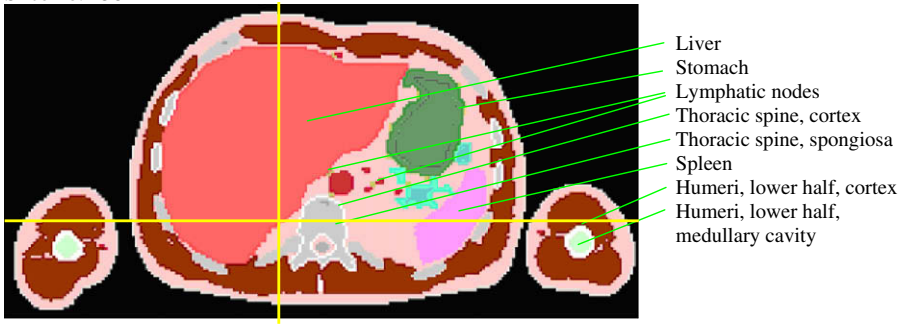

Slice no. 168

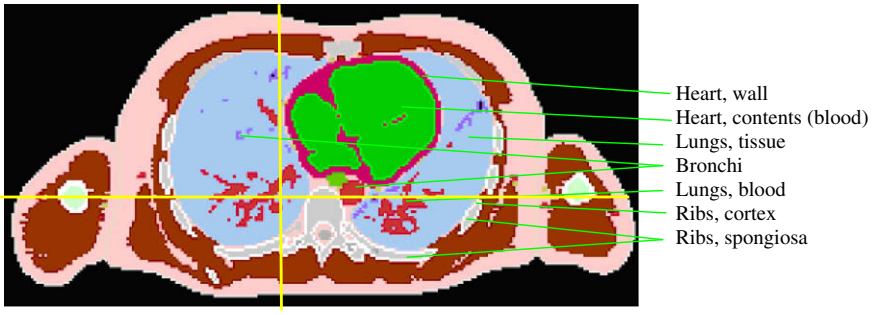

Slice no. 207

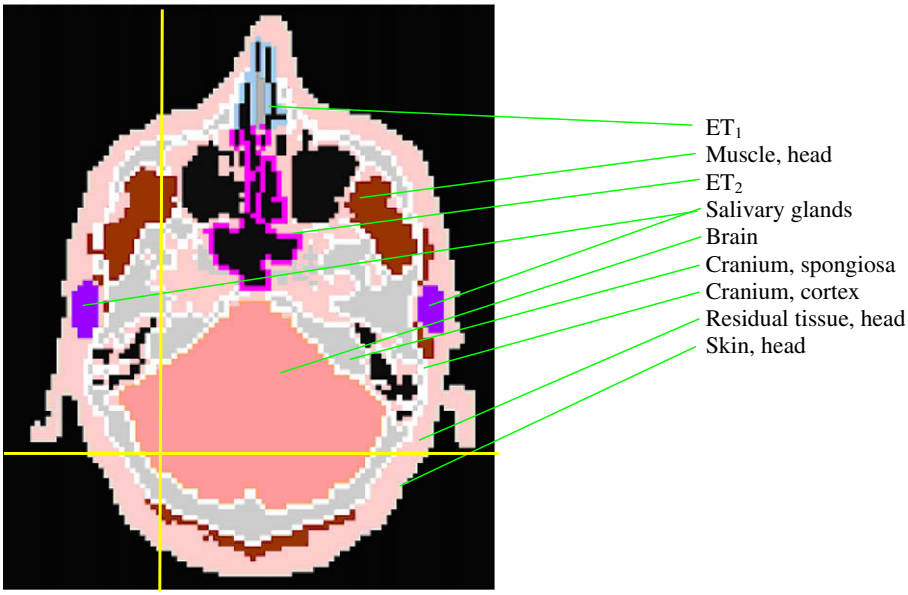
ET1
Muscle, head
ET2
Salivary glands
Brain
Cranium, spongiosa
Cranium, cortex
Residual tissue, head
Skin, head

G.1.2. Coronal and sagittal images

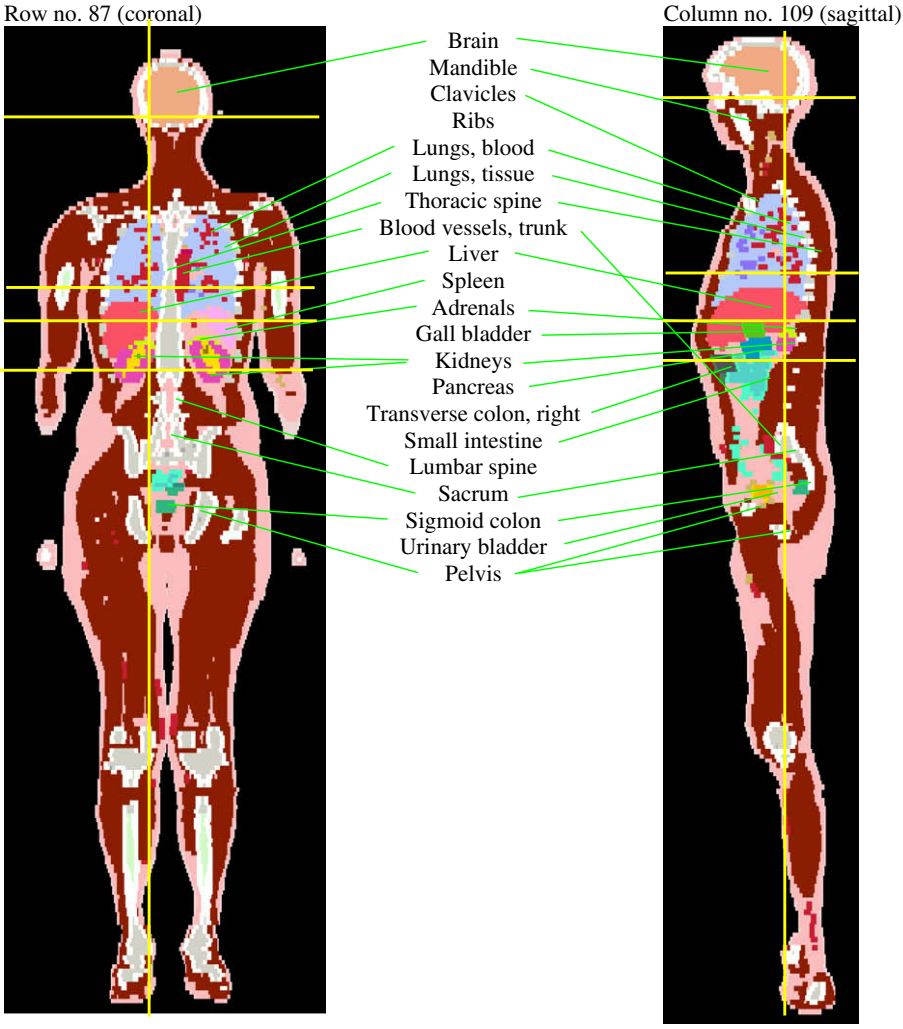

G.2. Images of the female reference computational phantom

G.2.1. Transverse (axial) images

Slice no. 187

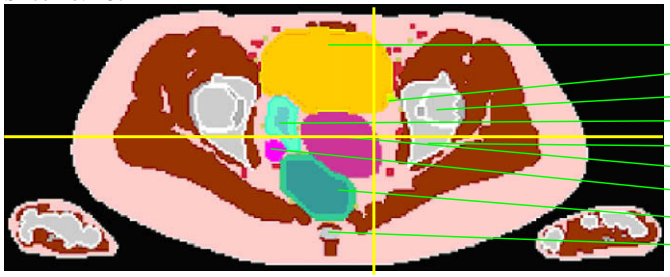

Slice no. 258

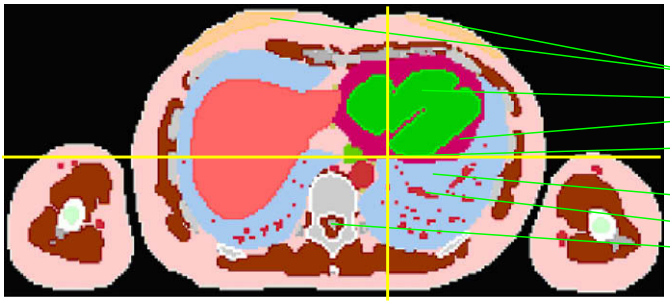

Slice no. 269

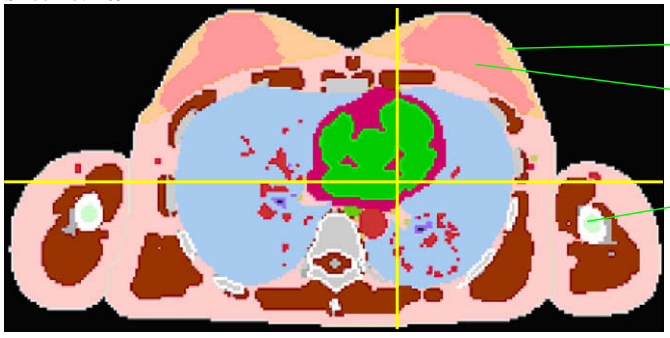

Slice no. 281

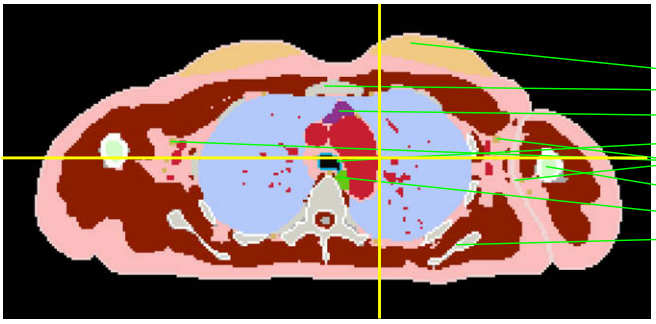

Slice no. 296

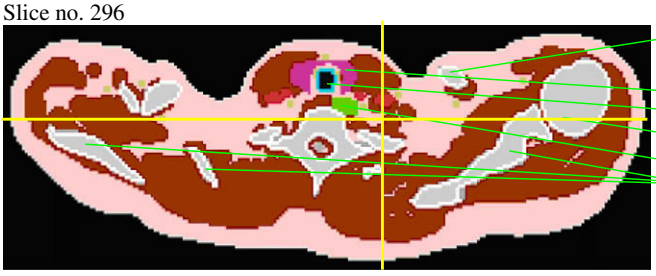

Slice no. 313

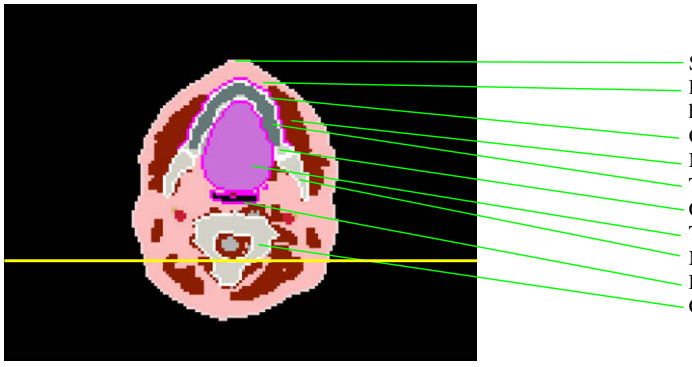

G.2.2. Coronal and sagittal images

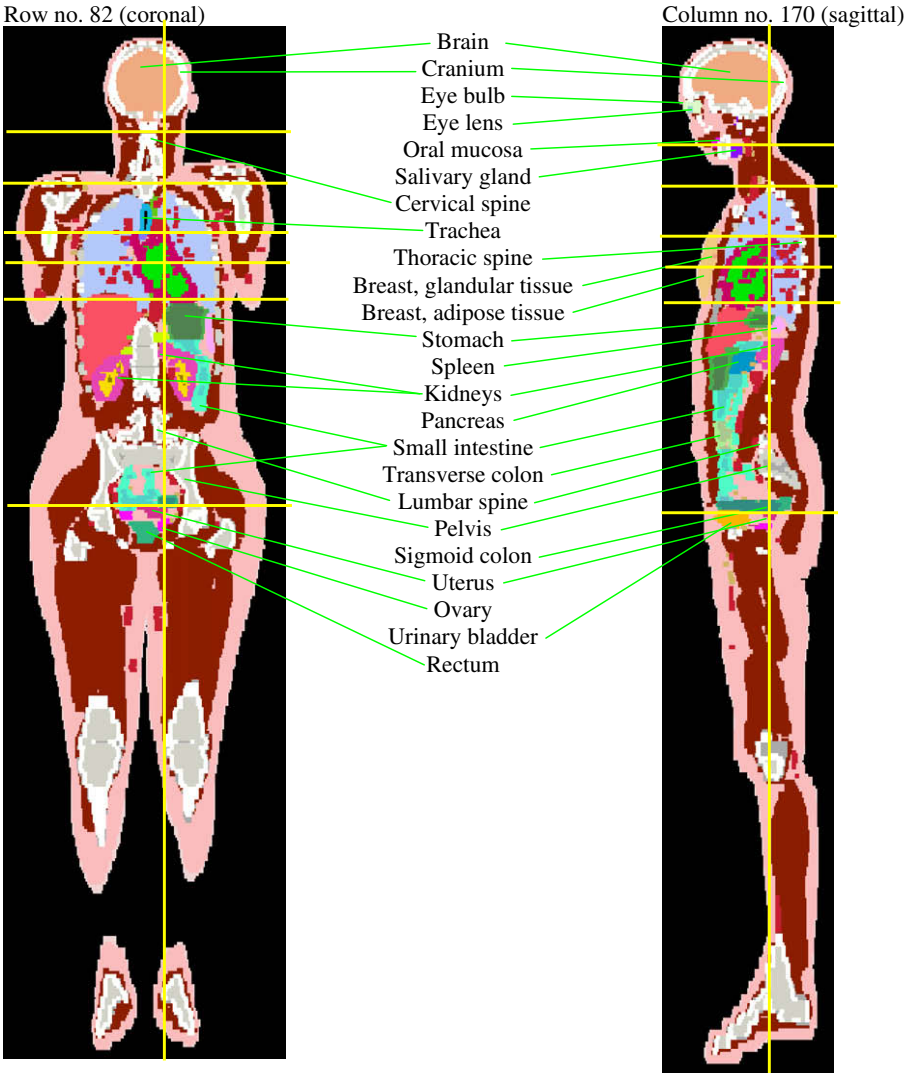

ANNEX H. SELECTED ORGAN DOSE CONVERSION COEFFICIENTS – EXTERNAL PHOTONS

(H 1) In this annex, selected organ dose conversion coefficients are given for external exposure to monoenergetic photons. The conversion coefficients are given in graphical form in terms of organ absorbed dose per air kerma free in air (in Gy/Gy). The geometries considered are unidirectional broad parallel photon beams impinging from the front (AP) and from the back (PA), as well as fully isotropic irradiation (ISO).

(H 2) The conversion coefficients are given for organs contributing to the quantity effective dose with the highest tissue weighting factors, namely colon, lungs, stomach, and breast. Conversion coefficients for the effective dose are also given.

(H 3) Figs. H.1–H.15 show data generated by the DOCAL Subgroup on External Dosimetry as part of the revision of *Publication 74* (ICRP, 1996) and ICRU Report 57 (ICRU, 1998) using the reference computational phantoms of this document and the radiation and tissue weighting factors of *Publication 103* (ICRP, 2007). The data were generated using the Monte Carlo codes EGSnrc (Kawrakow and Rogers, 2003), MCNPX (Waters, 2002; Hendricks et al., 2005) and GEANT4 (GEANT4, 2006a,b).

(H 4) The conversion coefficients for the adult male and female reference computational phantoms are compared with the respective conversion coefficients from *Publication 74* (ICRP, 1996) and ICRU Report 57 (ICRU, 1998). Thus, an indication is given of the magnitude of differences that can be expected between the present reference organ dose conversion coefficients and the reference values employing the new phantoms, as well as the revised tissue weighting factors (ICRP, 2007).

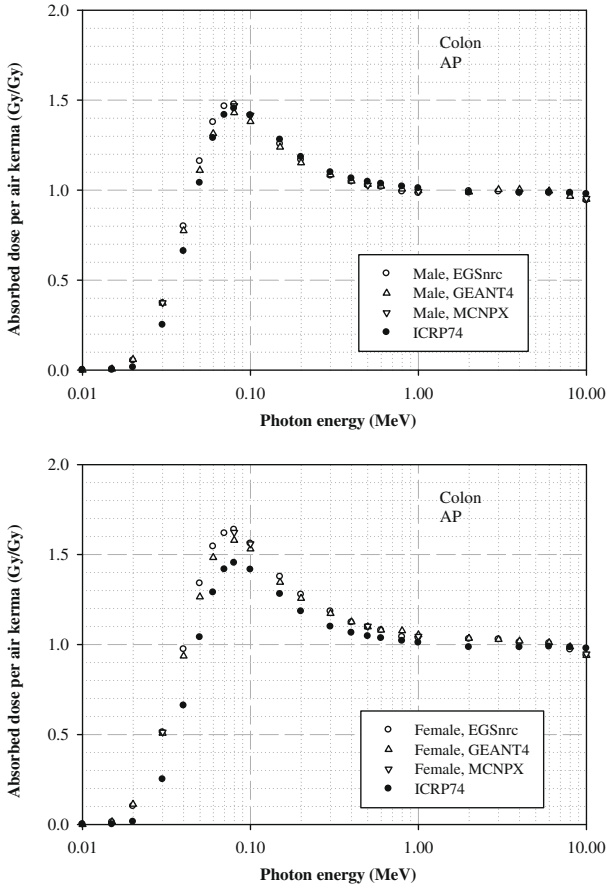

Fig. H.1. Colon absorbed dose per air kerma free-in-air for a broad parallel beam of monoenergetic photons impinging in anterior-posterior (AP) direction.

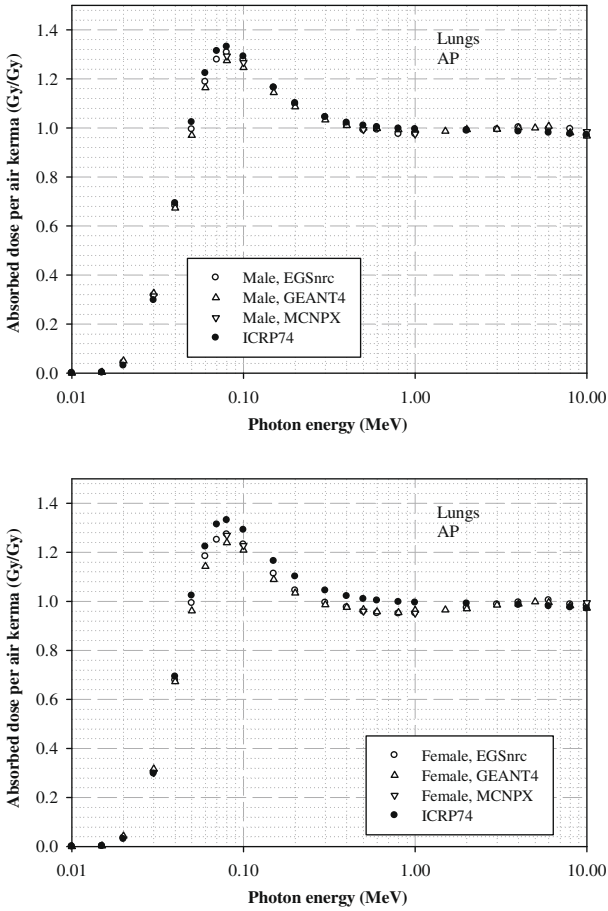

Fig. H.2. Lung absorbed dose per air kerma free-in-air for a broad parallel beam of monoenergetic photons impinging in anterior-posterior (AP) direction.

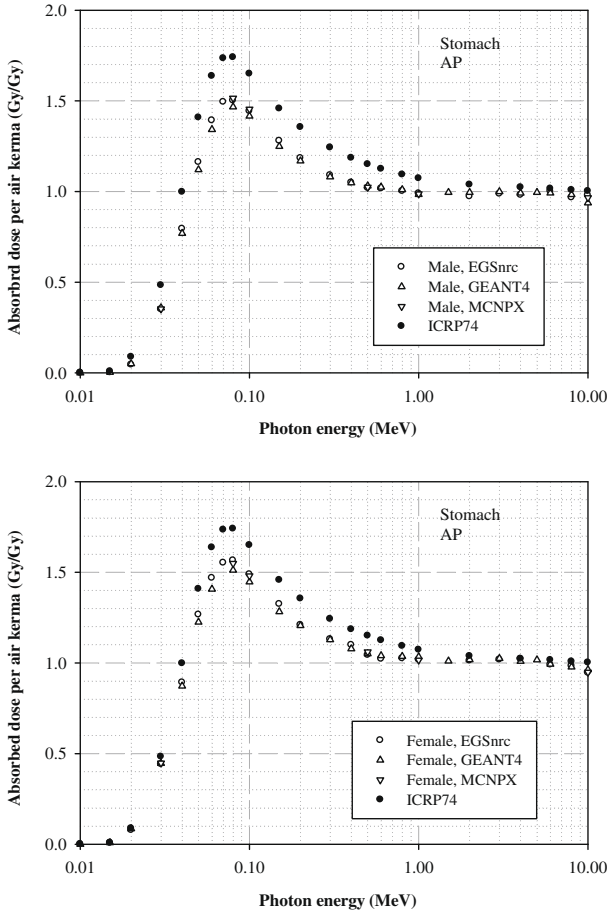

Fig. H.3. Stomach wall absorbed dose per air kerma free-in-air for a broad parallel beam of monoenergetic photons impinging in anterior-posterior (AP) direction.

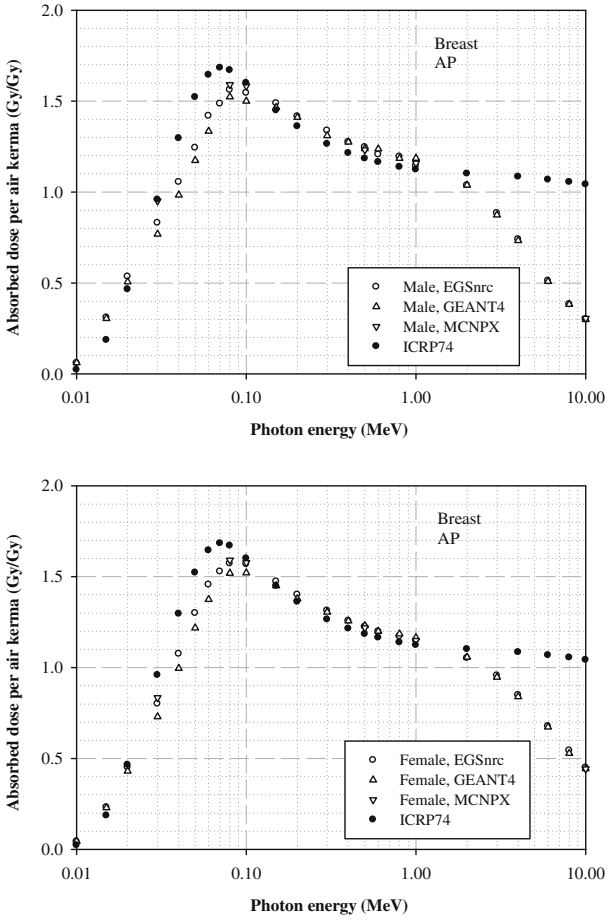

Fig. H.4. Breast absorbed dose per air kerma free-in-air for a broad parallel beam of monoenergetic photons impinging in anterior-posterior (AP) direction. The decline of the conversion coefficients for energies above 1 MeV is due to the escape of secondary electrons which has not been taken into account in the earlier calculations (ICRP, 1996; ICRU, 1998).

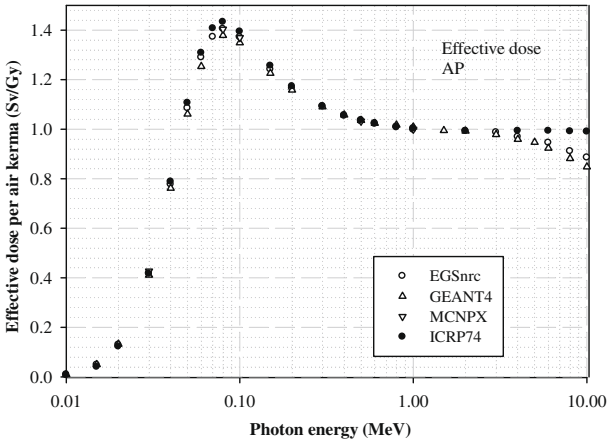

Fig. H.5. Effective dose per air kerma free-in-air for a broad parallel beam of monoenergetic photons impinging in anterior-posterior (AP) direction.

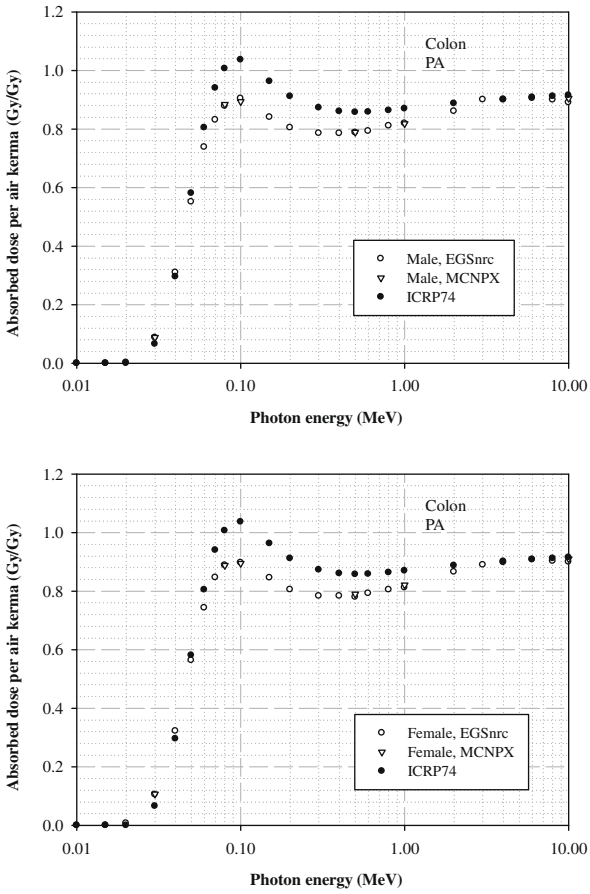

Fig. H.6. Colon absorbed dose per air kerma free-in-air for a broad parallel beam of monoenergetic photons impinging in posterior-anterior (PA) direction.

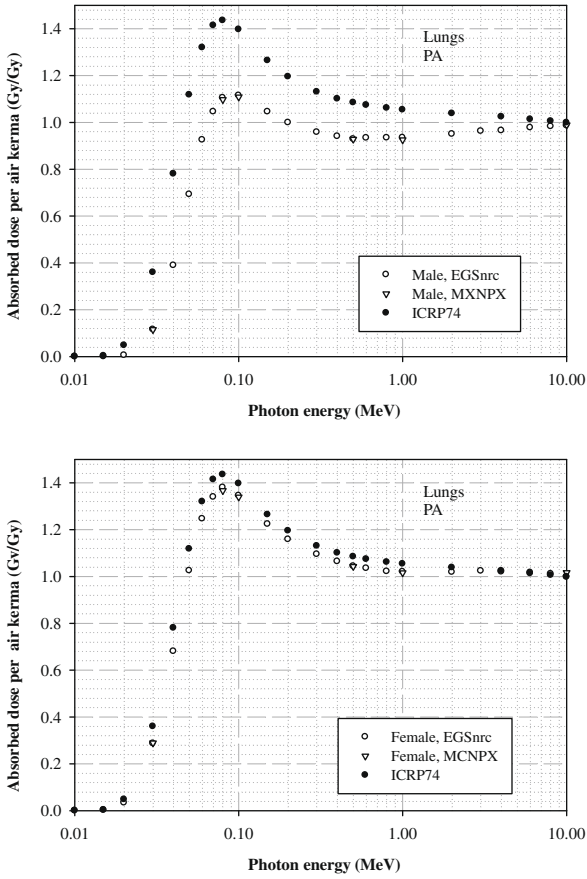

Fig. H.7. Lung absorbed dose per air kerma free-in-air for a broad parallel beam of monoenergetic photons impinging in posterior-anterior (PA) direction.

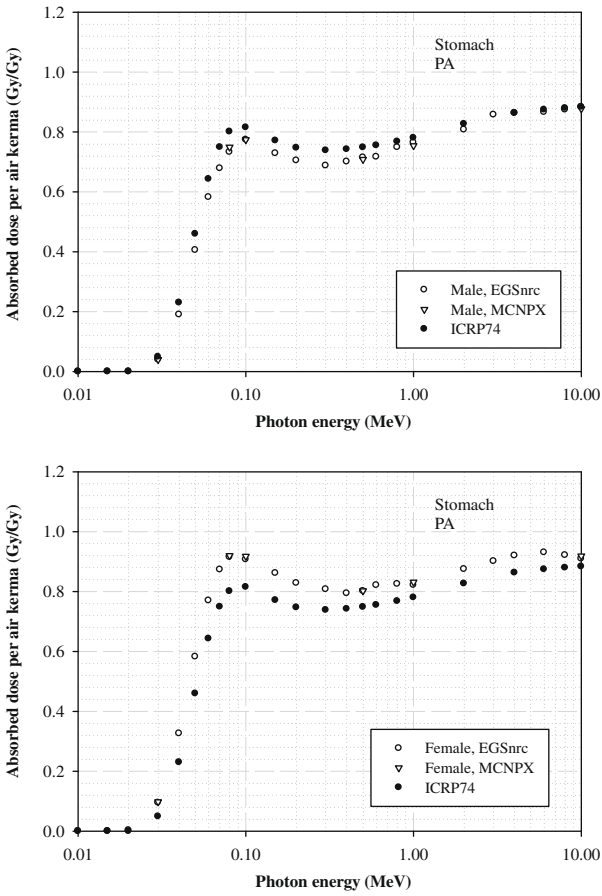

Fig. H.8. Stomach wall absorbed dose per air kerma free-in-air for a broad parallel beam of monoenergetic photons impinging in posterior-anterior (PA) direction.

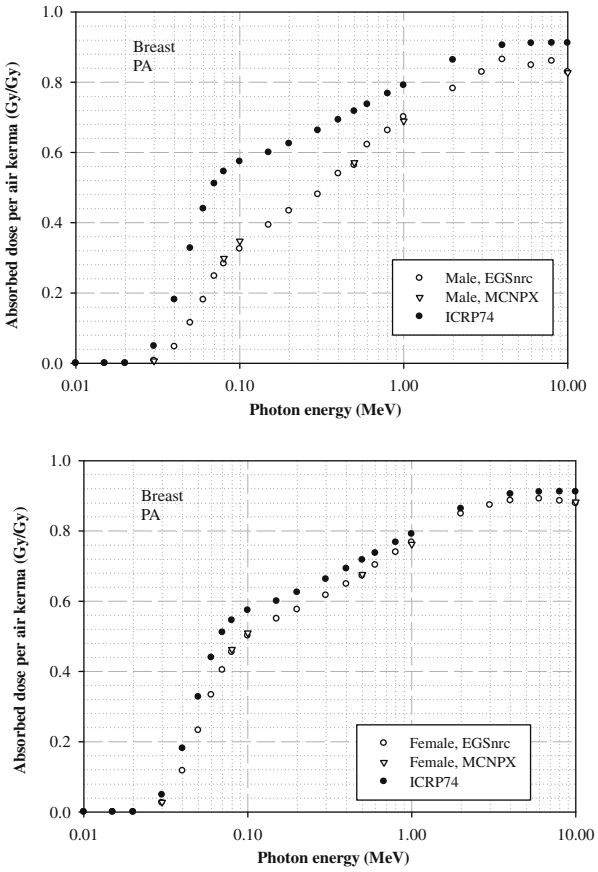

Fig. H.9. Breast absorbed dose per air kerma free-in-air for a broad parallel beam of monoenergetic photons impinging in posterior-anterior (PA) direction.

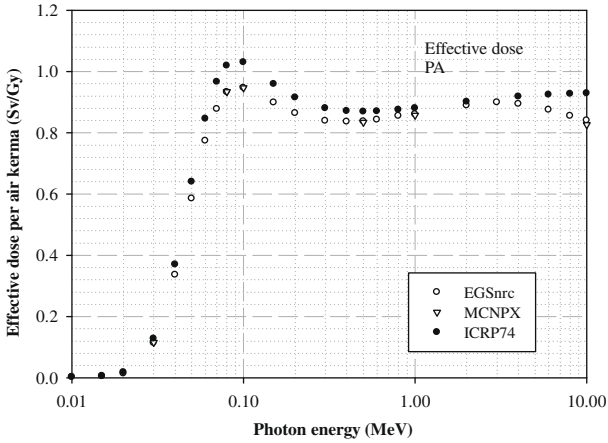

Fig. H.10. Effective dose per air kerma free-in-air for a broad parallel beam of monoenergetic photons impinging in posterior-anterior (PA) direction.

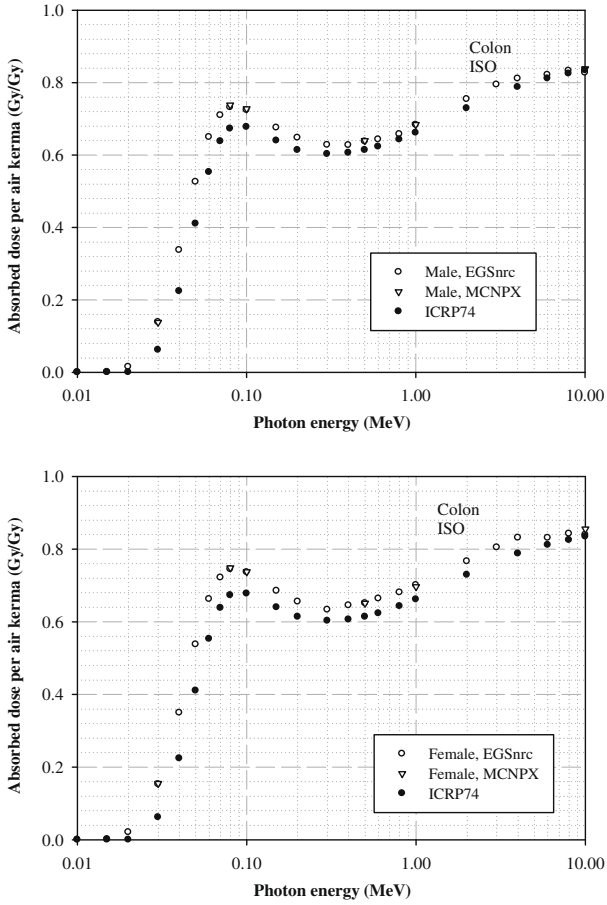

Fig. H.11. Colon absorbed dose per air kerma free-in-air for monoenergetic photons impinging isotropically (ISO).

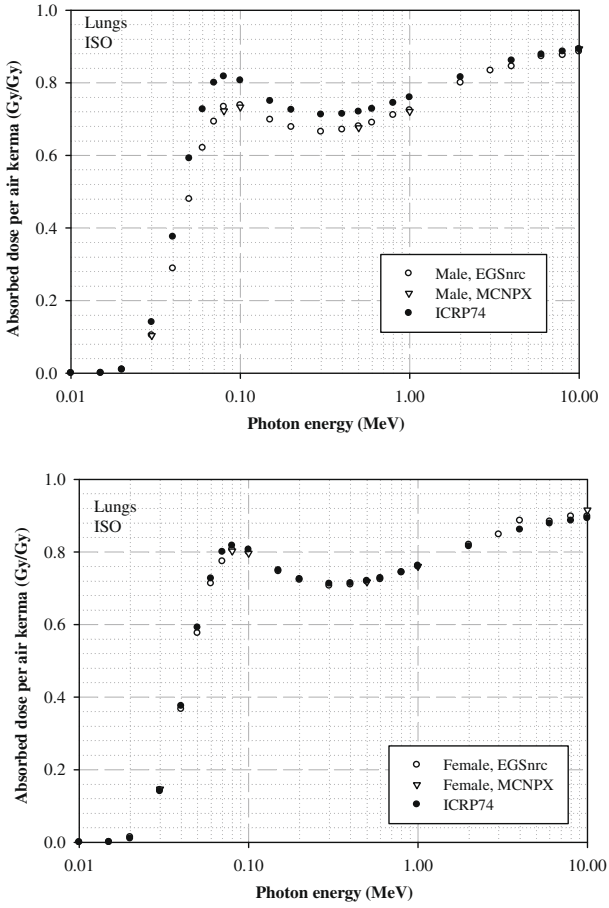

Fig. H.12. Lung absorbed dose per air kerma free-in-air for monoenergetic photons impinging isotropically (ISO).

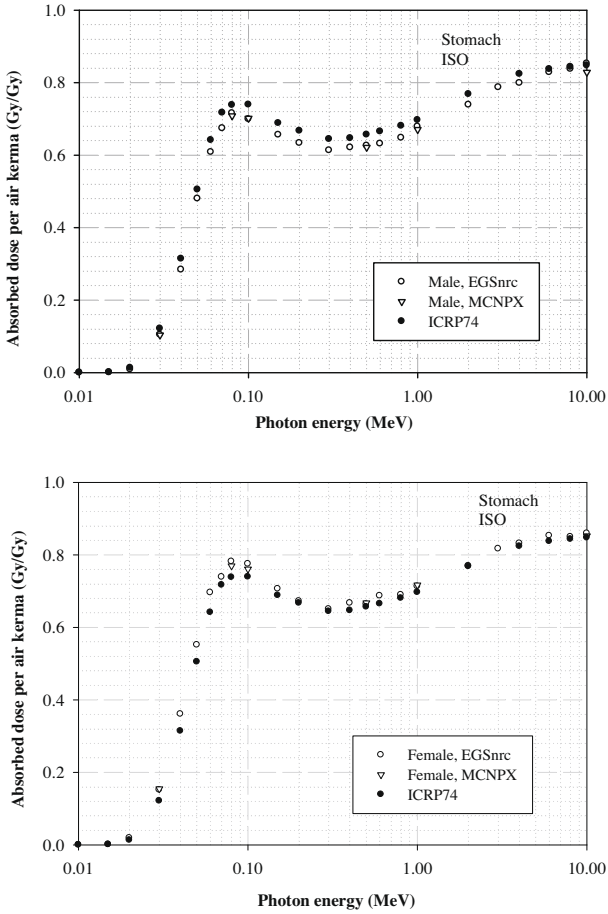

Fig. H.13. Stomach wall absorbed dose per air kerma free-in-air for monoenergetic photons impinging isotropically (ISO).

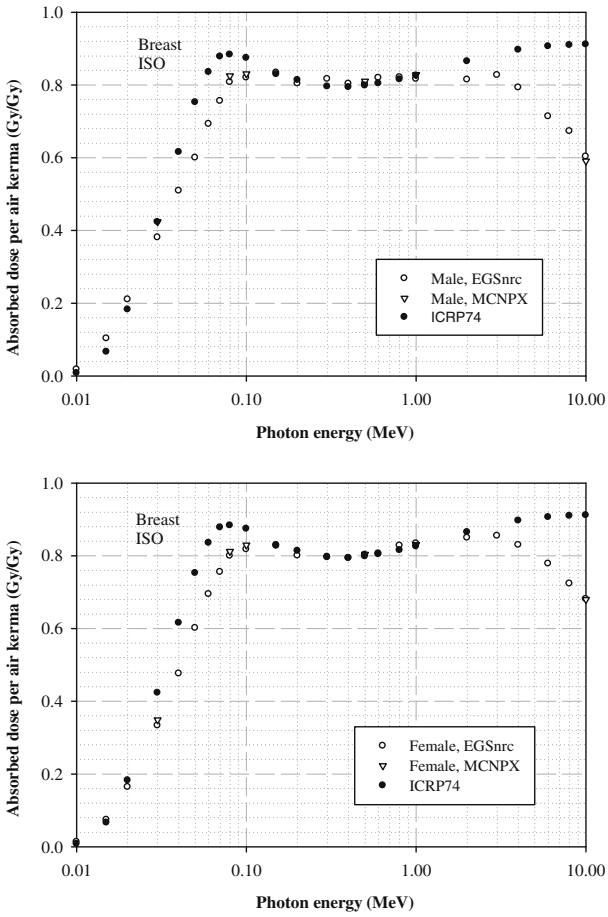

Fig. H.14. Breast absorbed dose per air kerma free-in-air for monoenergetic photons impinging isotropically (ISO). The decline of the conversion coefficients for energies above 1 MeV is due to the absence of secondary electron equilibrium which has not been considered in the earlier calculations (ICRP, 1996; ICRU, 1998).

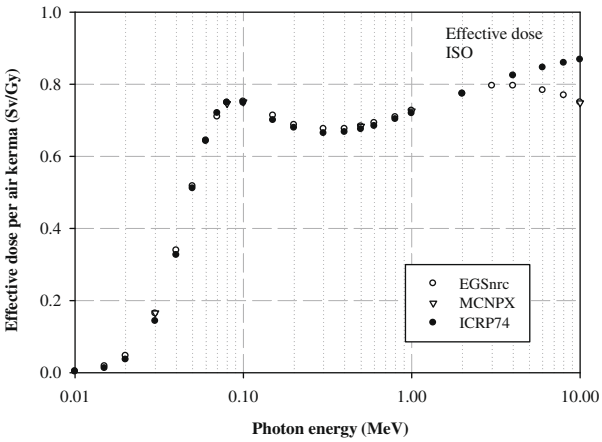

Fig. H.15. Effective dose per air kerma free-in-air for monoenergetic photons impinging isotropically (ISO).

H.1. References

GEANT4, 2006a. GEANT4: Physics Reference Manual. CERN, Geneva. Available at: http://geant4.web.cern.ch/geant4/support/userdocuments.shtml.

GEANT4, 2006b. GEANT4 User's Guide for Application Developers. CERN, Geneva. Available at: http://geant4.web.cern.ch/geant4/support/userdocuments.shtml.

Hendricks, J.S., McKinney, G.W., Waters, L.S., et al., 2005. MCNPX Extensions, Version 2.5.0. LA-UR-05-2675. LANL, Los Alamos, NM.

ICRP, 1996. Conversion coefficients for use in radiological protection against external radiation. ICRP Publication 74. Ann. ICRP. 26(3–4).

ICRP, 2007. The 2007 Recommendations of the International Commission on Radiological Protection. ICRP Publication 103. Ann. ICRP 37(2–4).

ICRU, 1998. Conversion Coefficients for Use in Radiological Protection Against External Radiation. ICRU Report 57. International Commission on Radiation Units and Measurements, Bethesda, MD.

Kawrakow, I., Rogers, D.W.O., 2003. The EGSnrc Code System: Monte Carlo Simulation of Electron and Photon Transport. PIRS Report 701. National Research Council of Canada, Ottawa.

Waters, L.S., 2002. MCNPX User's Manual, Version 2.3.0. Report LA-UR-02-2607. Los Alamos National Laboratory, Los Alamos, NM.

ANNEX I. SELECTED ORGAN DOSE CONVERSION COEFFICIENTS – EXTERNAL NEUTRONS

(I 1) In this annex, selected organ dose conversion coefficients are given for external exposure to monoenergetic neutrons. The conversion coefficients are given in graphical form in terms of organ absorbed dose per fluence (in Gy cm^2) for those organs contributing to the quantity effective dose with the highest tissue weighting factors, i.e. red bone marrow, colon, lungs, stomach, and breast.

(I 2) The geometries considered are unidirectional broad parallel beams impinging from the front (AP) and fully isotropic irradiation (ISO).

(I 3) Effective dose per fluence conversion coefficients are also given for unidirectional broad parallel beams impinging from the front (AP), the back (PA), and from the right (RLAT), as well as for fully isotropic irradiation (ISO).

(I 4) Figs. I.1–I.15 show data generated by the DOCAL Subgroup on External Dosimetry as part of the revision of *Publication 74* (ICRP, 1996) and ICRU Report 57 (ICRU, 1998) using the reference computational phantoms of this document and the radiation and tissue weighting factors of *Publication 103* (ICRP, 2007). The data were generated using the Monte Carlo codes PHITS (Iwase et al., 2002; Niita et al., 2006; Sato et al., 2009), FLUKA (Ferrari et al., 2005; Battistoni et al., 2006), and GEANT4 (GEANT4, 2006a,b).

(I 5) The conversion coefficients for the adult male and female reference computational phantoms are compared with the respective conversion coefficients from *Publication 74* (ICRP, 1996) and ICRU Report 57 (ICRU, 1998). Thus, an indication is given of the magnitude of differences that can be expected between the present reference organ dose conversion coefficients and the reference values employing the new phantoms, as well as the revised tissue and radiation weighting factors (ICRP, 2007).

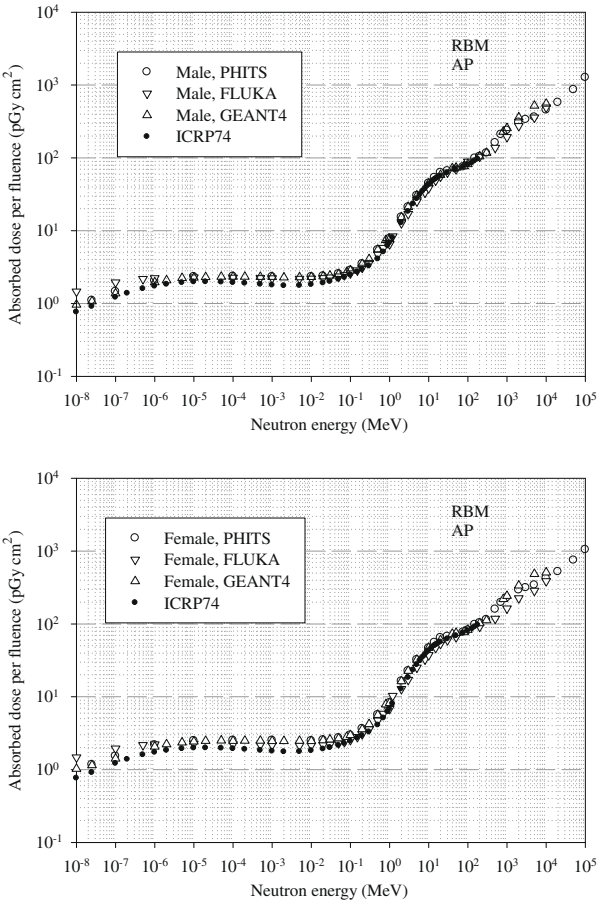

Fig. I.1. Red bone marrow (RBM) absorbed dose per particle fluence for monoenergetic neutrons impinging in anterior-posterior (AP) direction.

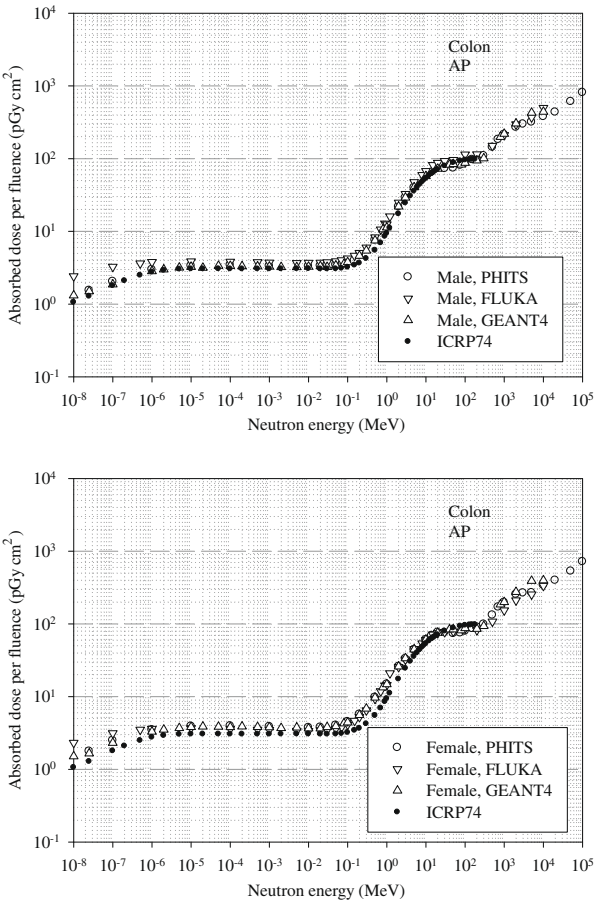

Fig. I.2. Colon absorbed dose per particle fluence for monoenergetic neutrons impinging in anterior-posterior (AP) direction.

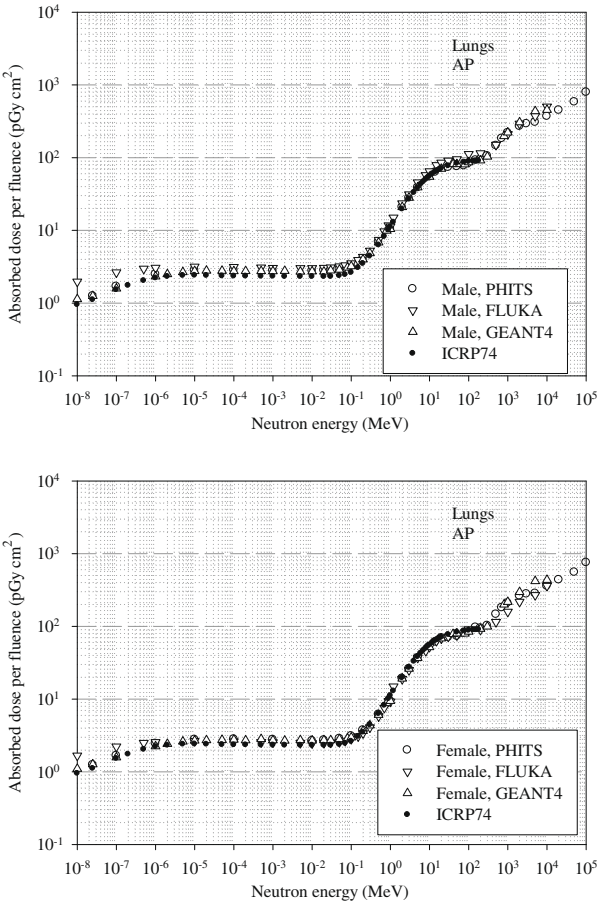

Fig. I.3. Lung absorbed dose per particle fluence for monoenergetic neutrons impinging in anterior-posterior (AP) direction.

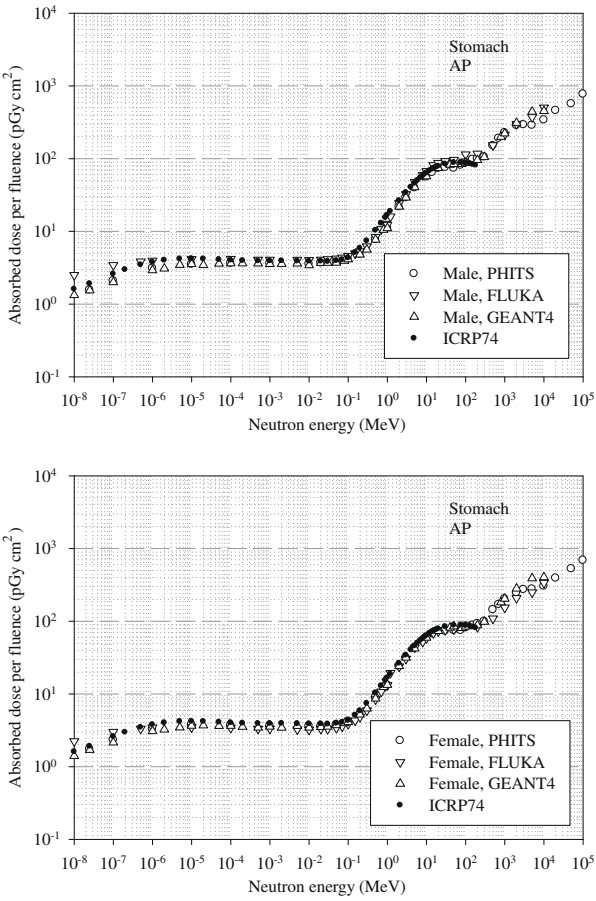

Fig. I.4. Stomach wall absorbed dose per particle fluence for monoenergetic neutrons impinging in anterior-posterior (AP) direction.

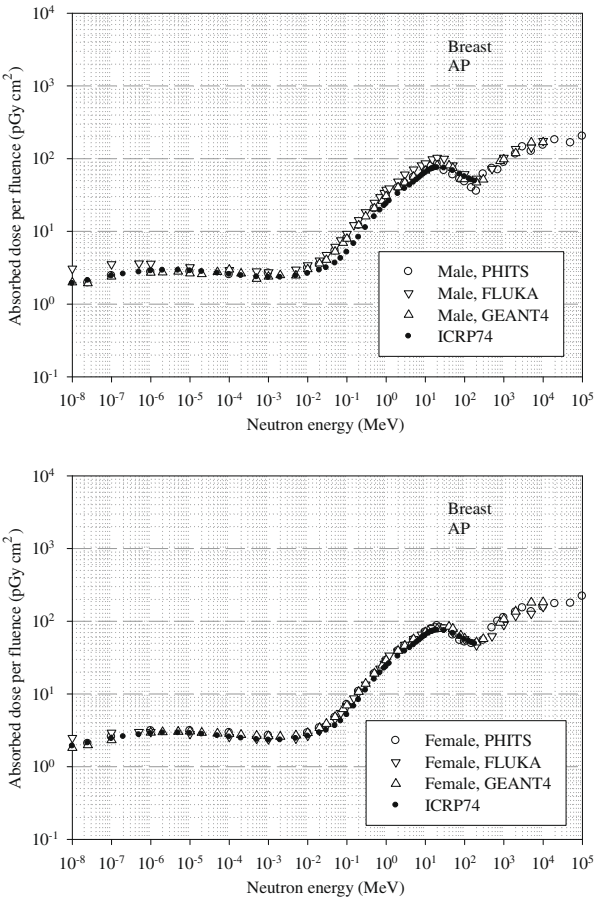

Fig. I.5. Breast absorbed dose per particle fluence for monoenergetic neutrons impinging in anterior-posterior (AP) direction.

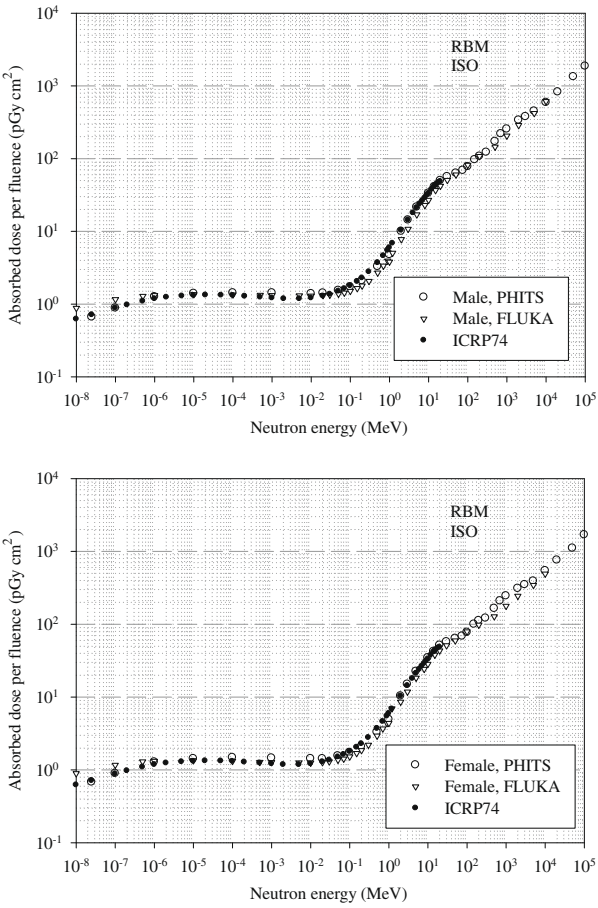

Fig. I.6. Red bone marrow (RBM) absorbed dose per particle fluence for monoenergetic neutrons impinging isotropically (ISO).

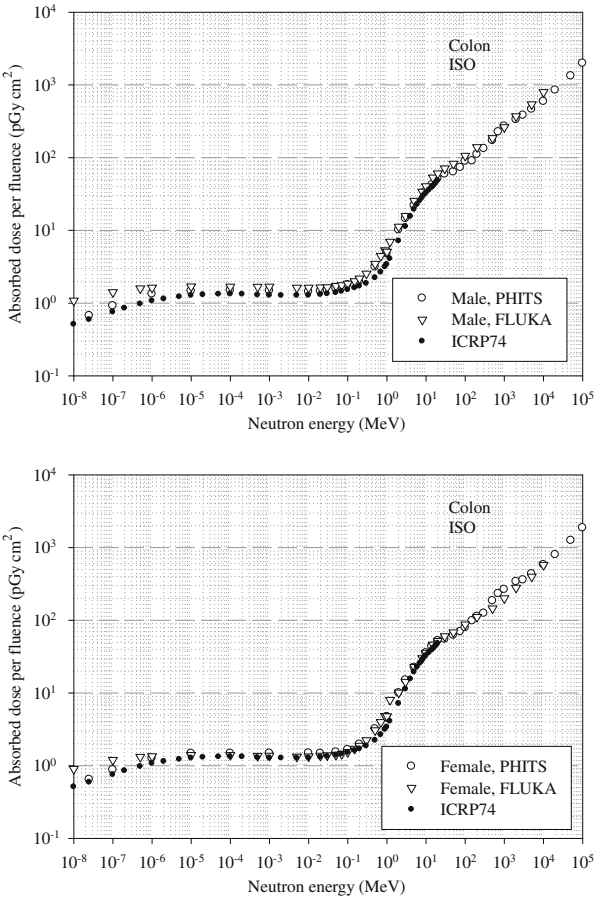

Fig. I.7. Colon absorbed dose per particle fluence for monoenergetic neutrons impinging isotropically (ISO).

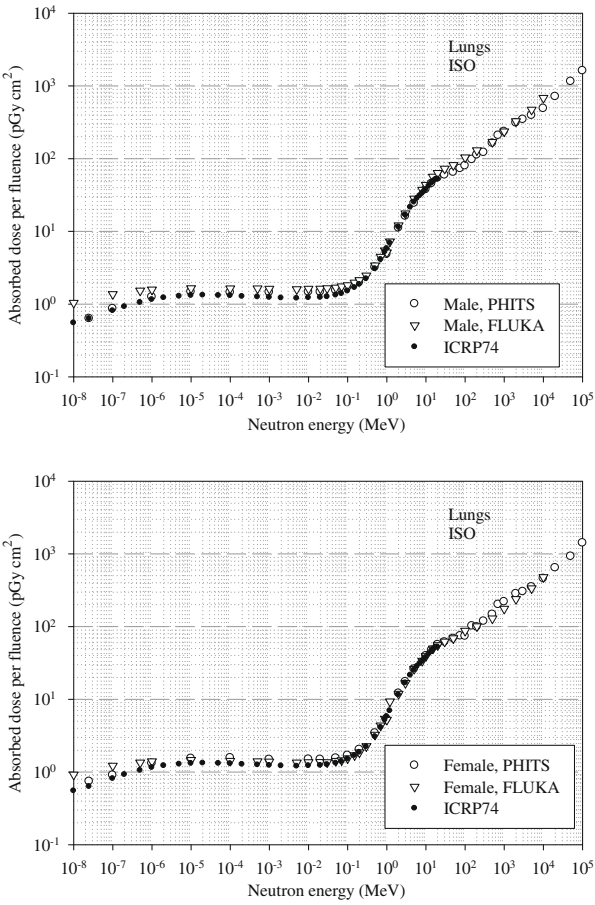

Fig. I.8. Lung absorbed dose per particle fluence for monoenergetic neutrons impinging isotropically (ISO).

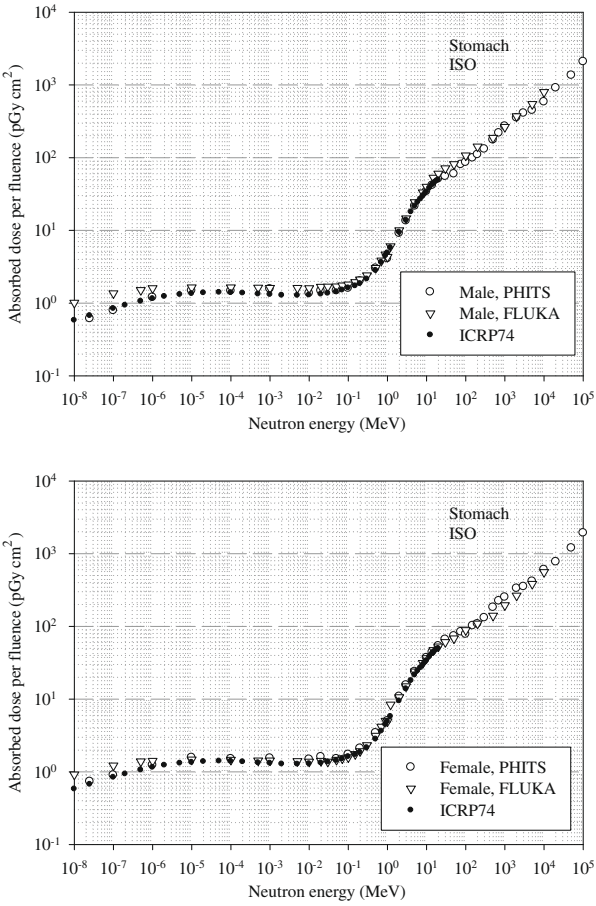

Fig. I.9. Stomach wall absorbed dose per particle fluence for monoenergetic neutrons impinging isotropically (ISO).

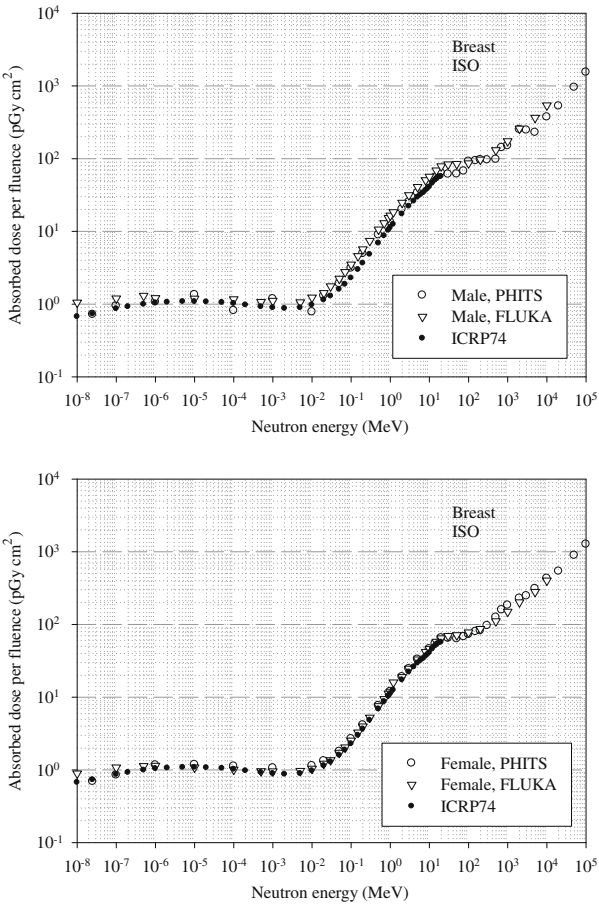

Fig. I.10. Breast absorbed dose per particle fluence for monoenergetic neutrons impinging isotropically (ISO).

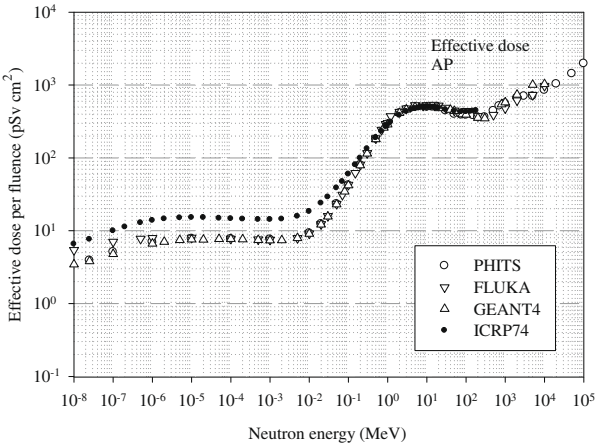

Fig. I.11. Effective dose per particle fluence for monoenergetic neutrons impinging in anterior-posterior (AP) direction.

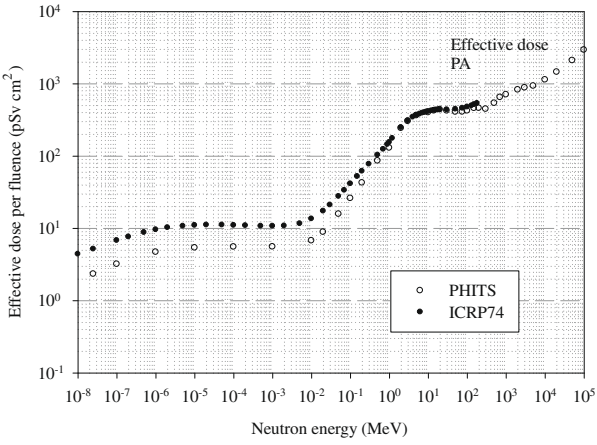

Fig. I.12. Effective dose per particle fluence for monoenergetic neutrons impinging in posterior-anterior (PA) direction.

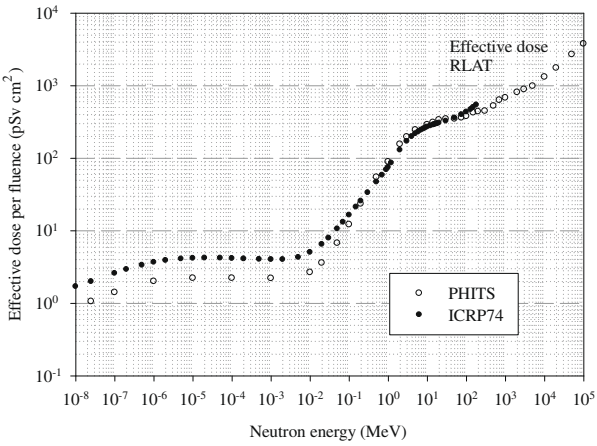

Fig. I.13. Effective dose per particle fluence for monoenergetic neutrons impinging in right lateral (RLAT) direction.

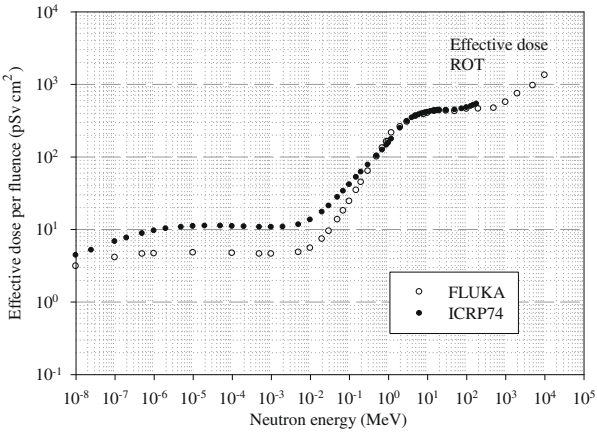

Fig. I.14. Effective dose per particle fluence for monoenergetic neutrons impinging in a full 360° rotation around the body length axis (ROT).

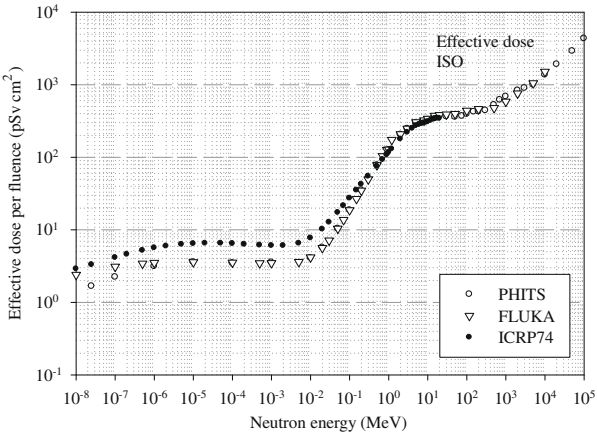

Fig. I.15. Effective dose per particle fluence for monoenergetic neutrons impinging isotropically (ISO).

I.1. References

Battistoni, G., Muraro, S., Sala, P.R., et al., 2006. The FLUKA code: description and benchmarking. In: Albrow, M., Raja, R. (Eds.), Hadronic Shower Simulation Workshop, Fermi National Accelerator Laboratory (Fermilab), Batavia, Illinois, AIP Conference Proceeding 896, pp. 31–49.

Ferrari, A., Sala, P.R., Fasso, A., et al., 2005. FLUKA: a Multi-particle Transport Code. CERN 2005-10, INFN/TC_05/11, SLAC-R-773. CERN, Geneva.

GEANT4, 2006a. GEANT4: Physics Reference Manual. Available at: http://geant4.web.cern.ch/geant4/support/userdocuments.shtml. CERN, Geneva.

GEANT4, 2006b. GEANT4: User's Guide for Application Developers. Available at: http://geant4.web.cern.ch/geant4/support/userdocuments.shtml. CERN, Geneva.

ICRP, 1996. Conversion coefficients for use in radiological protection against external radiation. ICRP Publication 74. Ann. ICRP 26(3–4).

ICRP, 2007. The 2007 Recommendations of the International Commission on Radiological Protection. ICRP Publication 103. Ann. ICRP 37(2–4).

ICRU, 1998. Conversion Coefficients for Use in Radiological Protection Against External Radiation. ICRU Report 57. International Commission on Radiation Units and Measurements, Bethesda, MD.

Iwase, H., Niita, K., Nakamura, T., 2002. Development of a general-purpose particle and heavy ion transport Monte Carlo code. J. Nucl. Sci. Technol. 39, 1142–1151.

Niita, K., Sato, T., Iwase, H., et al., 2006. PHITS – a particle and heavy ion transport code system. Radiat. Meas. 41, 1080–1090.

Sato, T., Endo, A., Zankl, M., et al., 2009. Fluence-to-dose conversion coefficients for neutrons and protons calculated using the PHITS code and ICRP/ICRU adult reference computational phantoms. Phys. Med. Biol. 54, 1997–2014.

ANNEX J. SELECTED ORGAN DOSE CONVERSION COEFFICIENTS – EXTERNAL HELIUM IONS

(J 1) Heavy charged particles are of concern mainly in space dosimetry. In the following, selected organ dose conversion coefficients are given for external exposure to monoenergetic helium ions as an example. The conversion coefficients are given in graphical form in terms of organ absorbed dose per fluence (in Gy cm^2). The geometries considered are a unidirectional broad parallel beam impinging from the front (AP), and isotropic irradiation (ISO).

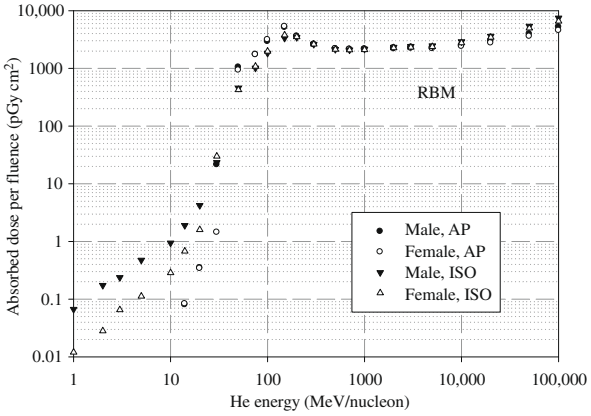

Fig. J.1. Red bone marrow (RBM) absorbed dose per particle fluence for monoenergetic helium ions impinging in anterior-posterior direction (AP) or isotropically (ISO).

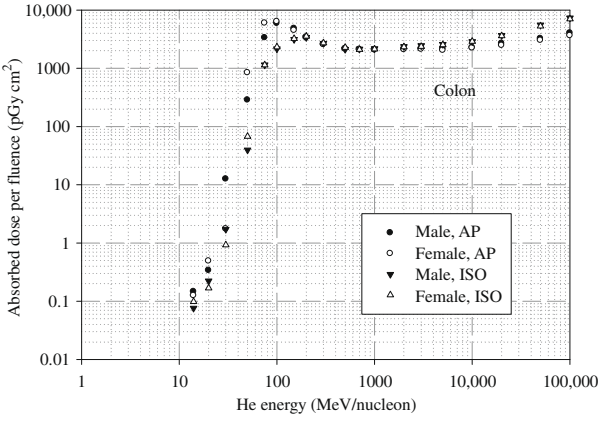

Fig. J.2. Colon absorbed dose per particle fluence for monoenergetic helium ions impinging in anterior-posterior direction (AP) or isotropically (ISO).

(J 2) The conversion coefficients are given for those organs contributing to the quantity effective dose with the highest tissue weighting factors, i.e. red bone marrow, colon, lungs, stomach, and breast.

(J 3) Figs. J.1–J.5 show data generated by the DOCAL Subgroup on External Dosimetry as part of the revision of *Publication 74* (ICRP, 1996) and ICRU Report 57 (ICRU, 1998) using the reference computational phantoms of this document and the tissue weighting factors of *Publication 103* (ICRP, 2007). The data were generated using the Monte Carlo code PHITS (Iwase et al., 2002; Niita et al., 2006).

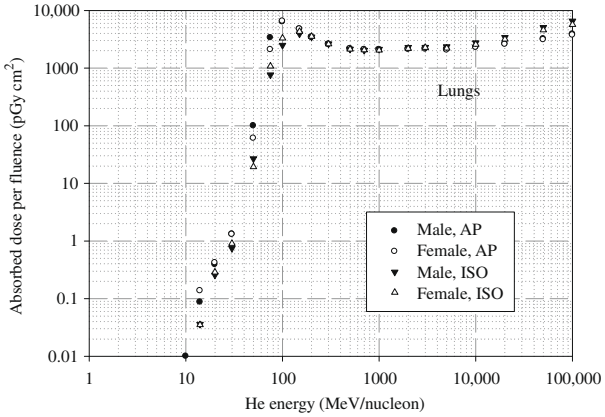

Fig. J.3. Lung absorbed dose per particle fluence for monoenergetic helium ions impinging in anterior-posterior direction (AP) or isotropically (ISO).

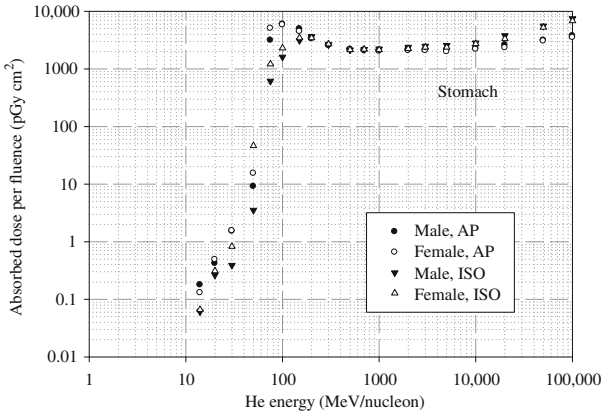

Fig. J.4. Stomach wall absorbed dose per particle fluence for monoenergetic helium ions impinging in anterior-posterior direction (AP) or isotropically (ISO).

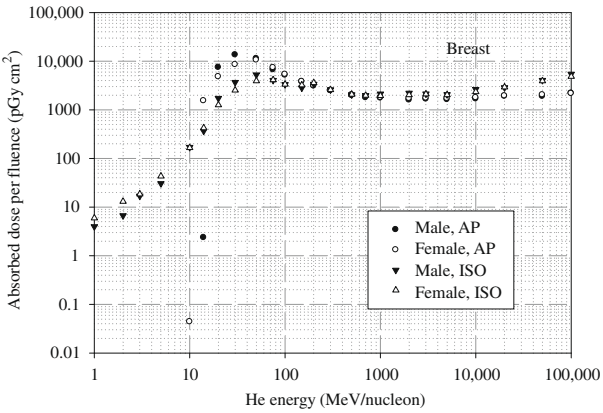

Fig. J.5. Breast absorbed dose per particle fluence for monoenergetic helium ions impinging in anterior-posterior direction (AP) or isotropically (ISO).

J.1. References

ICRP, 1996. Conversion coefficients for use in radiological protection against external radiation. ICRP Publication 74. Ann. ICRP 26(3–4).

ICRP, 2007. The 2007 Recommendations of the International Commission on Radiological Protection. ICRP Publication 103. Ann. ICRP 37(2–4).

ICRU, 1998. Conversion Coefficients for Use in Radiological Protection Against External Radiation. ICRU Report 57. International Commission on Radiation Units and Measurements, Bethesda, MD.

Iwase, H., Niita, K., Nakamura, T., 2002. Development of a general-purpose particle and heavy ion transport Monte Carlo code. J. Nucl. Sci. Technol. 39, 1142–1151.

Niita, K., Sato, T., Iwase, H., et al., 2006. PHITS – a particle and heavy ion transport code system. Radiat. Meas. 41, 1080–1090.

ANNEX K. SELECTED SPECIFIC ABSORBED FRACTIONS – PHOTONS

(K 1) In the following, specific absorbed fractions for monoenergetic photons are given for selected source and target region pairs in graphical form. The specific absorbed fraction is the fraction of energy emitted as a specified radiation type in a source region, S, that is absorbed per unit mass of target region, T (per kg).

(K 2) The source regions are liver, lungs, and thyroid, and the target regions are colon, lungs, stomach wall, and breast.

(K 3) Figs. K.1–K.12 show data generated by DOCAL using the reference computational phantoms of this document and the Monte Carlo codes EGSnrc (Kawrakow and Rogers, 2003) and MCNPX (Waters, 2002; Hendricks et al., 2005).

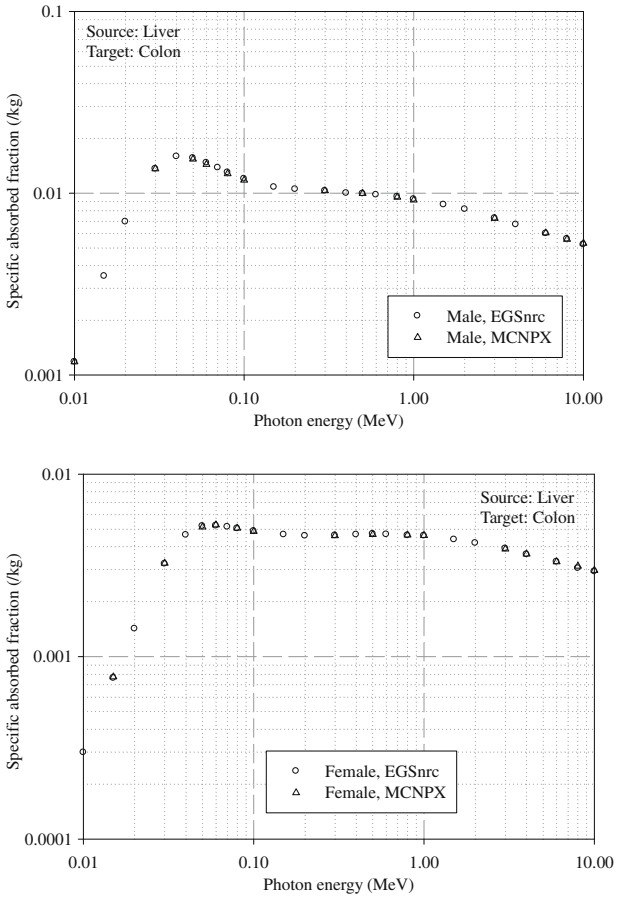

Fig. K.1. Specific absorbed fractions for monoenergetic photons for source region liver and target region colon wall.

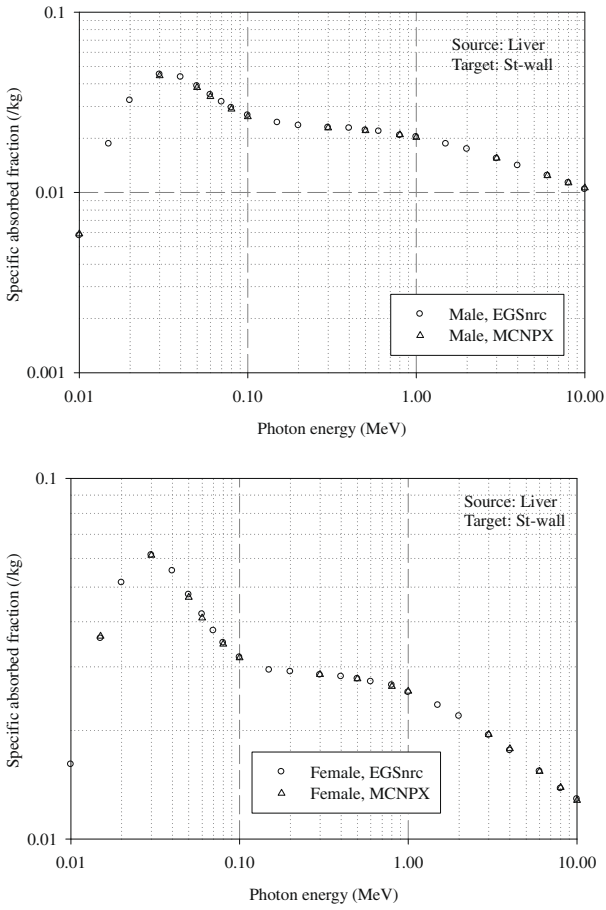

Fig. K.2. Specific absorbed fractions for monoenergetic photons for source region liver and target region lungs.

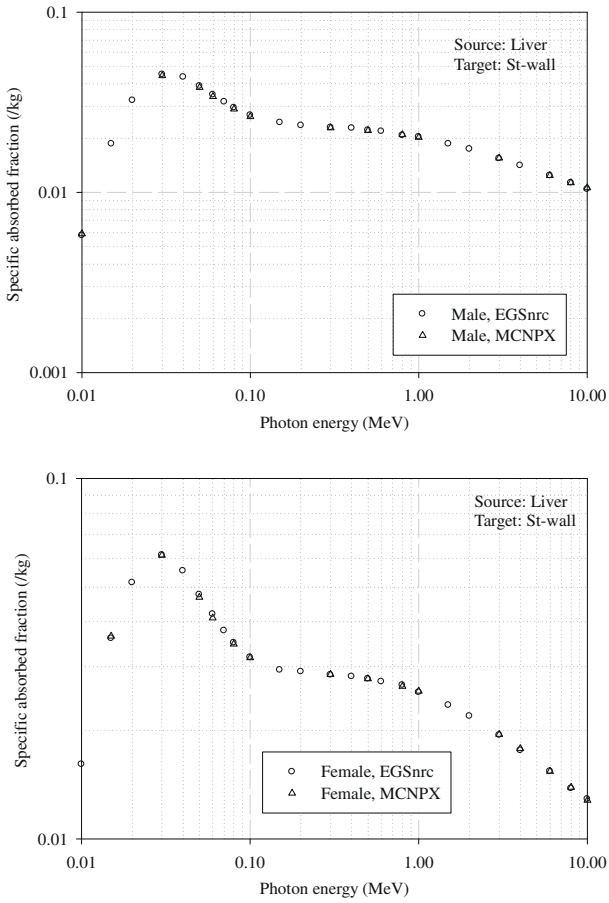

Fig. K.3. Specific absorbed fractions for monoenergetic photons for source region liver and target region stomach wall.

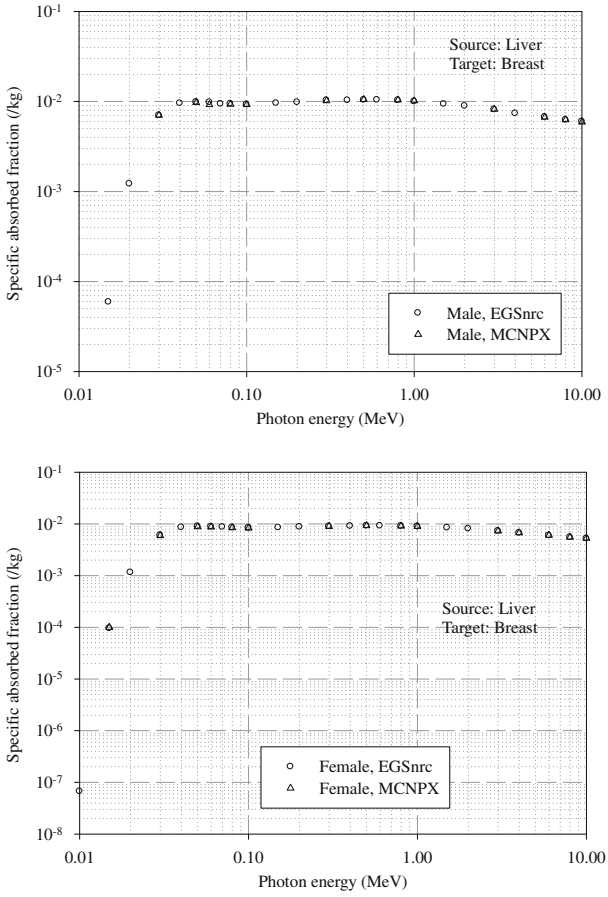

Fig. K.4. Specific absorbed fractions for monoenergetic photons for source region liver and target region breast.

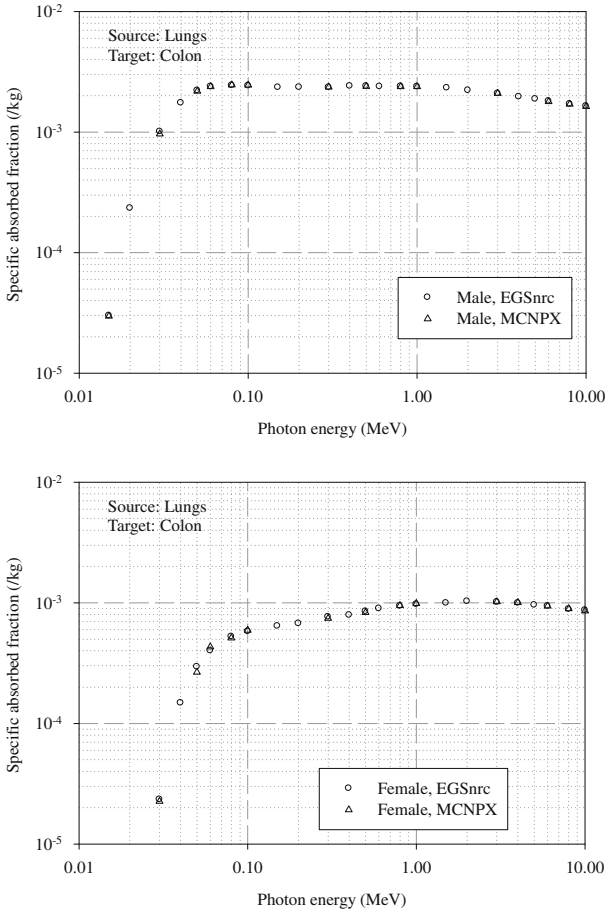

Fig. K.5. Specific absorbed fractions for monoenergetic photons for source region lungs and target region colon wall.

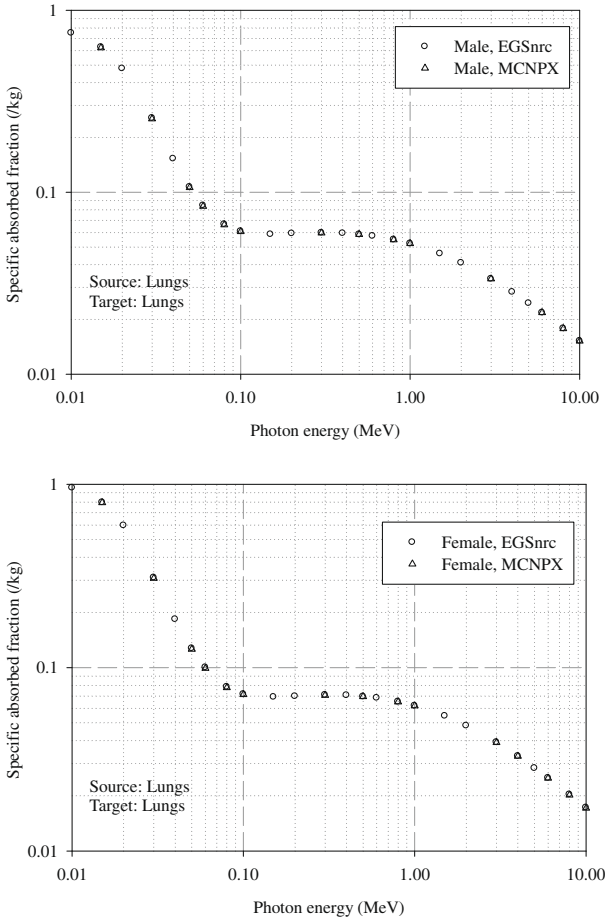

Fig. K.6. Specific absorbed fractions for monoenergetic photons for self-irradiation of the lungs.

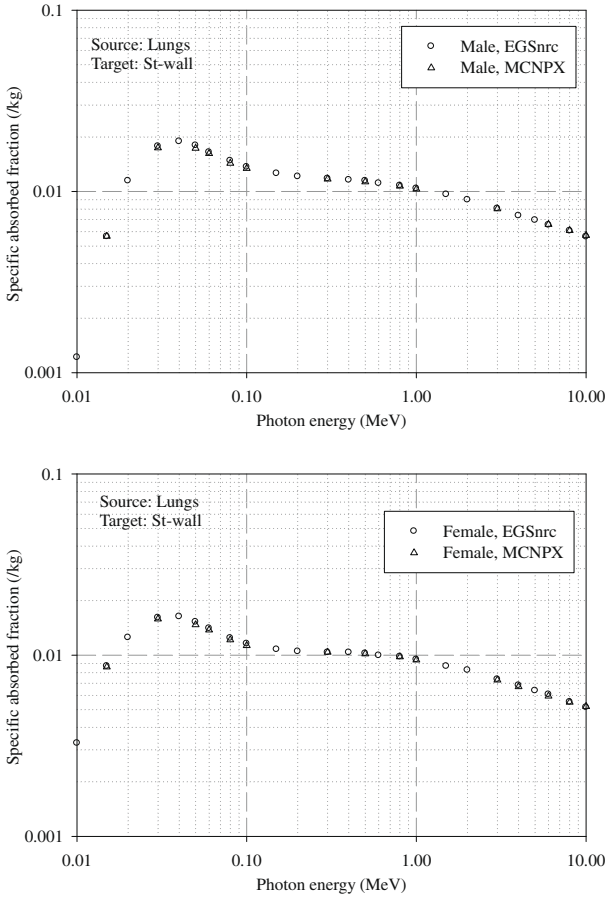

Fig. K.7. Specific absorbed fractions for monoenergetic photons for source region lungs and target region stomach wall.

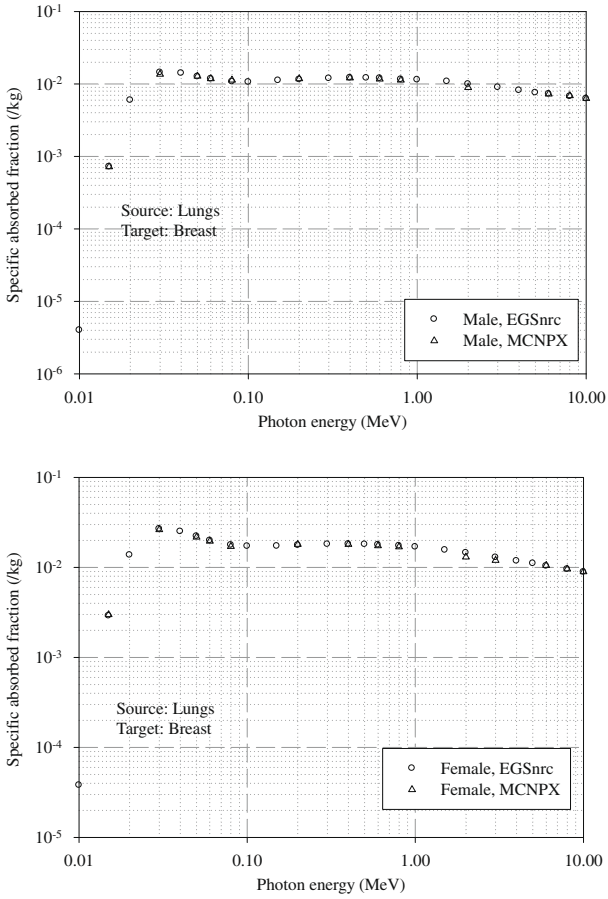

Fig. K.8. Specific absorbed fractions for monoenergetic photons for source region lungs and target region breast.

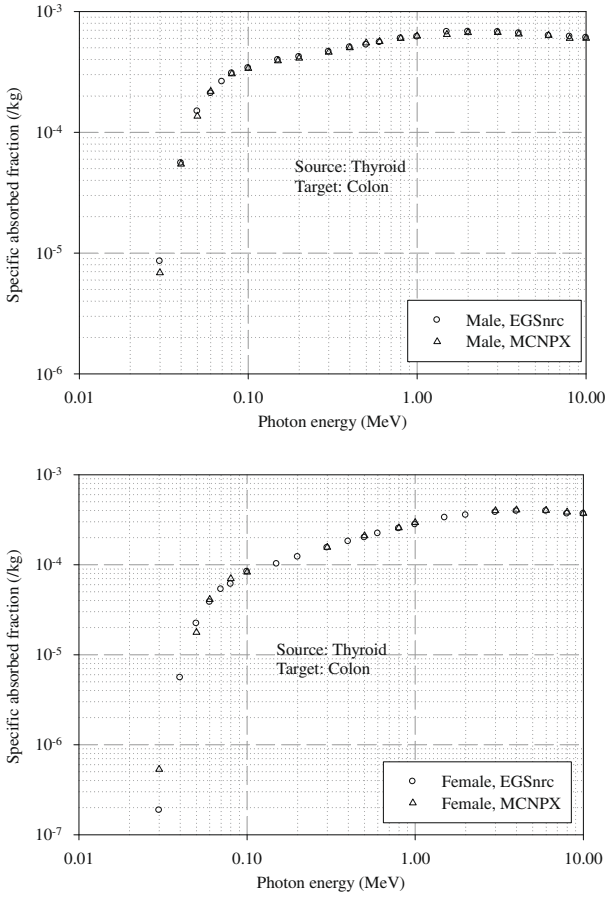

Fig. K.9. Specific absorbed fractions for monoenergetic photons for source region thyroid and target region colon wall.

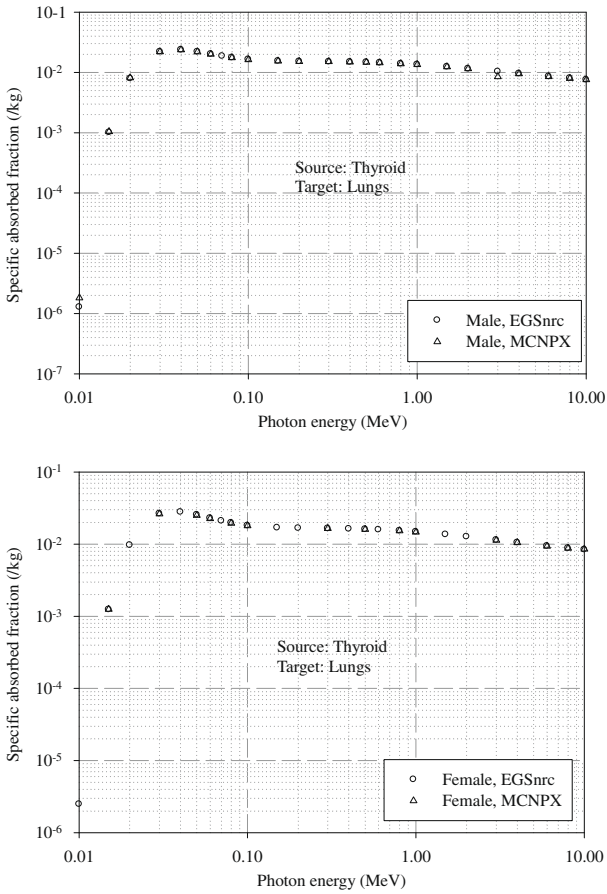

Fig. K.10. Specific absorbed fractions for monoenergetic photons for source region thyroid and target region lungs.

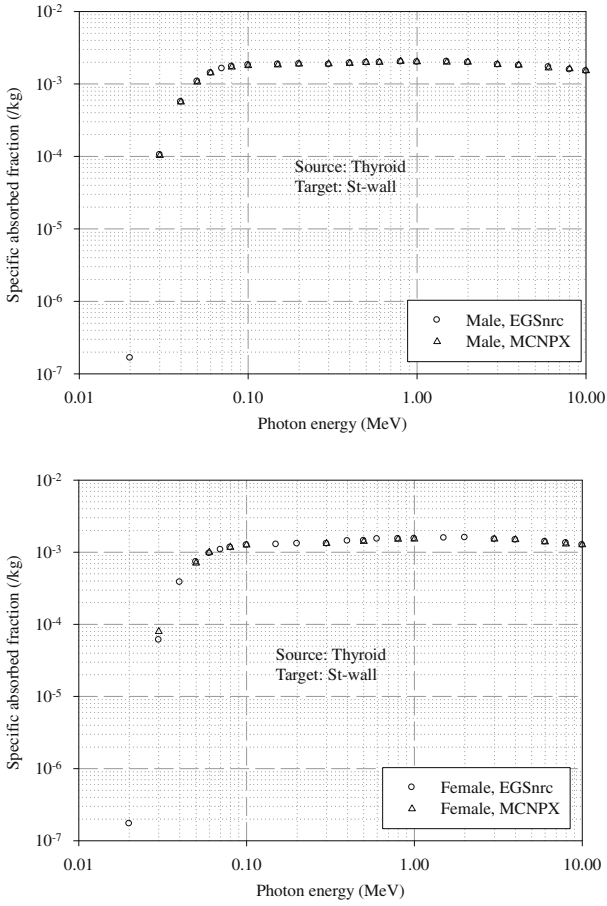

Fig. K.11. Specific absorbed fractions for monoenergetic photons for source region thyroid and target region stomach wall.

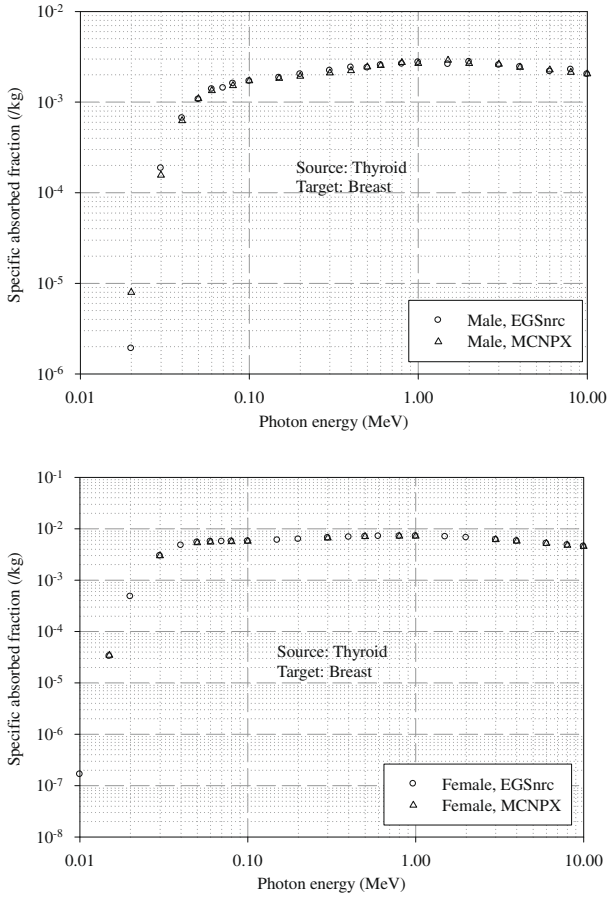

Fig. K.12. Specific absorbed fractions for monoenergetic photons for source region thyroid and target region breast.

K.1. References

Hendricks, J.S., McKinney, G.W., Waters, L.S., et al., 2005. MCNPX Extensions, Version 2.5.0. LA-UR-05-2675. LANL, Los Alamos, NM.

Kawrakow, I., Rogers, D.W.O., 2003. The EGSnrc Code System: Monte Carlo Simulation of Electron and Photon Transport. PIRS Report 701. National Research Council of Canada, Ottawa.

Waters, L.S., 2002. MCNPX User's Manual, Version 2.3.0. Report LA-UR-02-2607. Los Alamos National Laboratory, Los Alamos, NM.

ANNEX L. SELECTED SPECIFIC ABSORBED FRACTIONS – ELECTRONS

(L 1) In the following, specific absorbed fractions for monoenergetic electrons are given for selected source and target region pairs in graphical form. The specific absorbed fraction is the fraction of energy emitted as a specified radiation type in a source region, S, that is absorbed per unit mass of target region, T (per kg).

(L 2) The source regions are liver, lungs, and thyroid, and the target regions are colon wall, lungs, stomach wall, and breast.

(L 3) The present results confirm earlier findings that the previously applied simplifying assumption of electrons being fully absorbed in the source organ itself is not always true at higher energies (Chao and Xu, 2001). High energy electrons have the ability to escape from the source organ, as can be seen in Fig. L.6 where specific absorbed fractions for self-absorption in the lungs are shown. For organs in close vicinity, such as liver and stomach wall, high energy electrons escaping from the source organ may result in cross-fire specific absorbed fractions that can reach the same order of magnitude as those from photons (see Figs. K.3 and L.3).

(L 4) For distant organ pairs, however, such as thyroid and colon wall, electron specific absorbed fractions can be considered negligible.

(L 5) Figs. L.1–L.12 show data generated by DOCAL using the reference computational phantoms of this document and the Monte Carlo codes EGSnrc (Kawrakow and Rogers, 2003) and MCNPX (Waters, 2002; Hendricks et al., 2005).

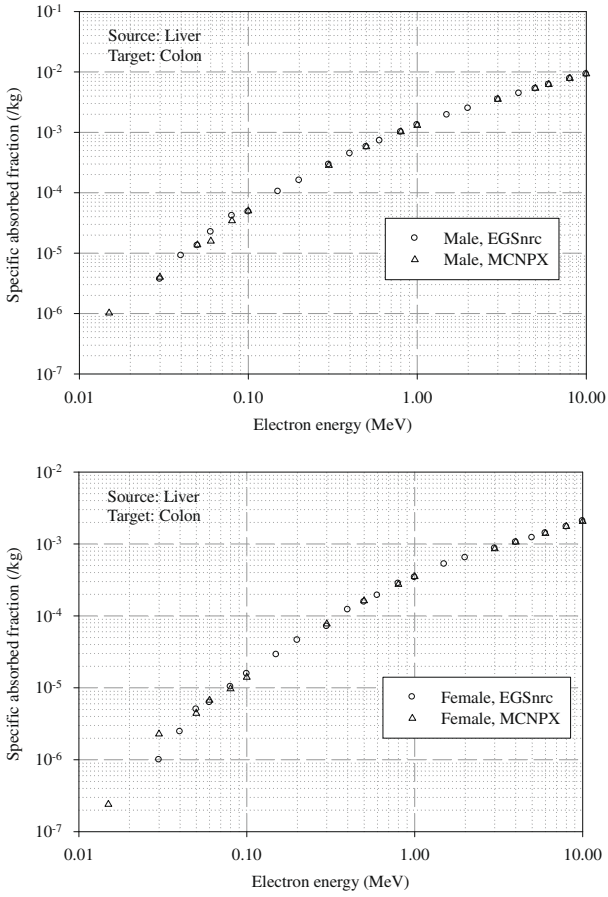

Fig. L.1. Specific absorbed fractions for monoenergetic electrons for source region liver and target region colon wall.

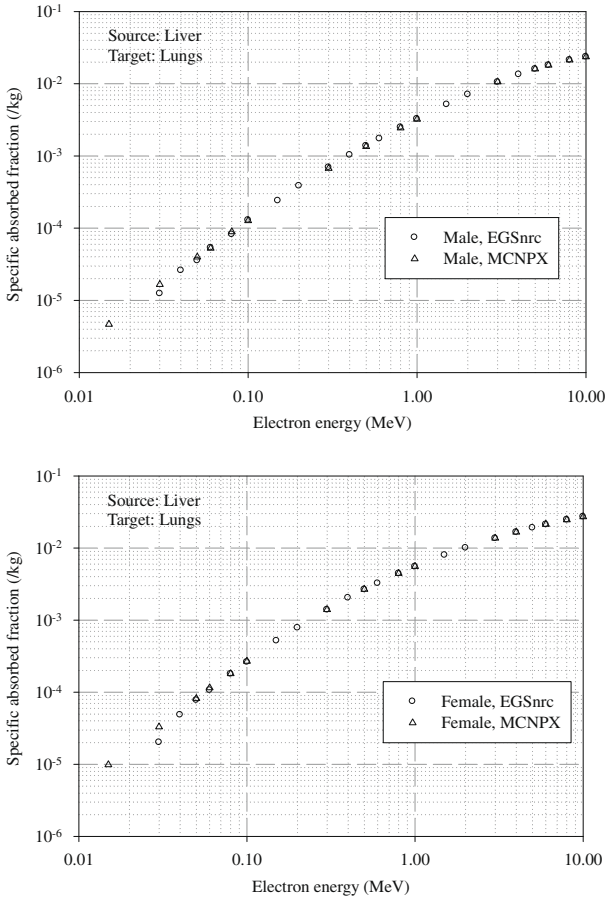

Fig. L.2. Specific absorbed fractions for monoenergetic electrons for source region liver and target region lungs.

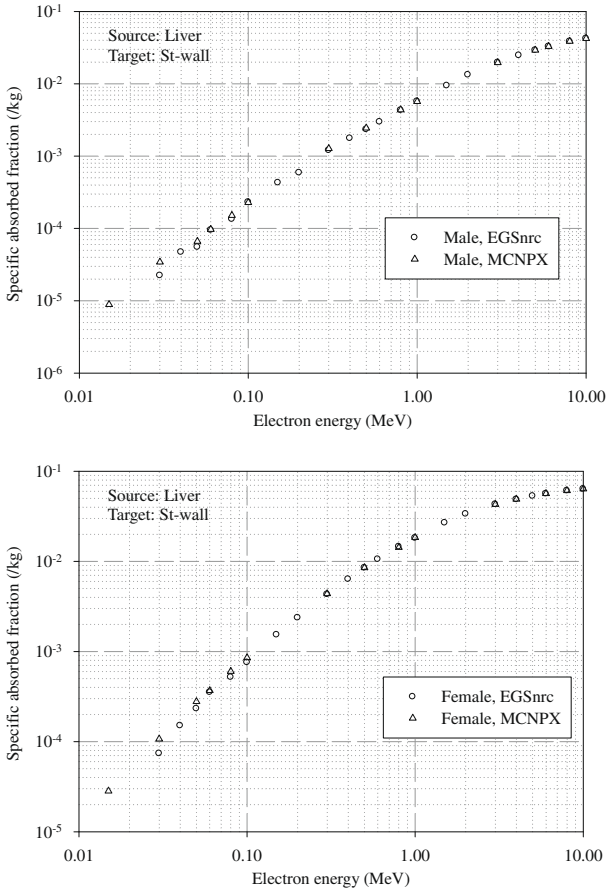

Fig. L.3. Specific absorbed fractions for monoenergetic electrons for source region liver and target region stomach wall.

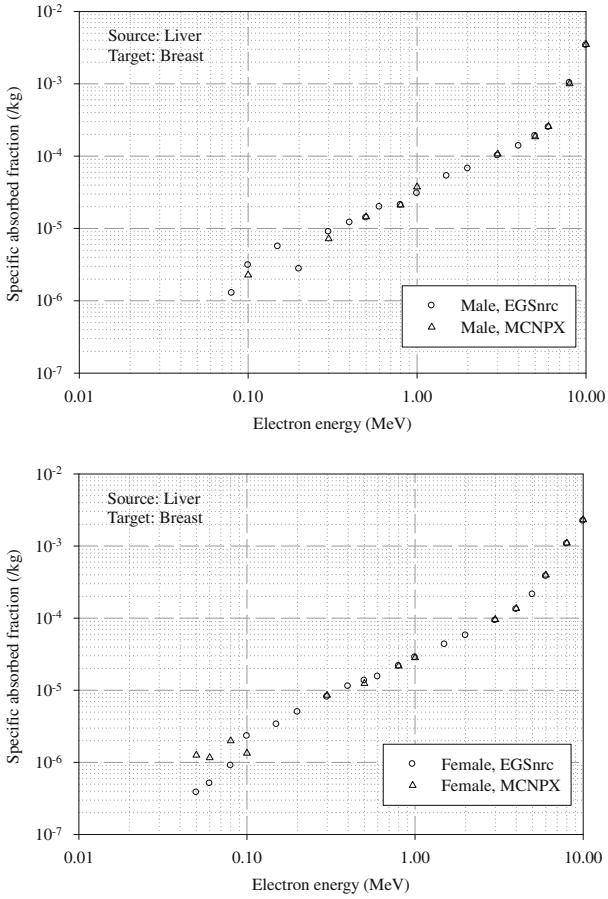

Fig. L.4. Specific absorbed fractions for monoenergetic electrons for source region liver and target region breast.

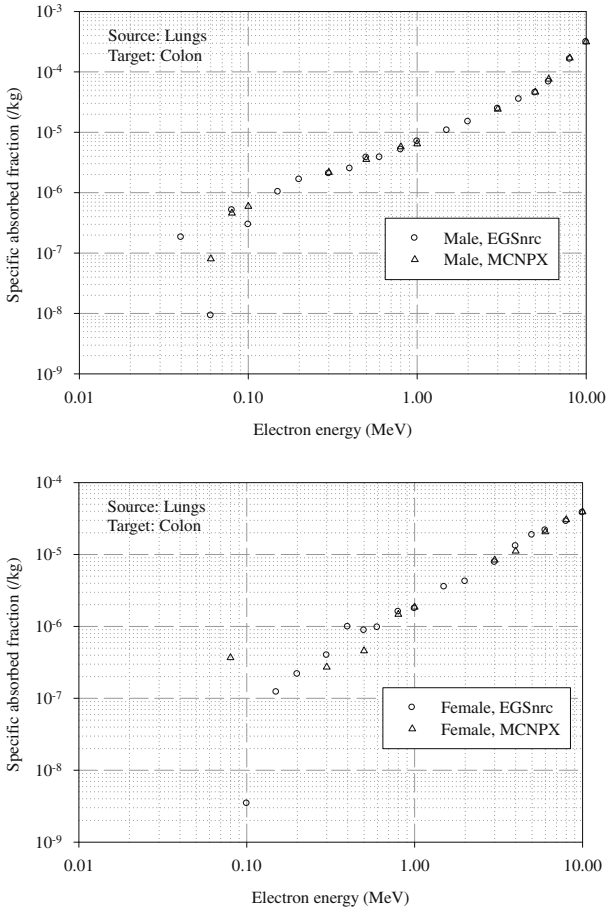

Fig. L.5. Specific absorbed fractions for monoenergetic electrons for source region lungs and target region colon wall.

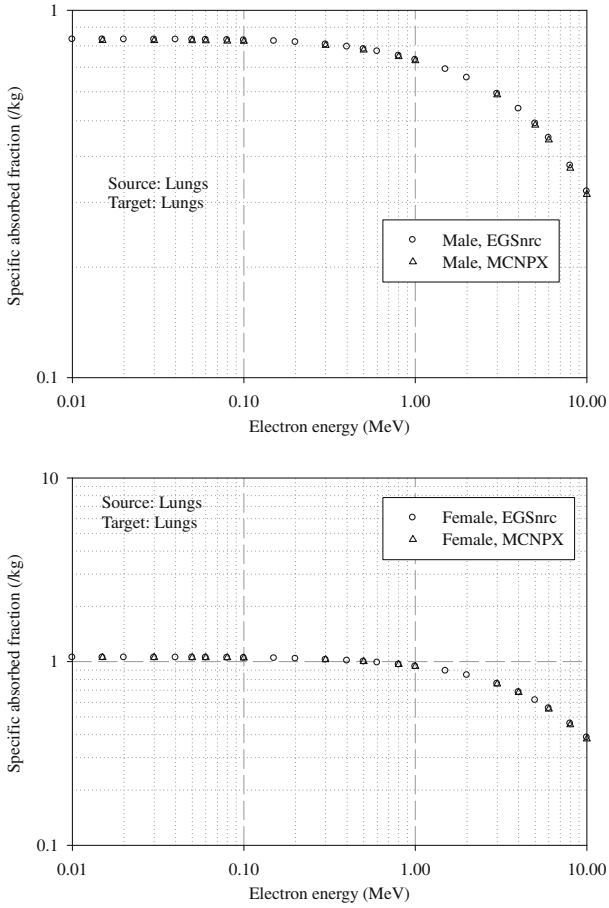

Fig. L.6. Specific absorbed fractions for monoenergetic electrons for self-irradiation of the lungs.

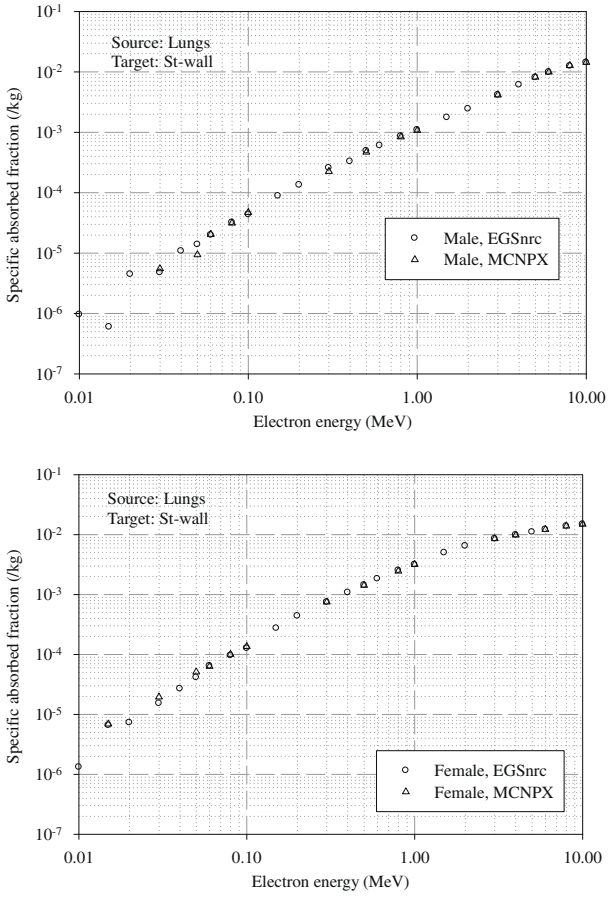

Fig. L.7. Specific absorbed fractions for monoenergetic electrons for source region lungs and target region stomach wall.

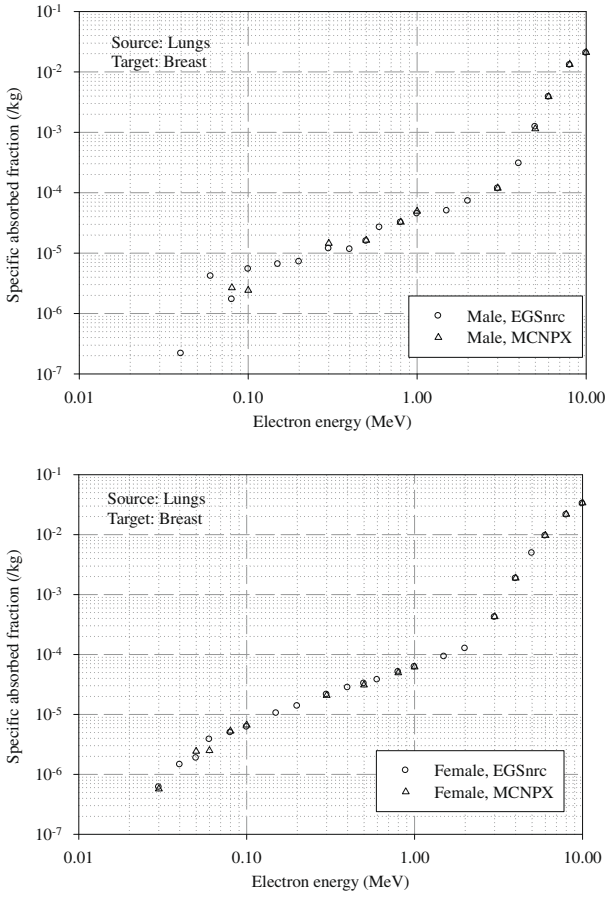

Fig. L.8. Specific absorbed fractions for monoenergetic electrons for source region lungs and target region breast.

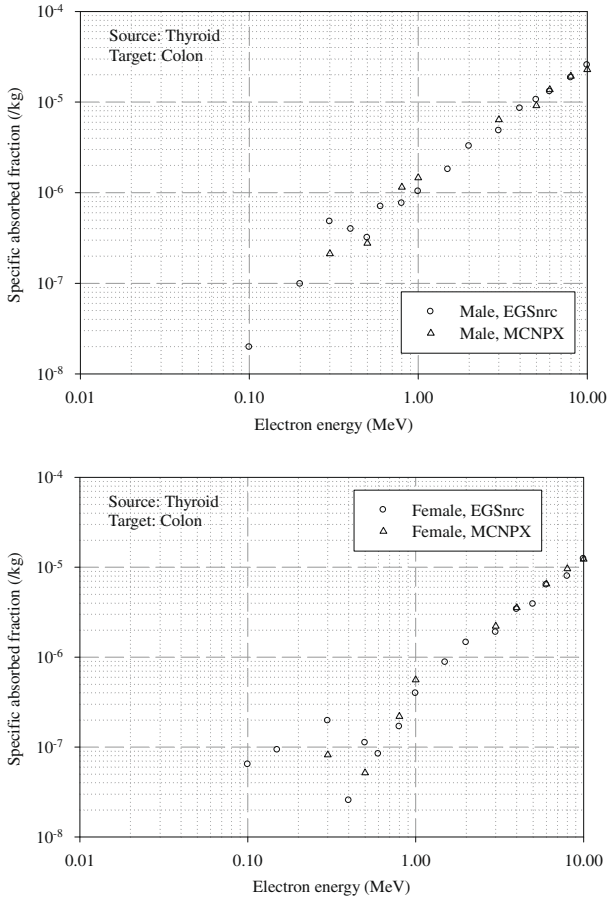

Fig. L.9. Specific absorbed fractions for monoenergetic electrons for source region thyroid and target region colon wall.

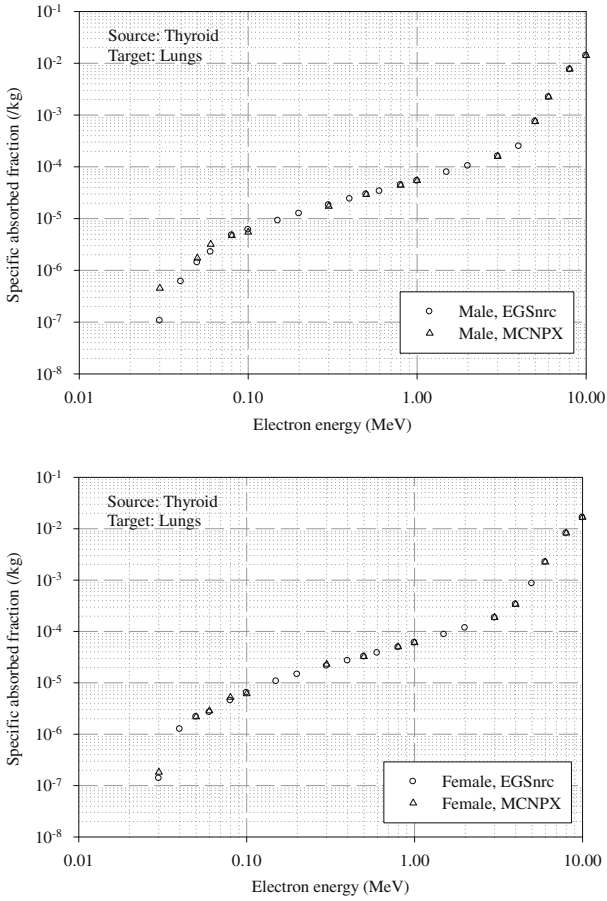

Fig. L.10. Specific absorbed fractions for monoenergetic electrons for source region thyroid and target region lungs.

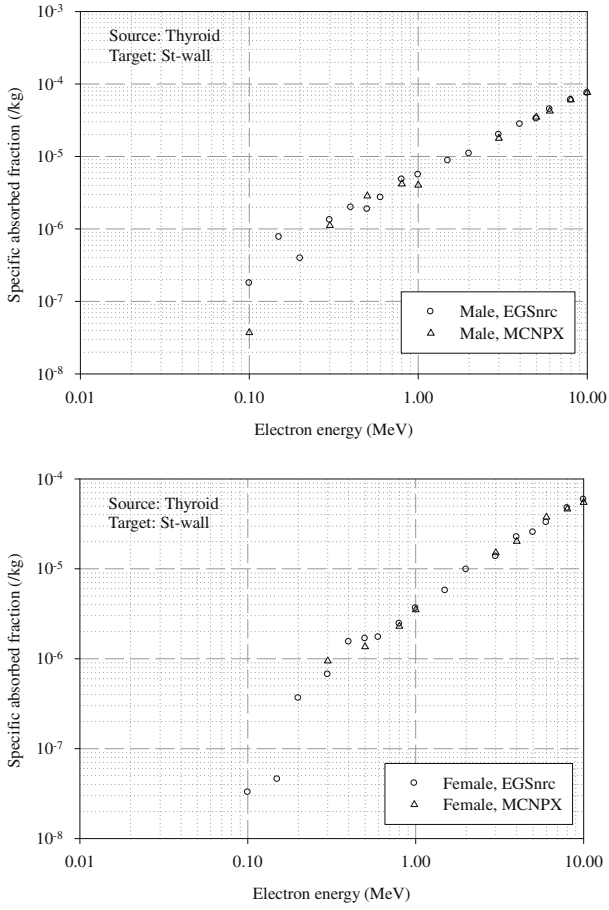

Fig. L.11. Specific absorbed fractions for monoenergetic electrons for source region thyroid and target region stomach wall.

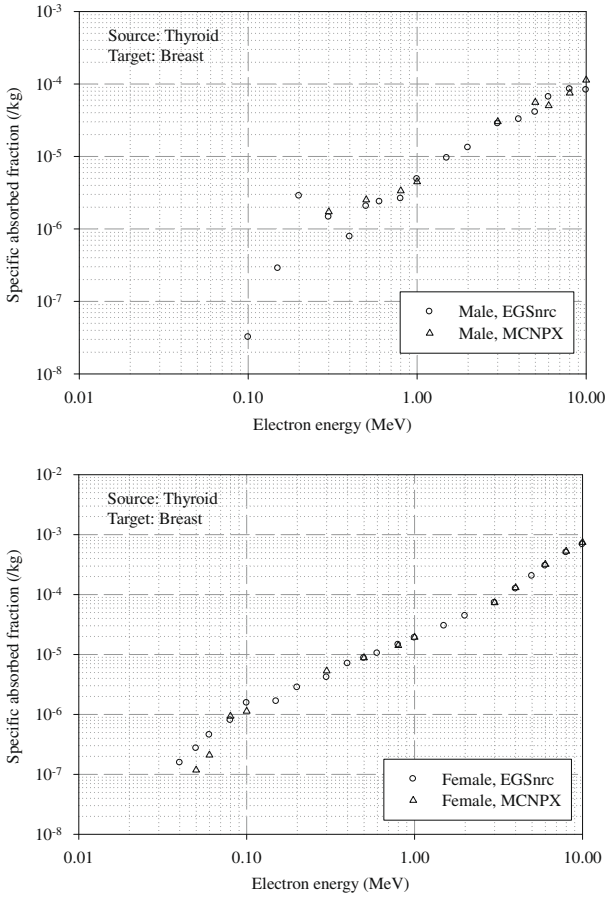

Fig. L.12. Specific absorbed fractions for monoenergetic electrons for source region thyroid and target region breast.

L.1. References

Chao, T.C., Xu, X.G., 2001. Specific absorbed fractions from the image-based VIP-Man body model and EGS4-VLSI Monte Carlo code: internal electron emitters. Phys. Med. Biol. 46, 901–927.

Hendricks, J.S., McKinney, G.W., Waters, L.S., et al., 2005. MCNPX Extensions, Version 2.5.0. LA-UR-05-2675. LANL, Los Alamos, NM.

Kawrakow, I., Rogers, D.W.O., 2003. The EGSnrc Code System: Monte Carlo Simulation of Electron and Photon Transport. PIRS Report 701. National Research Council of Canada, Ottawa.

Waters, L.S., 2002. MCNPX User's Manual, Version 2.3.0. Report LA-UR-02-2607. Los Alamos National Laboratory, Los Alamos, NM.

ANNEX M. SUMMARY OF THE CD CONTENTS

(M 1) It should be noted that the CD-ROM only stores data and does not contain 'active' software.

(M 2) The CD-ROM is organised into two main folders, one for each of the two reference phantoms (AM: adult male, AF: adult female). Each folder contains the following files:

- The array of organ ID numbers (in ASCII format); the file names are:

  AM.dat
  AF.dat

- A list of individually segmented structures, their identification numbers, and assigned media (Annex A); the file names are:

  AM_organs.dat
  AF_organs.dat

- A list of the media, their elemental compositions, and densities (Annex B); the file names are:

  AM_media.dat
  AF_media.dat

- The mass ratios of bone constituents (trabecular bone, red and yellow bone marrow) in the spongiosa regions; the file names are:

  AM_spongiosa.dat
  AF_spongiosa.dat

- The mass ratios of blood in various body tissues; the file names are:

  AM_blood.dat
  AF_blood.dat

(M 3) In the organ ID arrays, the organ IDs are listed slice by slice; within each slice, row by row; and within each row, column by column. That means, the column index changes fastest, then the row index, then the slice index. The numbers of columns, rows, and slices (i.e. the array dimensions) of both phantoms are given in Table 5.1 together with the voxel dimensions.

(M 4) The organ ID numbers are stored in groups of 16, but the number of columns is not a multiple of 16. Therefore, appropriate care has to be applied for reading the data. As an example, Fig. M.1 presents a FORTRAN programme reading the data of the female reference computational phantom and storing them into a $299 \times 137 \times 348$ array.

(M 5) Slice numbers increase from the toes up to the vertex of the body, row numbers increase from front to back, and column numbers increase from right to left.

```
      program readdata
*     Programme to read the voxel phantom data from ASCII file
*     AF.dat and store them in a three-dimensional array of
*     organ identification numbers
      dimension norgin(300),nodum(16),noid(300,200,350)
*     Numbers of columns, rows, and slices:
      ncol=299
      nrow=137
      nsli=348
      open (10,file='AF.dat')
*     Read phantom file, assign organ identification numbers to
*     array positions
*     The organ identification numbers are stored in groups of 16,
*     but the number of columns is not a multiple of 16.
*     Therefore, when ncol organ IDs are read, this ends right in
*     the middle of a line, and the rest of this line is ignored.
*     Hence, the next 'read' statement has to account for this:
*     The last line that has been read only partially, has to be
*     read again, whereby that first part that has been registered
*     already needs to be skipped. Therefore, the number 'ndum' of
*     these items has to be tracked.
      write (6,'('' Reading of phantom file started'')')
      nrorea=ncol/16
      ndifcol=ncol-16*nrorea
      ndum=0
      do 40 nsl=1,nsli
      do 40 nr=1,nrow
      if (ndum.ne.0) then
        backspace (10)
        read (10,*) (nodum(i),i=1,ndum), (norgin(i),i=1,ncol)
      else
        read (10,*) (norgin(i),i=1,ncol)
      endif
      do 30 nc=1,ncol
      noid(nc,nr,nsl)=norgin(nc)
   30 continue
      ndum=ndum+ndifcol
      if (ndum.ge.16) ndum=ndum-16
   40 continue
      write (6,'(''   … finished'')')
      close (10)
      end
```

Fig. M.1. FORTRAN programme reading the data of the female reference computational phantom and storing them into a $299 \times 137 \times 348$ array. Please note that for the male phantom, the numbers `ncol`, `nrow`, and `nsli` are different (see Table 5.1).

(M 6) There is skin with a different organ ID number at the top and bottom of the model (first and last slice). Thus, it can either be used or neglected (by assigning air or vacuum as medium) depending on the situation considered. If skin is assigned as the medium, it increases the body height as well as the total body mass.

ELSEVIER

ICRP Publication 110

Annals of the ICRP

Erratum

Erratum to P108

Due to an extremely unfortunate administrative oversight, the Committee responsible for publication 108, 'Environmental Protection: the Concept and Use of Reference Animals and Plants' were not credited in the preliminary pages of the report. To this end, please find below the Committee details as it should have appeared in that publication:

This report was drafted by Committee 5, under the chairmanship of R.J. Pentreath.

The Publisher apologies to the above Committee for this omission.

Annals of the ICRP

Annals of the ICRP is an essential publication for all:

- ☐ Regulatory and advisory agencies at regional, national and international levels
- ☐ Management bodies with responsibilities for radiological protection
- ☐ Professional staff employed as advisers and consultants
- ☐ Individuals, such as radiologists and nuclear medicine specialists, who make decisions about the use of ionising radiation.

Annals of the ICRP provides recommendations and guidance from the International Commission on Radiological Protection on protection against the risks associated with ionising radiation, from artificial sources as widely used in medicine, general industry and nuclear enterprises, and from naturally occurring sources. Each *Annals of the ICRP* provides an in-depth coverage of a specific subject area.

Annals of the ICRP are available as a journal subscription or can be purchased as individual books and in addition supporting CD-ROMs (currently 3 different ones) are available. *Annals of the ICRP* is also available in electronic format at www.sciencedirect.com.

Future publications of the ICRP

(Please note that these reports may be subject to late changes and alterations)

ICRP Publication 111 – *Application of the Commission's Recommendations to the Protection of People Living in Long Term Contaminated Areas after a Nuclear Accident or a Radiation Emergency*

ICRP Publication 112 – *Minimising Unintended Exposure in Radiation Therapy from New Technologies*

ISSN

0146-6453(200904)39:2;1-Z

ISBN

978-0-7020-4186-0(200904)39:2;1-Z

Printed by Polestar Wheatons Ltd. Exeter, UK